

# **CHARACTERIZATION OF POLARIZATION-MODE DISPERSION ON BURIED STANDARD SINGLE-MODE FIBERS**

by

Pradeep Kumar Kondamuri

B.Tech. (Electronics and Communications Engineering)

Sri Venkateswara University, Tirupathi, India, 2000

Submitted to the Department of Electrical Engineering and Computer Science and the Faculty of the Graduate School of the University of Kansas in partial fulfillment of the requirements for the degree of Master of Science

---

Professor in Charge

---

---

Committee Members

---

Date thesis accepted

*Dedicated to*  
*My parents and sisters*

## **ACKNOWLEDGEMENTS**

I would like to express my sincere thanks to Dr. Christopher Allen, my committee chair, for his guidance throughout this thesis and for his suggestions and support during my graduate studies here at University of Kansas. His encouragement and full support led me to the success of this work. I would like to thank Dr. Ronqing Hui for his valuable suggestions during my research work. I would also like to thank Dr. James Stiles for serving on my committee.

I would like to thank Juan Madrid who helped me in developing the visual basic software that controls the PMD measurement system. I would also like to thank Arun prasad chimata and Asvini Ganesh (other members of PMD compensation project) for helping me in my research work. Also, I would like to express my thanks to Sprint Corporation for their continued financial support and collaboration with lightwave lab. I learnt a lot working in such an advanced lightwave lab.

Finally, I would like to thank all my friends here at KU for making my stay here memorable.

## **ABSTRACT**

Polarization-mode dispersion (PMD) is a major impairment for high bit rate systems resulting in pulse broadening and distortion and thus leading to system performance degradation. Given the stochastic nature of PMD, it is extremely important to characterize PMD on buried fibers to gain a better understanding of its statistical characteristics. To characterize PMD on three different 95-km fibers within a slotted-core, direct buried, standard single-mode fiber-optic cable, we have configured an automated, long-term PMD measurement system, using a polarization analyzer, a tunable laser source and a PC. We report the detailed long-term measurement of differential group delay (DGD) on the above-mentioned fibers and make predictions regarding the probability, frequency and duration of high-DGD occurrences.

The plots of DGD showed DGD to change with time slowly but randomly and high-DGD events to be spectrally localized. Through analysis of measured DGD data, we were able to verify the Maxwellian distribution of DGD. The mean DGD, in most cases, was observed to vary by about 10 % or less during the measurements. The drift times obtained from the DGD data measured for a very long period agreed well with those reported by others. DGD bandwidths estimated on different fiber spans agreed well with the bandwidths found using the theoretical spectral autocorrelation fits. Outage analysis showed DGD excursions of three or more times the mean DGD to be infrequent and relatively short lived. This finding is significant for network operators who must assess the impact of PMD on network reliability.

# TABLE OF CONTENTS

<b>1. Introduction</b> .....	1
<b>2. Polarization-mode dispersion concepts</b> .....	5
2.1. Polarization effects in lightwave systems.....	5
2.2. What is PMD? .....	6
2.3. Causes of PMD .....	6
2.3.1. Birefringence .....	6
2.3.2. Mode coupling.....	8
2.4. PMD in short fibers .....	9
2.5. PMD in long fibers .....	10
2.6. Principal States model.....	12
2.7. PMD vector .....	13
2.8. Second-order PMD .....	14
2.9. Statistical nature of PMD.....	15
2.10. PMD in the presence of PDL.....	17
2.11. Emulation of PMD.....	17
2.11.1. Emulators with fixed orientations.....	18
2.11.2. Emulators with rotatable sections.....	19
2.11.3. Emulators with variable DGD elements.....	20
2.12. Numerical simulation of PMD.....	22
2.13. System impairments due to PMD .....	24
2.14. PMD tolerance of different modulation formats.....	26
2.15. PMD compensation techniques .....	27

2.15.1. Electrical PMD compensation .....	28
2.15.2. Optical PMD compensation .....	29
2.15.3. KU-PMD compensation system .....	33
<b>3. PMD measurement methods .....</b>	<b>35</b>
3.1. The pulse delay method .....	36
3.2. The modulation phase-shift method .....	37
3.3. The interferometric method.....	38
3.4. The Poincare arc method.....	40
3.5. The fixed analyzer method.....	41
3.6. The Jones Matrix Eigenanalysis (JME) method.....	43
<b>4. Measurement Setup.....</b>	<b>48</b>
<b>5. Measurement results and data analysis.....</b>	<b>50</b>
5.1. Tests & Plots .....	50
5.1.1. DGD color maps .....	50
5.1.2. DGD histograms .....	51
5.1.3. Temporal autocorrelation .....	51
5.1.4. Frequency autocorrelation .....	51
5.1.5. System outage analysis.....	52
5.1.6. Derivation of the expression for $R_{out}$ .....	53
5.2. Long-term measurements of individual buried fiber spans .....	55
5.2.1. Measurement setup.....	55
5.2.2. Plots of DGD vs. wavelength and time.....	56
5.2.3. Histograms of measured DGD data.....	59

5.2.4. Mean DGD variation with time.....	61
5.2.5. Temporal drift properties of DGD.....	63
5.2.6. Spectral behavior of DGD.....	65
5.2.7. System outage analysis.....	67
5.3. Long-term measurements of concatenated fiber spans.....	71
5.3.1. Measurement setup.....	71
5.3.2. Plots of DGD vs. wavelength and time.....	72
5.3.3. Histograms of measured DGD data.....	75
5.3.4. Mean DGD variation with time.....	77
5.3.5. Temporal drift properties of DGD.....	79
5.3.6. Spectral behavior of DGD.....	81
5.3.7. System outage analysis.....	83
5.4. Design rules based on DGD margin.....	86
5.5. Example scenarios (Single-span only).....	87
<b>6. Conclusions and future work.....</b>	<b>88</b>
6.1. Conclusions.....	88
6.2. Future work.....	89
<b>References.....</b>	<b>91</b>
Appendix A. Automated DGD measurements using polarization analyzer.	
Appendix B. Measured temporal and spectral PMD characteristics and their implications for network-level mitigation approaches.	
Appendix C. Analysis and comparison of measured DGD data on buried single- mode fibers.	

## LIST OF FIGURES

Fig. 2.1. Decorrelation of polarization in long fibers.....	8
Fig. 2.2. Spatial evolution of polarization caused by uniform birefringence.....	9
Fig. 2.3. Time-domain effect of PMD in a short fiber.....	10
Fig. 2.4. Model for a long fiber as a concatenation of birefringent sections with birefringence axes and magnitudes that change randomly along the fiber length.....	11
Fig. 2.5. Normalized Maxwellian distribution, with magnified tail portion.....	16
Fig. 2.6. PMD emulator with sections of PM fibers of unequal length and with rotatable connectors.....	19
Fig. 2.7. Schematic diagram of the PMD emulator with variable DGD elements.....	21
Fig. 2.8. General scheme for optical PMD compensation.....	29
Fig. 2.9. Optical compensation schemes. (a) PSP method (2 DOF), (b) 1 <sup>st</sup> order post comp (2 DOF), (c) 3 DOF post comp, (d) 4 DOF post comp, (e) 5 DOF post comp, (f) polarizer method (2 DOF). ....	31
Fig. 2.10. Block diagram of KU-PMD compensation system.....	33
Fig. 3.1. PMD measurement by the pulse-delay method.....	36
Fig. 3.2. PMD measurement by the modulation phase-shift method.....	37
Fig. 3.3. PMD measurement by the interferometric method.....	39
Fig. 3.4a. PMD measurement using the fixed analyzer method.....	42
Fig. 3.4b. Alternate setup for the fixed analyzer PMD measurement.....	42
Fig. 3.5. PMD measurement by the JME method.....	44



Fig. 4.1. Measurement setup used for making automated DGD measurements.....	48
Fig. 5.1. Measurement setup for characterizing individual buried fiber spans.....	55
Fig. 5.2. Measured, normalized DGD vs. wavelength and time for fiber span 1.....	57
Fig. 5.3. Measured, normalized DGD vs. wavelength and time for fiber span 2.....	57
Fig. 5.4. Measured, normalized DGD vs. wavelength and time for fiber span 3.....	58
Fig. 5.5. Histogram of measured, normalized DGD data on fiber span 1.....	59
Fig. 5.6. Histogram of measured, normalized DGD data on fiber span 2.....	60
Fig. 5.7. Histogram of measured, normalized DGD data on fiber span 3.....	60
Fig. 5.8. Frequency-averaged DGD and temperature vs. time for fiber span 1.....	61
Fig. 5.9. Frequency-averaged DGD and temperature vs. time for fiber span 2.....	62
Fig. 5.10. Frequency-averaged DGD and temperature vs. time for fiber span 3.....	62
Fig. 5.11. Normalized temporal ACF of frequency-averaged DGD data on fiber span 1 and its theoretical curve-fit.....	63
Fig. 5.12. Normalized temporal ACF of frequency-averaged DGD data on fiber span 2 and its theoretical curve-fit.....	64
Fig. 5.13. Normalized temporal ACF of frequency-averaged DGD data on fiber span 3 and its theoretical curve-fit.....	64
Fig. 5.14. Normalized spectral ACF of time-averaged DGD data from fiber span 1 and its adjusted theoretical curve-fit.....	65
Fig. 5.15. Normalized spectral ACF of time-averaged DGD data from fiber span 2 and its adjusted theoretical curve-fit.....	66
Fig. 5.16. Normalized spectral ACF of time-averaged DGD data from fiber	

span 3 and its adjusted theoretical curve-fit.....	66
Fig. 5.17. Calculated outage probability, $P_{out}$ , and mean outage rate $R_{out}$ , versus threshold/mean DGD for the three fiber spans.....	68
Fig. 5.18. Calculated mean outage duration, $T_{out}$ , as a function of threshold/mean DGD for the three fiber spans.....	68
Fig. 5.19. Measurement setup for characterizing the concatenated fiber spans.....	71
Fig. 5.20. Measured, normalized DGD vs. wavelength and time for fiber spans 1 and 2 concatenated (18 days).....	72
Fig. 5.21. Measured, normalized DGD vs. wavelength and time for fiber spans 2 and 3 concatenated (21 days).....	73
Fig. 5.22. Measured, normalized DGD vs. wavelength and time for fiber spans 1 and 3 concatenated (16 days).....	73
Fig. 5.23. DGD/Mean DGD vs. Time at 1560 nm on fiber spans 1 and 2 Concatenated.....	74
Fig. 5.24. DFT of DGD at 1560 nm with mean value subtracted from DGD data....	75
Fig. 5.25. Histogram of measured, normalized DGD data on fibers 1 and 2 concatenated.....	76
Fig. 5.26. Histogram of measured, normalized DGD data on fibers 2 and 3 concatenated.....	76
Fig. 5.27. Histogram of measured, normalized DGD data on fibers 1 and 3 concatenated.....	77
Fig. 5.28. Frequency-averaged DGD and temperature vs. time for fiber	

spans 1 and 2 concatenated.....	78
Fig. 5.29. Frequency-averaged DGD and temperature vs. time for fiber	
spans 2 and 3 concatenated.....	78
Fig. 5.30. Frequency-averaged DGD and temperature vs. time for fiber	
spans 1 and 3 concatenated.....	79
Fig. 5.31. Normalized temporal ACF of frequency-averaged DGD data on fiber	
spans 1 and 2 concatenated and its theoretical curve-fit.....	80
Fig. 5.32. Normalized temporal ACF of frequency-averaged DGD data on fiber	
spans 2 and 3 concatenated and its theoretical curve-fit.....	80
Fig. 5.33. Normalized temporal ACF of frequency-averaged DGD data on fiber	
spans 2 and 3 concatenated and its theoretical curve-fit.....	81
Fig. 5.34. Normalized spectral ACF of time-averaged DGD data on fiber	
spans 1 and 2 and it's adjusted theoretical curve-fit.....	82
Fig. 5.35. Normalized spectral ACF of time-averaged DGD data on fiber	
spans 2 and 3 and it's adjusted theoretical curve-fit.....	82
Fig. 5.36. Normalized spectral ACF of time-averaged DGD data on fiber	
spans 1 and 3 and it's adjusted theoretical curve-fit.....	83
Fig. 5.37. Calculated outage probability, $P_{out}$ , and mean outage rate $R_{out}$ , versus	
threshold/mean DGD for the concatenated fiber spans.....	84
Fig. 5.38. Calculated mean outage duration, $T_{out}$ , as a function of	
threshold/mean DGD for the concatenated fiber spans.....	84

## LIST OF TABLES

Table. 3.1. Summary of different PMD measurement methods.....	47
Table. 5.1. Predicted mean time between outages (MTBOs) and mean outage durations for different DGD tolerances.....	69
Table. 5.2. Values of $P_{out}$ , $R_{out}$ and $T_{out}$ for different values of threshold / mean DGD on fiber span 1.....	70
Table. 5.3. Predicted mean time between outages (MTBOs) and mean outage durations for different DGD tolerances.....	85

# 1. INTRODUCTION

Over the years, many forms of communication systems have been devised. The basic motivations behind each new form were to improve the transmission fidelity, to increase the data rate and to enhance the transmission distance between repeater stations. The bit rate-distance product  $BL$ , where  $B$  is the transmission bit rate and  $L$  is the repeater spacing, measures the transmission capacity of communication links [5]. The advent of telegraphy began the era of electrical communications with a very low bit rate using wire pairs as the channel. But, it is the invention of telephone and the development of worldwide telephone networks that led to many advances in the design of electrical communication systems. Coaxial cables replaced the wire pairs thereby increasing the system capacity considerably. However, losses in the coaxial cable were found to be frequency dependent and increase rapidly beyond 10 MHz. This led to the development of microwave communication systems operating at frequencies of 1 to 10 GHz. Both coaxial and microwave systems operate at data rates of up to a few hundred Megabits/ second (Mb/s), but microwave communication systems allow for a larger repeating spacing than coaxial systems. Further, it was realized in the later half of 20<sup>th</sup> century that a multi-fold increase in  $BL$  product can be achieved by using optical carrier over a fiber and this realization led to the era of fiber optic communications [4].

The fiber-optic communication technology is barely three decades old but it has made tremendous progress over a short period. The first generation fiber-optic systems operated with a wavelength near  $0.8 \mu\text{m}$  at bit rates of few tens of Mb/s and a

repeater spacing of about 10 km. The repeater spacing of these systems was limited by the fiber loss at the operating wavelength of 0.8  $\mu\text{m}$  and the inter-modal dispersion in multi-mode fibers. The second-generation fiber optic systems operated near 1.3  $\mu\text{m}$  where fiber loss is less than 1 dB/km and the chromatic dispersion is minimum. These systems operated at bit rates of up to 1.7 Gb/s on single-mode fibers with a repeater spacing of about 50 km. The repeater spacing was further enhanced for third generation systems that operated near 1.55  $\mu\text{m}$  (where the fiber loss is  $\sim 0.25$  dB/km) with data rates of up to 4 Gb/s over distances in excess of 100 km. But these systems faced the problem of large fiber dispersion near 1.55  $\mu\text{m}$ , which was overcome by using single-longitudinal-mode lasers with either single-mode fiber (SMF) with dispersion compensating fiber (DCF) or dispersion shifted fiber (DSF) [4].

The current fourth generation of fiber-optic systems makes use of optical amplification for increasing the repeater spacing and of wavelength-division multiplexing (WDM) for increasing the data rate. The development of erbium-doped fiber amplifiers (EDFAs) has revolutionized the design of fiber-optic links by replacing the electronic repeaters. These fourth generation WDM systems can operate at bit rates of 40 Gb/s per wavelength over distances of a few thousand kilometers. However, in spite of using dispersion compensation schemes, the residual dispersion accumulates over such long distances resulting in the reduction of achievable transmission distances. To combat this problem, the use of solitons is proposed for the next (fifth) generation fiber optic systems. Solitons are optical pulses that preserve their shape during propagation in a fiber by counteracting the effect of dispersion

through the fiber non-linearity [4]. However, as the bit rate approaches 10 Gb/s and beyond, both the fourth and fifth generation systems face a different type of dispersion impairment called polarization-mode dispersion (PMD) that imposes detrimental effects if not handled properly.

PMD is caused by optical birefringence and is a fundamental property of single-mode optical fiber and components in which signal energy at a wavelength is resolved into two orthogonal polarization modes of slightly different propagation velocity. PMD is a major impairment for high bit rate systems resulting in pulse broadening and distortion and leading to system performance degradation. Unlike the chromatic dispersion, PMD varies stochastically in time making it particularly difficult to assess, counter or cope with [3]. Therefore, a thorough understanding of the statistical characteristics of PMD is essential for system engineers to ensure reliable communication at high bit rates over fiber-optic links.

This thesis is an attempt to characterize PMD on buried fibers made available by Sprint. While PMD is a vector quantity, with a magnitude (DGD) and a direction (PSP), this thesis deliberately focuses exclusively on DGD, as this is a readily measured parameter on installed optical networks. The statistical distribution and behavior of PSPs has been extensively studied and reported elsewhere. Long-term DGD measurements were made on the fiber links and the data captured is analyzed to understand the temporal, spectral, distributional and system outage properties of PMD. Chapter 2 of this report discusses the different aspects of PMD including the causes of PMD, PSP model, and emulation and mitigation techniques. Different time-

domain and frequency-domain methods used to measure PMD are described in Chapter 3. Chapter 4 gives a detailed description of the measurement setup used and the procedure followed to perform long term, automated PMD measurements on buried fibers. The results obtained and the detailed analysis of the captured data is presented in Chapter 5. Finally, a few conclusions regarding the work done and recommendations for future work are made.



## **2. POLARIZATION-MODE DISPERSION CONCEPTS**

### **2.1 Polarization effects in lightwave systems**

Polarization implies a definite direction and phase relationship between electric fields of a propagating wave. Polarization effects have historically played a minor role in the development of lightwave systems because commercial optical receivers are insensitive to polarization as they detect optical power rather than the optical field. But because of the recent developments like the optical amplifier, which has dramatically increased the optical path lengths achievable, and new transmitter and receiver technologies, which have pushed the capacity of optical fiber to its limit, small effects such as polarization-mode dispersion (PMD) and polarization-dependent loss (PDL) can accumulate in a span to the point where they become an important consideration for lightwave system developers [2]. PMD is discussed in detail in the remaining sections of this chapter.

PDL is a measure of the peak-to-peak difference in transmission of an optical component or system with respect to all possible states of polarization. It is the ratio of the maximum and the minimum transmission of an optical device with respect to all polarization states, defined as  $10\log(T_{\max} / T_{\min})$  (dB) where T is the optical transmittance or power taken over the entire polarization-state space. Fiber bending, angled optical interfaces and oblique reflection are some of the causes of PDL. The impact of PDL on network performance is increased signal distortion, and consequently, higher bit-error-rate. PDL is usually characterized as a localized

component effect in contrast to the distributed nature of PMD. However, it interacts with PMD in nonlinear ways to dramatically increase system bit-error-rate [1].

## **2.2 What is PMD?**

PMD is a property of a single-mode fiber or an optical component in which signal energy at a given wavelength is resolved into two orthogonal polarization modes with different propagation velocities [3]. The resulting difference in propagation time between polarization modes, known as differential group delay (DGD), leads to pulse broadening which causes a number of serious capacity impairments.

## **2.3 Causes of PMD**

The underlying cause of PMD in a fiber or an optical component is a phenomenon called *birefringence*. It is defined as the difference in refractive indices of a pair of orthogonal polarization states. The description of PMD in a fiber is further complicated by the fact that polarization modes can couple to each other, a phenomenon known as *mode coupling* [6].

### **2.3.1 Birefringence**

Any optical wave of arbitrary polarization can be represented as the linear superposition of two orthogonally polarized  $HE_{11}$  modes in a waveguide. In the ideal case, where the waveguide has cylindrical symmetry, these two modes are indistinguishable or degenerate in terms of their propagation properties. The loss of degeneracy of polarization modes can be termed as birefringence. Birefringence can be attributed to both intrinsic and extrinsic factors. Intrinsic factors like non-circular

core or built-in asymmetric stress in a fiber result from processes during the fiber's manufacture. A noncircular core gives rise to *geometric* birefringence, whereas a nonsymmetrical stress field creates *stress* birefringence. These factors cause the index of one polarized mode to differ slightly from other, resulting in different propagation velocities for the two modes. A light pulse traveling along the polarization mode with smaller refractive index travels with higher speed and so that polarization mode is termed as fast-axis and the other as slow-axis. PMD is more predominant in older fibers than newer fibers because modern process controls minimize all the stress and asymmetry in the fibers during manufacture.

Extrinsic factors result from mechanical stress. Stress may occur due to twisting and bending of the fiber, or from environmental effects like temperature changes. Twisting and bending can occur during cabling process and so PMD is a strong function of cable design [24]. Fiber twist creates circular birefringence whereas all the other perturbations mentioned above create linear birefringence in which the electric field vectors of the two linearly polarized waveguide modes are aligned with the symmetry axes of the fiber. Birefringence resulting from the above mentioned intrinsic and extrinsic factors may be of opposite sign and may add or subtract from each other. PMD in optical components may be caused by the birefringence of its sub-components, which may include segments of asymmetric fiber. Certain components exhibit PMD because of the parallel-path mechanism in which a signal propagates along parallel paths of slightly different optical length, where the splitting is a function of polarization, resulting in differential group delay.

### 2.3.2 Mode coupling

The birefringence of a single-mode fiber varies randomly along its length owing to the variation in the drawing and cabling process [3]. As mentioned earlier, modeling of birefringence with the length of fiber gets complicated because of mode coupling. To understand the concept of mode coupling, consider a light pulse that is plane polarized in the fast-axis injected into the fiber. As the pulse propagates across the fiber, some of the energy will couple into the orthogonal slow-axis polarization state, this in turn will also couple back into the original state until eventually, for a sufficiently long distance, both states are equally populated, as illustrated in Fig. 2.1.

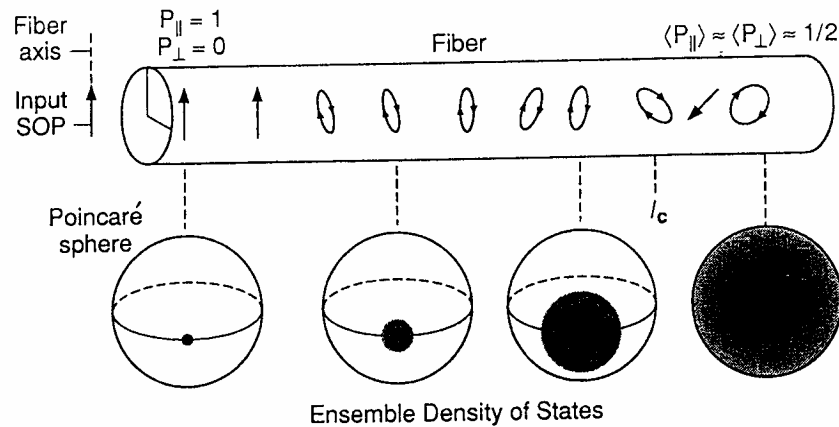


Fig. 2.1. Decorrelation of polarization in long fibers [2].

The length of the fiber at which the ensemble average power in one orthogonal polarization mode is within  $1/e^2$  of the power in the starting mode is called the *coupling length* or *correlation length*  $L_c$ . It is a statistical parameter that varies with wavelength, position along the length of the fiber and temperature. Typical values of coupling length range from tens of meters to almost a kilometer [6].

## 2.4 PMD in short fibers ( $L \ll L_c$ )

If the length of the fiber ( $L$ ) is much less than the correlation length ( $L_c$ ), then it is termed as ‘short’ fiber. In a short fiber, the birefringence can be considered uniform and the mode coupling is absent. Birefringence in a short fiber can be expressed as the difference between the propagation constants of the slow and fast modes as

$$\Delta\beta = \frac{\omega \cdot n_s}{c} - \frac{\omega \cdot n_f}{c} = \frac{\omega \cdot \Delta n}{c} \quad (2.1)$$

where  $\omega$  is the angular optical frequency,  $c$  is the speed of light, and  $\Delta n = n_s - n_f$  is the effective differential refractive index between the slow and fast modes [2].

In short fibers, for a given input polarization state the state of polarization evolves in a cyclic fashion as the light propagates down the fiber, i.e., from linear to elliptical to circular and back through elliptical to a linear state as shown in Fig. 2.2. In the frequency-domain, for a fixed-input polarization state, as the light frequency is varied, the output polarization traces out a circle on the surface of a Poincare sphere.

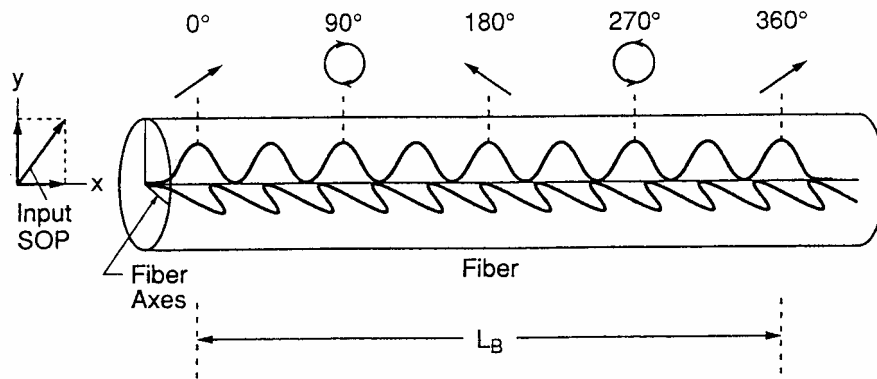


Fig. 2.2. Spatial evolution of polarization caused by uniform birefringence [2].

*Beat length*  $L_b$ , is defined as the propagation distance for which a  $2\pi$  phase difference accumulates between the two modes or, equivalently, the polarization rotates through a full cycle and is given by  $L_b = \lambda/\Delta n$ , where  $\lambda$  is optical wavelength and  $\Delta n$  is the differential refractive index. A typical value of beat length is  $\sim 10$  m for standard telecommunications-type fibers [2].

Due to the absence of mode coupling in the short fibers, DGD ( $\Delta\tau$ ) accumulates linearly with fiber length.  $\Delta\tau$  can be found from the frequency derivative of the difference in propagation constants as

$$\frac{\Delta\tau}{L} = \frac{d}{d\omega} \left( \frac{\Delta n \cdot \omega}{c} \right) = \left( \frac{\Delta n}{c} \right) + \left( \frac{\omega}{c} \right) \frac{d}{d\omega} (\Delta n) \quad (2.2)$$

The effect of PMD in the time-domain in a short fiber is illustrated in Fig. 2.3, where a pulse launched with equal power on the two birefringent axes results in two pulses at the output separated by the DGD.

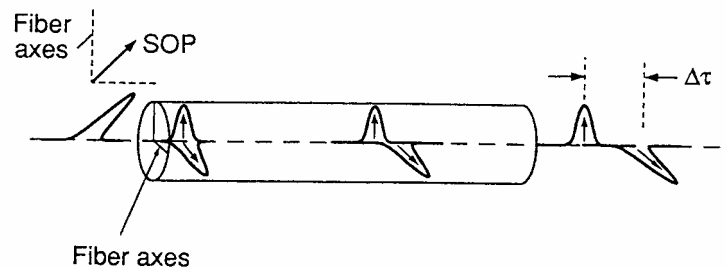


Fig. 2.3. Time-domain effect of PMD in a short fiber [2].

## 2.5 PMD in long fibers ( $L \gg L_c$ )

Fibers of length ( $L$ ) much greater than the correlation length ( $L_c$ ) are termed 'long' fibers. In long fibers birefringence is no longer uniform owing to the randomness in perturbations and presence of polarization-mode coupling discussed in

Sec. 2.3.2. Long fibers can be modeled as a concatenation of birefringent sections whose birefringence axes and magnitudes change randomly as shown in Fig. 2.4.

Birefringence in each section of a long fiber may either add to or subtract from the total birefringence and so DGD does not accumulate linearly with fiber length, unlike the short fiber case. Instead, DGD accumulates as a three-dimensional random walk, and on average increases with the square root of distance. Since the

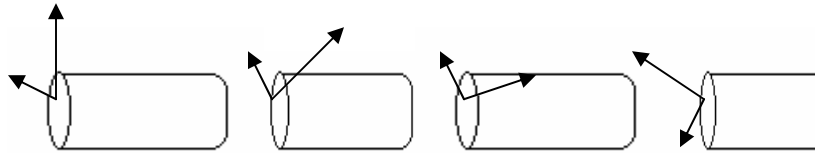


Fig. 2.4. Model for a long fiber as a concatenation of birefringent sections with birefringence axes and magnitudes that change randomly along the fiber length [1]. mode coupling, and hence DGD, varies with the fiber's environment, a statistical approach should be adopted for analysis of PMD in long fibers. Transmission systems are generally in the long-length regime and so fiber PMD is often specified using a PMD coefficient having units of  $\text{ps}/(\text{km})^{1/2}$ . Fibers manufactured today have mean PMD coefficients smaller than  $0.1 \text{ ps}/(\text{km})^{1/2}$  whereas “legacy” fibers installed in the 1980s may exhibit PMD coefficients greater than  $0.8 \text{ ps}/(\text{km})^{1/2}$  [2]. In the frequency-domain, as the wavelength is varied, the output state of polarization (SOP) of a long fiber will trace out an irregular path on the Poincare sphere. Any portion of this path, over a small wavelength interval, can be represented as an arc of a circle, the center of which when projected normal to the plane of the circle to the surfaces of the sphere,

locates two diametrically opposed, orthogonal states of polarization known as principal states of polarization (PSPs) [3].

## **2.6 Principal States model**

The Principal States model was developed by Poole and Wagner in 1986. This model provides both a time domain and a frequency domain characterization of PMD. It assumes that the coherence time of the source is greater than the PMD-induced time shift and also that PDL is negligible.

According to this model, in the frequency-domain, for a length of fiber, there exists for every frequency a special pair of input polarization states, called the input Principal States of Polarization (PSPs). A PSP is defined as that input polarization for which the output state of polarization is independent of frequency to first order. This means that an optical pulse that is aligned with a PSP at the input of a fiber will emerge at the output with its spectral components all having the same state of polarization. The PSPs are orthogonal in the absence of PDL [3]. In short fibers the principal states simply correspond to the polarization modes of the fiber whereas in long fibers these are determined by the cumulative effects of the birefringence over the entire span. An important characteristic of these PSPs is that they locate the axis of the sphere about which the output state of polarization rotates as wavelength is changed over a narrow wavelength interval. Each pair of input PSPs has a corresponding pair of orthogonal PSPs at the fiber output. The input and output PSPs are related by the fiber's transmission matrix, just as any input polarization is related to a polarization at the fiber output [2]. In the case of long single-mode fiber paths,



where mode coupling is significant, the principal states of polarization move randomly about the sphere as a function of wavelength and can be considered fixed only over narrow wavelength intervals. But in the case of optical components where mode coupling is absent, the principal states of polarization are fixed; as wavelength changes, the output state of polarization orbits regularly around the principal states axis on the sphere [3].

The time-domain description of Principal States model states that light pulse launched in any PSP results in an output light pulse that is undistorted to first-order. PSPs have group delays, which are the maximum, and minimum mean time delays and the difference between these two delays is called differential group delay (DGD) [7]. According to this model, complete description of the PMD of a particular fiber at a given time requires specification of both the differential group delay and the principal states of polarization as functions of wavelength.

## **2.7 PMD vector**

The polarization-mode dispersion vector  $\Omega$  provides an intuitive representation of PMD. The PMD-vector  $\Omega(z, t, \omega)$  is a three-component polarization vector in Stokes space that varies randomly with fiber length  $z$ , time  $t$  and the optical frequency  $\omega$  [8]. The PMD-vector originates at the center of the Poincare sphere and points toward the PSP about which the output SOPs rotate in a counter clock wise direction with increasing optical frequency. The length or magnitude of the PMD-vector represents the DGD.

Any SOP can be expressed as a three-dimensional vector  $\mathbf{s}$  composed of normalized Stokes parameters that can be located on the Poincare sphere. For a given constant input polarization to the fiber, PMD will manifest as a change in output polarization Stokes vector with frequency according to the relation [3]:

$$d\mathbf{s}/d\omega = \boldsymbol{\Omega} \times \mathbf{s} \quad (2.3)$$

A measure of DGD is the rate of rotation of the output SOP about the principal states axis regardless of degree of mode coupling. Therefore DGD can be expressed as [3]

$$\Delta\tau = \Delta\theta / \Delta\omega \quad (2.4)$$

where  $\Delta\tau$  is the DGD in seconds,  $\Delta\theta$  is the amount of rotation about the principal states axis in radians and  $\Delta\omega$  is the optical frequency change that produced the arc, in radians/seconds. For highly mode-coupled devices the above relation must be evaluated over wavelength increments small enough that the PSPs remain fixed.

The above representation of the PMD-vector has several advantages in that it is the underlying model for most of statistical treatments of PMD and so it forms the basis for most of the known statistical properties (discussed in the next section) of the PMD-vector. Also the above representation provides an elegant concatenation rule for the PMD-vector of a sequence of birefringent elements [8]. The drawback is that it does not incorporate the effects of polarization-dependent losses (PDL) in a straightforward way.

## 2.8 Second-order PMD

PMD variation with wavelength can be represented by a vector in Stokes space as  $\boldsymbol{\Omega}(\omega) = \Delta\tau\mathbf{q}$ , where  $\omega$  is angular frequency of the carrier,  $\Delta\tau$  is the DGD and

$\mathbf{q}$  is a unit Stokes vector pointing in the direction of fast PSP. Second-order PMD is described by the frequency derivative of  $\mathbf{\Omega}$  as

$$\mathbf{\Omega}_\omega = \Delta\tau_\omega \mathbf{q} + \Delta\tau \mathbf{q}_\omega, \quad (2.5)$$

where the subscript  $\omega$  indicates differentiation with respect to  $\omega$ . The first component in the above equation,  $\Delta\tau_\omega \mathbf{q}$ , is parallel to  $\mathbf{\Omega}$ , while the second component,  $\Delta\tau \mathbf{q}_\omega$ , is orthogonal to  $\mathbf{\Omega}$  since  $\mathbf{q} \cdot \mathbf{q}_\omega = 0$ . The term  $\Delta\tau \mathbf{q}_\omega$  describes PSP depolarization, a rotation of the PSPs with frequency, while  $\Delta\tau_\omega$  causes polarization-dependent chromatic dispersion (PCD) resulting in pulse compression or broadening. It can be viewed as polarization-dependent change in chromatic dispersion DL, of the fiber, described by an effective dispersion, [9]

$$DL_{eff} = DL \pm \tau_\lambda \quad (2.6)$$

where

$$\tau_\lambda = -(\pi c/\lambda^2) \Delta\tau_\omega = \frac{1}{2} \frac{d\Delta\tau}{d\lambda} \quad (2.7)$$

is the PCD and the plus and minus signs correspond to alignment with the two PSPs.

## 2.9 Statistical nature of PMD

As discussed in the earlier sections, PMD in a fiber varies randomly with wavelength and also with environmental conditions. This is because of the randomness of mode coupling and core deformation due to external stress in the fiber. The PMD-vector can be decomposed into three orthogonal vectors along the axes of the Poincare sphere, each of which is an independent random variable with zero mean and can be described statistically by the Gaussian distribution. The magnitude of the PMD-vector is the DGD given by the square root of the sum of the squares of the orthogonal

components. The impact of PMD on telecommunication systems can be predicted from the distribution of DGD ( $\Delta\tau$ ). It has been shown that in the random mode-coupled or long fiber regime,  $\Delta\tau$  follows a Maxwellian distribution, given by (2.8) and shown in Fig. 2.5. This means that the distribution of values of  $\Delta\tau$  measured over a wide wavelength range or over time at a fixed wavelength, if a changing environment acts upon the path, will be Maxwellian [3]. As a result of this variability, the PMD of a path is expressed statistically as mean DGD  $\langle\Delta\tau\rangle = \sigma\sqrt{8/\pi}$  or rms DGD  $\langle\Delta\tau^2\rangle^{1/2} = \sigma\sqrt{3}$

$$p(\Delta\tau) = \sqrt{\frac{2}{\pi}} \frac{\Delta\tau^2}{\sigma^3} e^{\left(\frac{-\Delta\tau^2}{2\sigma^2}\right)} \quad (2.8)$$

for  $0 < \Delta\tau < +\infty$  where  $\Delta\tau$  is DGD and  $\sigma^2$  is the variance.

The probability density function of  $\Delta\tau_\omega$  has been derived [9] as

$$p(\Delta\tau_\omega) = \frac{2}{\langle\Delta\tau\rangle^2} \operatorname{sech}^2\left(\frac{4 \cdot \Delta\tau_\omega}{\langle\Delta\tau\rangle^2}\right), \text{ where } \langle\Delta\tau\rangle \text{ is the mean DGD} \quad (2.9)$$

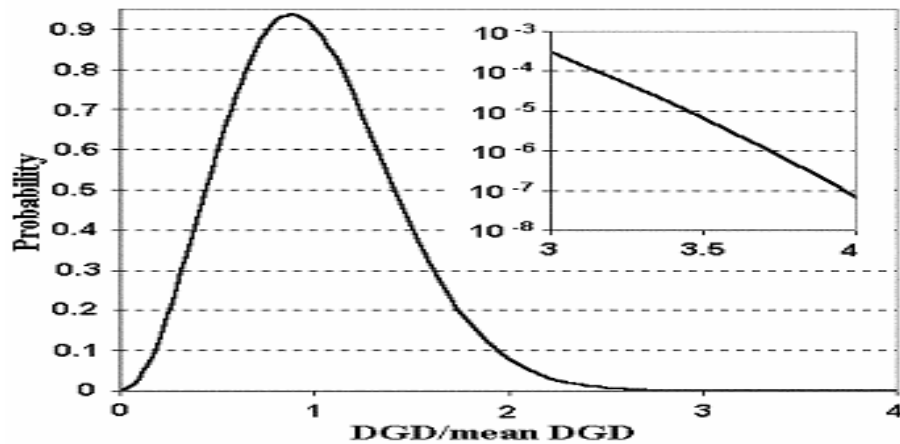


Fig. 2.5. Normalized Maxwellian distribution, with magnified tail portion [32].

## **2.10 PMD in the presence of PDL**

The concepts explained in the preceding sections of this chapter and the remaining parts of this report were based on the assumption that the PDL in the fibers and components is negligible. In the presence of PDL, the long-fiber model described in Sec. 2.5, where it is assumed to be a concatenation of small birefringent sections, and the PSP model become invalid. It has been shown that, in general, the two PSPs are no longer orthogonal in the presence of PDL [11]. Also with PDL, the two PSPs are not necessarily the fastest and slowest states and the maximum pulse spreading can be even larger than the DGD [10]. A comprehensive model for PMD in the presence of PDL is yet to be investigated.

## **2.11 Emulation of PMD**

An important issue for designers of high-performance systems is to measure performance degradation due to high PMD fiber spans. Present-day fibers have very low PMD values and so high-PMD fibers are not commercially available. Even if high-PMD fiber were available, it would be difficult to use it to rapidly explore a large number of different fiber ensembles, which are required to determine the distribution of penalties due to PMD [12]. Thus, to test optical systems that may be affected by PMD and also to characterize PMD compensators, it is critical to be able to accurately emulate first- and higher-order PMD and quickly cycle through a large number of different fiber PMD states [13].

Any PMD emulator that emulates transmission through communication fiber should have two key properties: [12][13][16]

1. The DGD should be Maxwellian-distributed over an ensemble of fiber realizations at any fixed optical frequency.
2. When averaged over an ensemble of fiber realizations, the frequency autocorrelation function of the PMD emulator should tend towards zero as the frequency separation increases.

Different models for PMD emulators have been proposed in recent years. The most easily implemented emulator of first-order PMD is a length of polarization maintaining (PM) fiber [1]. The three popular emulator models are emulators with fixed orientations, emulators with rotatable sections and emulators with variable DGD elements.

#### **2.11.1. Emulators with fixed orientations**

In this model, a PMD emulator is realized by connecting several short spans of PM fiber with some fixed angular offset between each section. This approach does not guarantee that the emulator has the PMD characteristics of a real fiber [15]. However, the emulator can be optimized to obtain a DGD distribution in good agreement with a Maxwellian distribution over an ensemble of frequencies. But the practical use of such emulators is limited due to the wide frequency range that one needs to sweep in order to obtain good statistics. One must assume that the behavior of the fiber remains the same at all frequencies even when studying only a single channel, which is not a realistic assumption. Also, it is not possible to study WDM systems using an emulator with fixed sections. In WDM systems, the frequency dependence of the dispersion, the gain and the loss, and system components greatly

affect the system performance. Thus, even if it were possible to vary the frequency of the laser sources while keeping their spacing fixed, it is still not possible to reproduce the correct system behavior of an ensemble of different fiber realizations [16]. Thus, in practice the use of PMD emulators with fixed orientations is very limited.

### 2.11.2 Emulators with rotatable sections

Khosravani et al. [12] describes another model to emulate PMD using rotatable connectors between sections of PM fibers that generate an ensemble of high PMD fiber realizations by randomly rotating the connectors. The accuracy of the statistical properties of PMD using this model depends on the number of sections used, the more the number of sections used, the better the accuracy.

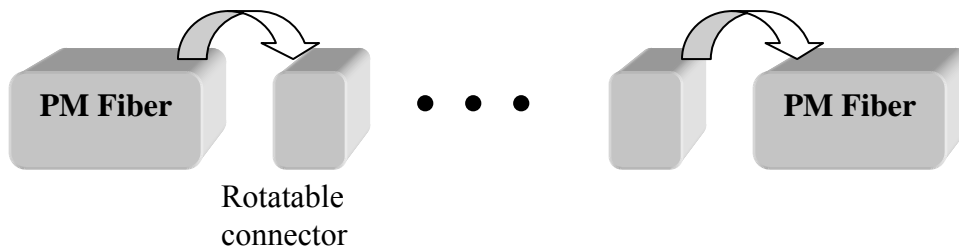


Fig. 2.6. PMD emulator with sections of PM fibers of unequal length and with rotatable connectors [12].

Fig. 2.6 shows the experimental setup of the PMD emulator with sections of PM fiber connected by rotatable-key connectors. Rotatable connectors allow the polarization axes of any two adjacent fibers to be rotated with respect to each other. The length of the PM fibers can be chosen using a Gaussian random variable. The total loss of the emulator varies with the angles between the PM fiber sections but it can be made more uniform by careful consideration of the connectors themselves. A large collection of DGD values can be obtained by emulating different fiber realizations either by changing the wavelength of the optical carrier after fixing the

angles between the PM fiber sections or by rotating the angles between each section of PM fiber. But in WDM systems, it is not feasible to change the optical frequency over a wide range.

Khosravani et al. [12] demonstrated that using 15 sections of PM fiber, a Maxwellian DGD distribution can be obtained by randomly rotating the angles between the fibers over a number of times at a fixed wavelength. Also, the second-order PMD distribution is close to the ideal second-order PMD distribution (has the form of energy density of a first-order optical soliton [9]). A PMD emulator with rotatable sections also satisfies another condition required in WDM systems that the PMD vectors of different channels should be uncorrelated. Khosravani et al. [12] shows that negligible correlation between PMD vectors can be obtained by properly choosing the channel spacing.

### **2.11.3 Emulators with variable DGD elements**

The PMD emulator models described in earlier sections require a large number of sections to obtain the desired statistical properties. In addition, the configuration of these emulators should be changed to emulate various statistics. Furthermore, the probability distribution generated by these emulators typically had much smaller value than the exact Maxwellian distribution thereby underestimating the system outage probabilities of the rare DGD events. Lee et al. [14] describes a model for PMD emulator that overcomes all the above-mentioned drawbacks of the other emulator models.



The schematic diagram of the proposed emulator is shown in Fig. 2.7. It uses variable-DGD elements, polarization controllers and a microprocessor. Multiple variable-DGD elements are concatenated with polarization controllers between them.

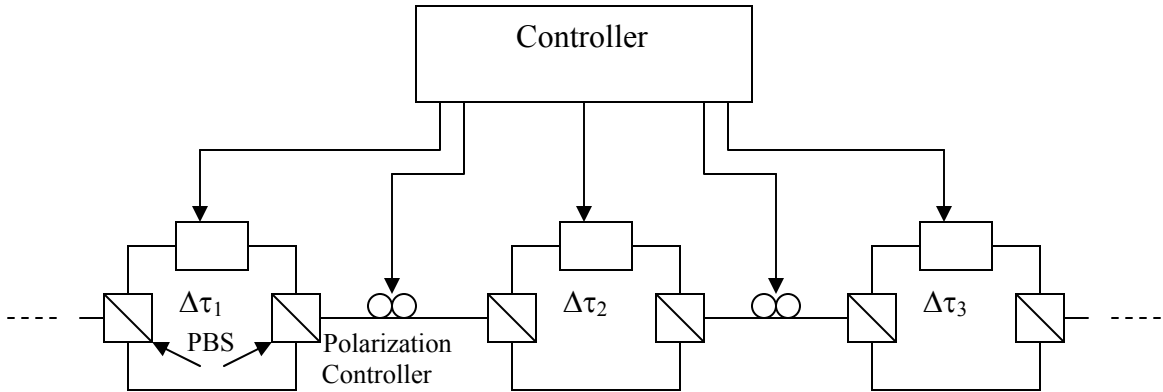


Fig. 2.7. Schematic diagram of the PMD emulator with variable DGD elements [14].

The polarization controllers can produce arbitrary rotation on the Poincare sphere after each DGD element. Thus, by controlling the DGD of each element to have Maxwellian distribution and the polarization controllers to scatter each PMD vector uniformly on the Poincare sphere, it is possible to emulate PMD with exact Maxwellian distribution, regardless of the number of DGD sections. Lee et al. [14] demonstrates that it is possible to generate PMD with real fiber's characteristics at a fixed wavelength by using only three sections of DGD elements. However, this is not true for WDM systems where the PMD characteristics of each channel should be statistically independent. Lee et al. [14] shows that to emulate the statistically independent PMD in each WDM channel, it is required to use relatively large number of variable-DGD elements.

The PMD emulator model described in this section has several advantages over other emulator models. The statistical characteristics obtained using this model are exact unlike the other models. This model allows the generation of various statistics without changing its physical configuration. Also, using this model it is possible to generate the first- and second-order PMD separately. The first-order PMD can be generated without higher-order PMD by controlling only one DGD element. The frequency-dependent PSP can be included by using one additional DGD element. To add the frequency-dependent DGD, more than two DGD elements should be controlled [14].

## **2.12 Numerical simulation of PMD**

Numerical simulation, like emulation, is another way of testing system robustness to PMD-induced outage. Simulation can be used to explore the behavior of system performance in the presence of PMD, to understand the behavior of PMD compensators and to provide insight into the statistics of PMD [1]. The simulator model is similar to that of an emulator model (i.e., a series of birefringent elements sandwiched between polarization adjustments). Simulations usually use more sections than emulators and can use more sophisticated polarization adjustment than emulators. The flexibility inherent in numerical calculation allows randomness to be achieved more easily than in emulators.

Dal Forno et al. [17] describes a model for numerical simulation using coarse-step method. It considers a SMF as a concatenation of unequal length segments with a given mean birefringence and random coupling angles. The Jones matrix  $T(\omega)$  that

describes a concatenation of unequal sections of birefringent fiber can be expressed as [17]

$$T(\omega) = \prod_{n=1}^N B_n(\omega) R(\alpha_n) \quad (2.10)$$

$$= \prod_{n=1}^N \begin{bmatrix} e^{j\left(\sqrt{\frac{3\pi}{8}} b \omega \sqrt{h_n} / 2 + \phi_n\right)} & 0 \\ 0 & e^{-j\left(\sqrt{\frac{3\pi}{8}} b \omega \sqrt{h_n} / 2 + \phi_n\right)} \end{bmatrix} \begin{bmatrix} \cos\alpha_n & \sin\alpha_n \\ -\sin\alpha_n & \cos\alpha_n \end{bmatrix} \quad (2.11)$$

where N is number of segments,  $B_n(\omega)$  represents the birefringence matrix of  $n^{\text{th}}$  segment with  $h_n$  length,  $R(\alpha_n)$  is the matrix of a rotator that represent the random coupling angle between the segment axes, b is the PMD coefficient of the fiber in ps/ $\sqrt{\text{km}}$  and  $\omega$  is the optical frequency.

For a given value of total PMD and fiber length L, the size of the each segment is randomly generated from a Gaussian distribution around the mean length L/N with standard deviation varying from 0-30% of the mean length. The phase  $\phi_n$  in (2.11) accounts for the small temperature fluctuations along the fiber and it is a stochastic variable with a uniform distribution between 0 and  $2\pi$ .  $\alpha_n$  is the random coupling angle between the segment axes and is a random variable with uniform distribution between 0 and  $\pi$ . The DGD,  $\Delta\tau$ , for a single wavelength can be calculated by calculating the Eigen values of the matrix  $T_\omega(\omega) * T^{-1}(\omega)$ , where  $T_\omega(\omega)$  is the frequency derivative of the transmission matrix.  $T_\omega$  can be approximated as

$[T(\omega+\Delta\omega)-T(\omega)]/\Delta\omega$  for a small frequency step,  $\Delta\omega$ . The DGD is determined using the expression [3],

$$\Delta\tau = \left| \frac{\tan^{-1}\left(\frac{\rho_1}{\rho_2}\right)}{\Delta\omega} \right| \quad (2.12)$$

where  $\rho_1$  and  $\rho_2$  are the Eigen values described above.

### 2.13 System impairments due to PMD

Digital light wave systems rely on undistorted transmission of optical pulses through long lengths of fiber. Dispersive effects such as PMD cause pulse spreading and distortion and thus can lead to system penalties.

The differential group delay between the two pulses propagating in the fiber when the input polarization of the signal does not match the PSP of the fiber induces inter-symbol interference (ISI) impairment in a single digital transmission channel [1]. This impairment can be expressed as a power penalty  $\varepsilon$  of the form

$$\varepsilon(dB) = \left(\frac{A}{T^2}\right)\Delta\tau^2\gamma(1-\gamma) = A\left(\frac{\Delta\tau}{2T}\right)^2 \sin^2\theta \quad (2.13)$$

where the penalty, expressed in dB, is assumed to be small. In (2.13)  $T$  is the bit interval,  $\gamma$  ( $0 \leq \gamma \leq 1$ ) is the power-splitting ratio and  $\theta$  is the angle between the input polarization and the input PSP. 'A' is a dimensionless parameter that depends on pulse shape, modulation format and specific receiver characteristics and is determined

by simulation and experiment. The DGD value  $\Delta\tau$  in the above expression is the instantaneous DGD and is assumed to be constant during the penalty measurement.

In real systems, the power penalty caused by PMD will vary randomly owing to the random variation of the parameters  $\gamma$  and  $\Delta\tau$ . As per the industry standards, penalties in excess of 1 dB are unacceptable [2]. Assuming a Maxwellian distribution for  $\Delta\tau$  and a uniform distribution of  $\gamma$  and statistical independence of  $\Delta\tau$  and  $\gamma$ , it can be shown that  $\varepsilon$  has an exponential probability density function [2],

$$p(\varepsilon) = \eta \exp(-\eta\varepsilon) \quad (2.14)$$

where  $\eta = 16 T^2 / (A\pi\langle\Delta\tau\rangle^2)$  and  $\langle\Delta\tau\rangle$  denotes the average differential delay. The probability of observing a penalty greater than 1 dB is obtained by integrating the expression for  $p(\varepsilon)$  from 1 to infinity and is given by [2]

$$\Pr(\varepsilon \geq 1) = \int_1^{\infty} \eta e^{-\eta\varepsilon} d\varepsilon = e^{-\eta} \quad (2.15)$$

Using (2.15), the ratio of  $\langle\Delta\tau\rangle/T$  for a given value of  $\Pr(\varepsilon \geq 1)$  can be expressed in terms of the known parameters which establishes a PMD limit.

System impairments due to second- and higher-order PMD occur for large signal bandwidths, particularly when these PMD components combine with chromatic fiber dispersion or signal chirp. The simplest second-order impairment mechanism is polarization-dependent chromatic dispersion (PCD) described in Sec. 2.8. But PCD is a relatively minor component of the second-order PMD vector compared to the depolarization component that refers to the rotation of the PSPs with frequency. Pulse distortions caused by depolarization include overshoots and

generation of satellite pulses [1]. PSP depolarization can also have a detrimental effect on first-order PMD compensators.

PMD impairments due to inter-channel effects occur in polarization-multiplexed transmission systems. In polarization interleaved WDM systems, adjacent wavelength channels are launched with orthogonal polarizations in order to suppress nonlinear impairments such as cross-phase modulation (XPM) and four-wave mixing (FWM). PMD destroys the orthogonality of these polarizations resulting in leakage of signal between the neighboring channels. This leads to coherent cross talk at the channel receivers resulting in system impairments [1].

## **2.14 PMD tolerance of different modulation formats**

Different modulation formats have different sensitivities to the pulse distortion caused by PMD. The formats usually considered are non-return-to-zero (NRZ), return-to-zero (RZ), pre-chirped RZ (CRZ), conventional solitons and dispersion-managed solitons (DMS).

Experiments on systems with an optically pre-amplified receiver [18] have shown RZ format to be more tolerant to first-order PMD than NRZ. As the PMD is increased, power in isolated zeros rises more quickly for NRZ signals than for RZ signals. This is because, the pulse energy for RZ signals is more confined to the center of each bit slot even after transmission. The increased power in isolated zeros leads to a greater penalty for NRZ format when using an optically pre-amplified receiver [1]. Also, in general, pulses with shorter duty cycles like in RZ, CRZ, soliton and DMS formats, perform better because they have a wider margin which allows

them to retain their pulse power during a bit time [19]. Khosravani et al. [19] also shows that CRZ can be more tolerant to PMD than RZ and NRZ. For CRZ pulses that undergo an initial compression in the dispersive fiber, the average dispersion is adjusted to give maximum compression at the end of the transmission leading to a better performance.

Conventional solitons are more robust to PMD than NRZ. Xie et al. [20] has shown that the amount of group-velocity-dispersion [GVD] and soliton energy has significant effects on the soliton robustness to PMD. By optimizing both GVD and soliton energy, the soliton pulse width can be maintained even at high PMD. Xie et al. [21] has shown that DM solitons are more robust to PMD than conventional solitons and that the robustness of DM solitons can be enhanced by increasing both the map strength and the average GVD. In conclusion, RZ, CRZ, solitons and DM solitons are more robust to PMD than NRZ, but CRZ outperforms other formats at higher PMD [19].

## **2.15 PMD compensation techniques**

Because of the stochastic nature of PMD, reducing the impact of PMD does not necessarily imply the complete cancellation of the effect, but the reduction of the probability of outage due to PMD. Several PMD compensation techniques have been proposed in the past few years that can be separated into two main categories: [25]

- Electrical PMD compensation
- Optical PMD compensation

This section presents a brief discussion of these techniques followed by a block diagram description of the PMD compensator being developed at University of Kansas.

### **2.15.1 Electrical PMD compensation**

Electrical compensation of PMD involves equalizing the electrical signal before the receiver but after the photodiode. This equalization can be implemented in many ways. One way is to use a linear transversal filter (TF) that is realized using a tapped delay line model. The TF divides the signal, delays the copies by constant delay stages and superimposes the differentially delayed signals at the output port. The tap weights are adjusted to maximize the receive signal quality. Another way of equalization is to use non-linear decision feedback equalizer (DFE). The basic principle of DFE is that once a decision is made on a particular bit as a one or zero, the inter-symbol interference that this bit induces on future bits can be subtracted out before deciding on future bits. This method requires fast signal processing for coupling the decided bit back in time [1]. One other way of equalization is based on phase diversity detection where two photo diodes detect the signals on the PSPs of the fiber and infer a DGD value and a controlled delay is generated on one arm before electrical recombination [25].

Electrical compensation schemes, in general, are robust and will improve the signal against all kinds of transmission impairments. On the other hand, they do not perform as good as optical PMD compensators and also they require high-speed electronics for better performance [26].



### 2.15.2 Optical PMD compensation

The goal of optical PMD compensation is to reduce the total PMD impairment caused by the transmission fiber and the compensator. The block diagram of a general optical PMD compensation scheme is shown in Fig. 2.8. It has an adaptive counter element, a feedback signal and a control algorithm.

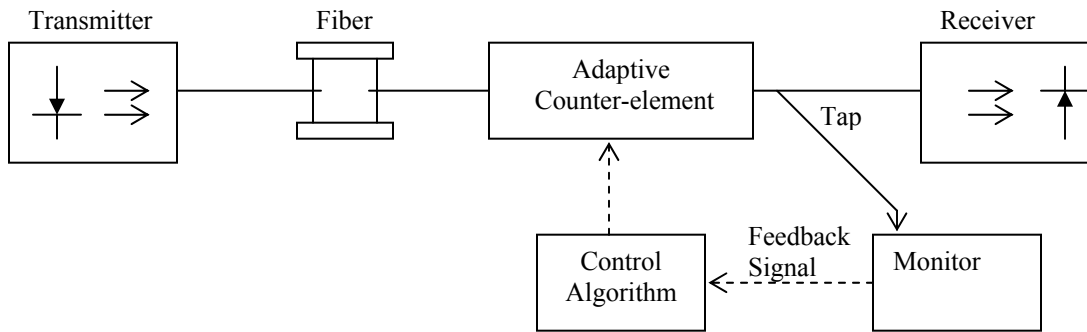


Fig. 2.8. General scheme for optical PMD compensation [1].

The adaptive counter element is the core of any PMD compensator. It must be able to counteract PMD impairments and be tunable. High birefringent elements like polarization-maintaining (PM) fibers, LiNbO<sub>3</sub> delays, and Bragg gratings etc. separated by polarization controllers are used as adaptive counter elements. Different schemes vary in the number of birefringent elements used, their tunability and the technology used for polarization control. The feedback signal is required to provide the PMD information to the controlling algorithm of the compensator. Important characteristics of a feedback signal are (i) its sensitivity to PMD, (ii) its correlation with BER and (iii) its response time. The common feedback signals used in various schemes are the degree of polarization (DOP), RF spectral width, total RF power and

eye opening. Of all these, DOP feedback signal has the advantages of being bit rate independent and having quick response time. Finally, the controlling algorithm controls the adaptive counter element based on the feedback signal. It is generally implemented as some kind of gradient search method. The parameters of the algorithm are chosen carefully to avoid the sub-optimum operating points, which can have disastrous impact on the transmission quality [27].

Sunnerud et al. [28] and Karlsson [26] present a unique way of classifying the optical compensators based on the number of degrees of freedom (DOF) in the compensator, which is the number of elements or parameters in the compensating element that are controlled by the control algorithm. The DOF is a good estimate of the complexity and hence the cost of the compensator. Fig. 2.9 shows six different PMD compensation methods and their corresponding DOF. The PSP method shown in Fig. 2.9a is a pre-transmission compensation technique in which a polarization controller (PC) is used to align the SOP with one of the input PSPs of the fiber link. It is a first order compensator with two DOF. A first-order post-compensator with a PC and a fixed time delay (2 DOF) is shown in Fig. 2.9b. This is sometimes referred to as a half-order compensator. In Fig. 2.9c, a post-compensator with a PC and a variable delay (3 DOF) is demonstrated. Fig. 2.9d shows a double-stage compensator with two PCs and two fixed delays (4 DOF). Another double-stage compensator with two PCs and one fixed and one variable delay (5 DOF) is illustrated in Fig. 2.9e. The double-stage compensators can compensate for higher order PMD. Fig. 2.9f shows a PC and

a polarizer in combination (2 DOF), where the average power through the polarizer could act as an error signal.

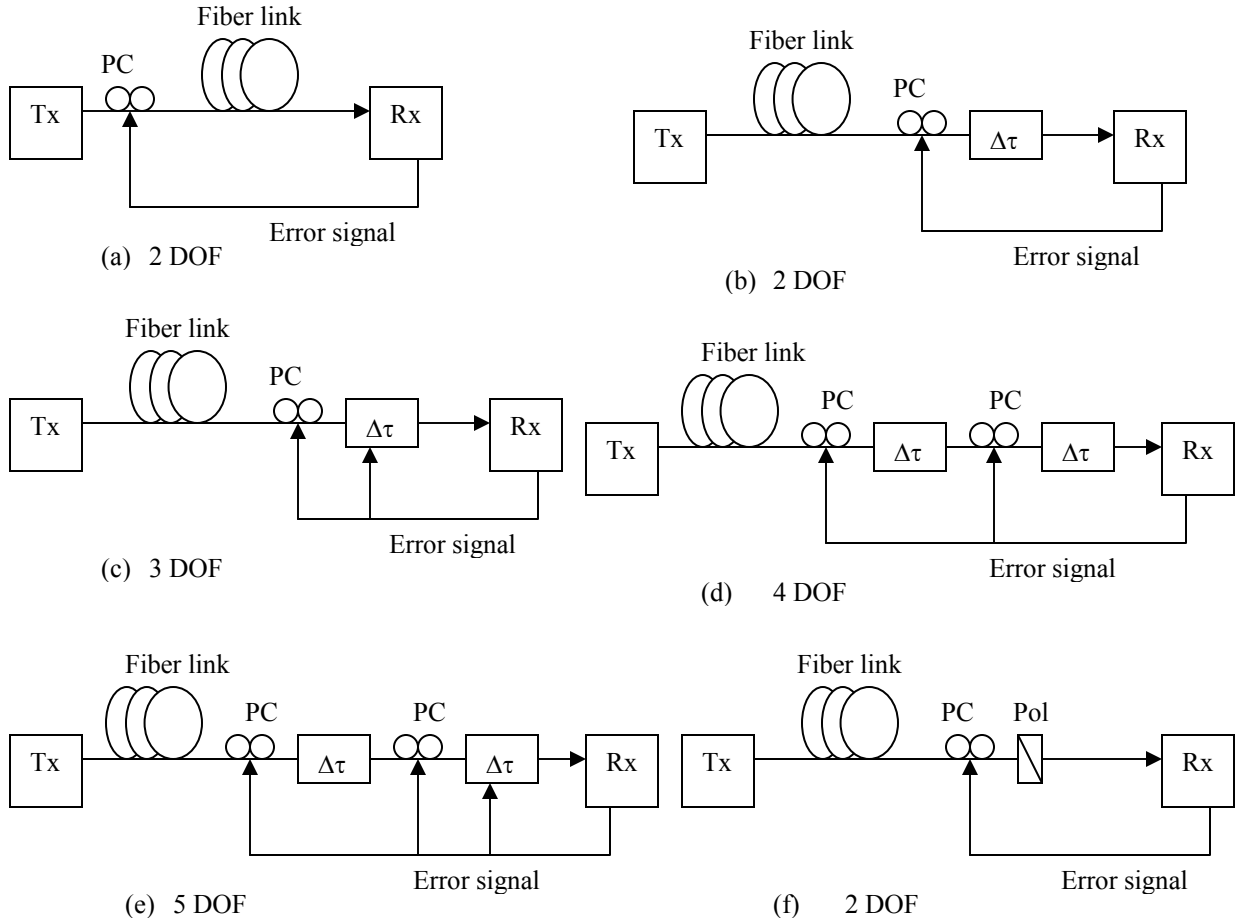


Fig. 2.9. Optical compensation schemes. (a) PSP method (2 DOF), (b) 1<sup>st</sup> order post comp (2 DOF), (c) 3 DOF post comp, (d) 4 DOF post comp, (e) 5 DOF post comp, (f) polarizer method (2 DOF) [28],[26].

By means of numerical simulations, Sunnerud et al. [28] concludes that a single-stage compensator with a variable delay (3 DOF), shown in Fig 2.9c performs better than the first-order compensators of Figs. 2.9a and b. This is because it has a well-defined optimum and it can compensate for higher-order PMD to some extent. The double-stage compensators (4 DOF, 5 DOF), shown in Figs. 2.9d and e, have

several sub-optima. They are better than first-order compensators when operating at the global optimum, but they could be trapped in a local optimum unless a good way to reach the global optimum is reached. As a consequence, these schemes perform worse than first-order compensator at low PMD (relative to bit period), but still better at high PMD [28]. The polarizer method (2 DOF) shown in Fig. 2.9f has only one optimum and it performs better than first-order compensators at large PMD because it does not add any DGD. At low PMD, the performance is worse than first-order compensators but an improvement is achieved compared to the uncompensated case [28]. Of all the compensators discussed in the section, the single-stage compensator with a variable delay line is optimum with respect to the performance and complexity.

To conclude, use of any of the compensation techniques discussed in this section does not necessarily guarantee complete cancellation of PMD, but can reduce the probability of outage due to PMD. Using PMD compensators is an expensive proposition, especially in WDM systems. This is because PMD compensators are band-limited and so each compensator can work at the most on a few consecutive channels and therefore many compensators have to be used to compensate for PMD on all the channels of a WDM system. Moreover, researchers have shown that use of advanced modulation formats like the ones discussed in Sec. 2.14 will result in same performance as that of the single-stage compensators. They can be expected to be a realistic alternative if used in combination with error correcting codes [26].

### 2.15.3 KU-PMD compensation system

This section gives a brief description of the PMD compensation system patented by University of Kansas [38]. This scheme compensates the PMD effect after the signal has traveled along the fiber link. The block diagram of it is shown in Fig. 2.10. It is a first-order, single-stage post compensator with a PC and a variable delay line. The DOP of the output signal is used as the feedback signal.

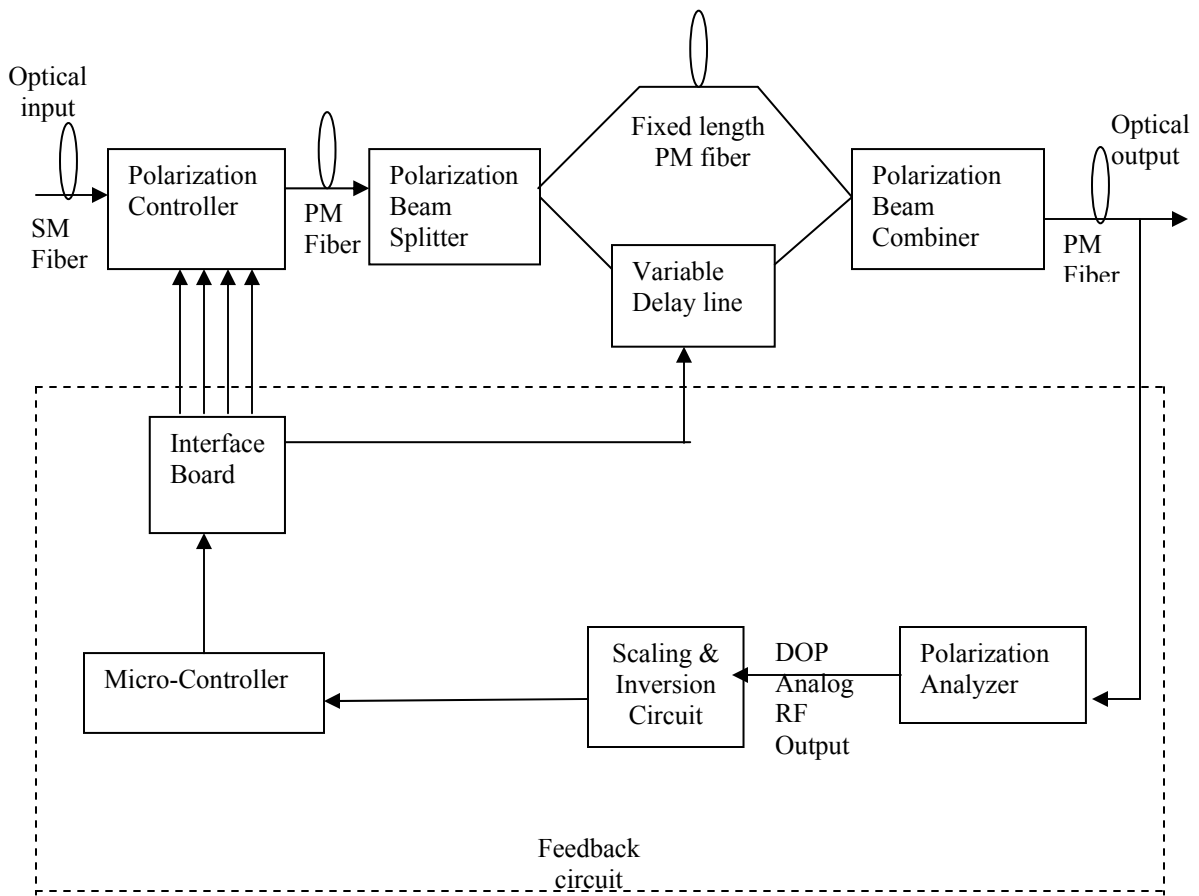


Fig. 2.10. Block diagram of KU-PMD compensation system [38].

In this scheme, the polarization beam splitter (PBS), variable delay line, fixed length PM fiber and the polarization beam combiner (PBC) constitute the adaptive

counter element. The signal first enters a polarization controller, where the link's output PSP is adjusted to match a linearly polarized PBS. The PBS divides the incoming signal into two components with a time offset between them resulting from the link PMD. To compensate the time offset, one of the components of the signal is fed to a variable delay line adjusted to the DGD value present in the signal. The two components are then merged in PBC, and the resulting output is fed to the receiver and to a feedback circuit that controls the polarization controller and the delay line. The DOP of the output signal is determined and a voltage signal proportional to the DOP is obtained. The algorithm running on the micro-controller makes use of this voltage signal to determine the optimum settings for the polarization controller and the variable delay line.

For optimum performance of this compensating scheme, the optical power should be equally split between the PSPs of the transmission fiber. Specifically, the performance of the compensator will be poor if the total optical power is aligned to any one PSP. But, in reality, there is no guarantee that this situation doesn't occur. However, using a polarizing scrambler at the transmitter side would alleviate this problem considerably. Scrambling the input signal at the transmitter will assure that the optical power is not aligned entirely to any one PSP, but more or less equally split between the two PSPs and thus avoids the worst-case situation [29].

### **3. PMD MEASUREMENT METHODS**

After chromatic dispersion, PMD is the most likely effect limiting the transmission bandwidth of single-mode fiber in high-speed systems. As we approach ultra-high bit rates, it is increasingly important to measure PMD, so that action can be taken to improve a fiber link. A considerable number of techniques for the measurement of PMD have been proposed. Some of these measure the scalar instantaneous DGD; others determine the mean DGD and a few allow measurement of the instantaneous PMD vectors as a function of frequency [1]. PMD measurement methods can be broadly classified into two categories:

- Time-domain methods
- Frequency-domain methods

Time domain methods operate by sensing pulse delays whereas the frequency domain methods operate by detecting changes of polarization with frequency. Measurement capabilities of various instruments range from around 1 fs to about 100 ps of DGD. The smaller ranges are needed for the measurement of the instantaneous DGD of optical components or short pieces of fiber, whereas the larger ranges are used to characterize long communication spans [1].

The following discussion will focus on six popular PMD measurement methods, three time-domain methods and three frequency-domain methods. The three time-domain methods that are discussed are pulse delay, modulation phase-shift and interferometric methods; the frequency-domain methods that are discussed are Poincare arc, fixed analyzer and Jones Matrix Eigenanalysis (JME) methods.

### 3.1 The pulse delay method

This method is one of the earliest and conceptually simplest methods of measuring DGD at a given wavelength. This method involves launching short pulses into a fiber, varying the input polarization state and measuring the maximum differential time of flight using an oscilloscope triggered by the same clock source as the input pulses. The measurement setup is shown in Fig. 3.1.

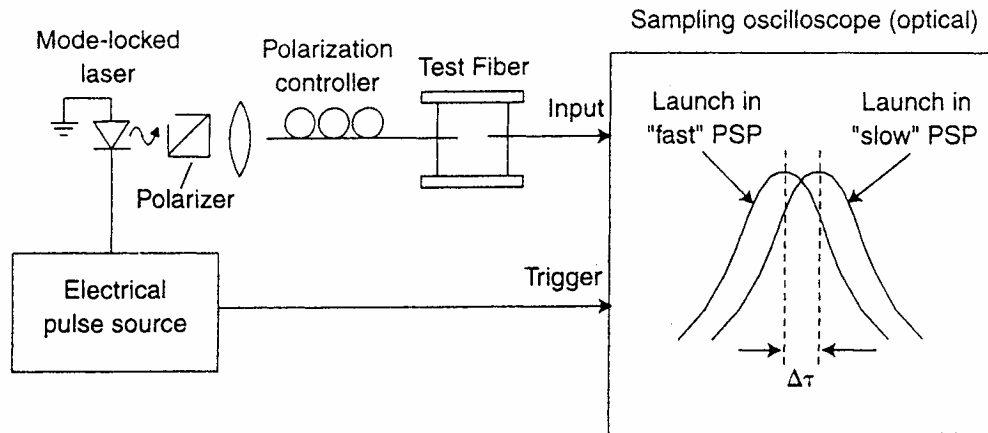


Fig. 3.1. PMD measurement by the pulse-delay method [3].

Implementation of this method is complicated by the need to search the range of input polarization states to find the two principal states. To resolve small differential group delays ultra-short pulses are required and so this method works best with large values of PMD [2]. Also, this method measures only instantaneous DGD at a specific wavelength and not the average DGD.



### 3.2 The modulation phase-shift method

In this method, instantaneous DGD is determined from the difference in modulation phase between the principal states of polarization. The measurement setup is shown in Fig. 3.2.

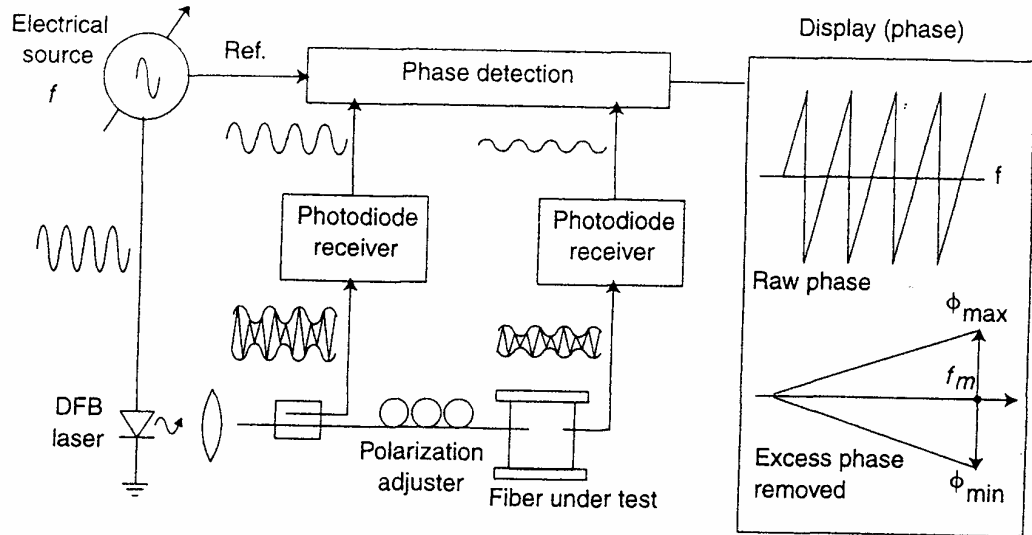


Fig. 3.2. PMD measurement by the modulation phase-shift method [3].

A high-frequency sinusoidal intensity-modulated light wave is injected into the fiber. The output is detected and the modulation phase is measured relative to the electrical modulation source using a network analyzer or lightwave component analyzer. The input polarization is then varied to produce maximum and minimum excursion of phase. At the maximum and minimum delays, the input state of polarization is aligned with the fiber's PSPs [24]. The difference between the maximum and minimum phase delays is used to determine the instantaneous DGD at a particular modulation frequency as [3]

$$\Delta \tau = \frac{\phi_{\max} - \phi_{\min}}{360 f_m}, \quad (3.1)$$

where  $f_m$  is the modulation frequency.

Although this technique is simple and intuitive, like the pulse delay method, it requires the experimental determination of the PSPs. In other words, the measurement must be carried out many times with different input states of polarization to determine which states of polarization correspond to the PSPs of the fiber. Another drawback of this method is that it requires a stable operating temperature and isolation from environmental perturbations and so it is not suitable for field measurements of optical fibers [24].

### **3.3 The interferometric method**

This is another time domain method based on direct measurement of a time delay. A variety of interferometric techniques for PMD measurement have been developed and standardized. The principle of any interferometric PMD measurement method is based upon measurement of the electric-field autocorrelation or mutual coherence, of two signals derived from the same wide band source. This method usually employs a Michelson interferometer or a Mach-Zehnder interferometer. Often the interferometer is implemented using a fiber-directional coupler constructed with PM fiber. An interferometric measurement setup using a Michelson interferometer is shown in Fig. 3.3.

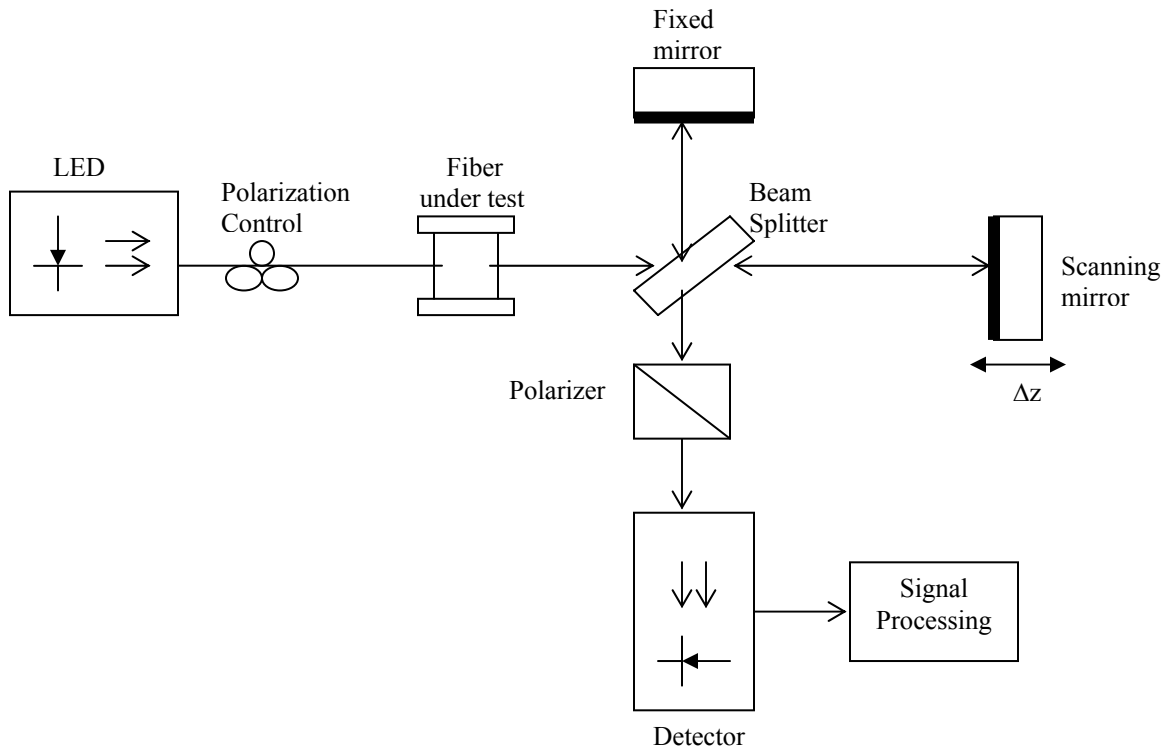


Fig. 3.3. PMD measurement by the interferometric method [1].

As shown in Fig. 3.3, the interferometer has a fixed-mirror arm and an arm with a scanning mirror. The maximum DGD that can be measured using this method depends on the maximum scanning range of the scanning mirror. The light from a broadband source (like an LED) is sent through the fiber and split into two parts in the interferometer. These two parts are delayed relative to each other by a time delay,  $\Delta T$ , proportional to the scan distance  $\Delta x$  from the interferometric balance [the point where both paths are of equal length] given by  $\Delta T = 2 \Delta x / c$  where  $c$  is the speed of light. The delayed parts are recombined for interference at the detector. The fringe pattern (autocorrelation) created at the detector by scanning the mirror distance is used to extract the DGD information [1]

The interferometric method is applicable to both optical components and long fibers, but the algorithmic approach to analyze the fringe patterns created is different. For optical components that are non-mode-coupled, the fringe pattern has a central interference peak when the interferometer is balanced. As the mirror is scanned away from balance, the fringe pattern shows two side peaks when  $\Delta T = \pm\Delta\tau$ , providing DGD information. For long fibers that are mode-coupled, the fringe patterns are complex and are difficult to analyze. The mean DGD, averaged over the spectral width of the source, is extracted from the fringe patterns by determining the second moment of the fringe distribution or by using a Gaussian fit to the fringe pattern [1].

The interferometric method is tolerant of movement along the fiber path during the measurement. Movement changes the details of the interferogram, but not the overall shape [3]. A significant drawback of this method is its inability to make PMD measurements in optical components having a narrow optical bandwidth like many WDM devices [24].

### **3.4 The Poincare arc method**

In the frequency domain, polarization dispersion manifests as a frequency-dependent state of polarization. In Poincare arc method, the PMD information (like the PSPs, the DGD and its wavelength dependency) are derived from the arc traced out on the Poincare sphere by the point representing the output polarization state as a function of wavelength, for a constant input polarization state [22]. The magnitude and the direction of the dispersion vector,  $\Omega$ , at a given wavelength can be determined from

$$\frac{d \hat{s}}{d \omega} = \hat{\Omega} \otimes \hat{s} \quad (3.2)$$

by differentiating the measured data with respect to frequency and by making measurements for at least two input polarizations. DGD can also be determined using the expression

$$\Delta \tau = \frac{\Delta \theta}{\Delta \omega} \quad (3.3)$$

where  $\Delta \theta$  is angular width of the arc described by the Stokes vector on the Poincare sphere in the frequency window of width  $\Delta \omega$  [3].

This method can be used either to measure instantaneous DGD values at specific wavelengths or to determine the average delay over a wavelength band. Unlike the other measurement methods described above, this method can be used to determine high-order dispersion by measuring the complete dispersion vector. Also, this method is accurate for both large and small values of PMD but its accuracy is limited by the stability of the fiber under test [2].

### 3.5 The fixed analyzer method

This method is also referred to as the wavelength-scanning method. An experimental setup using a broadband source and an optical spectrum analyzer is shown in Fig. 3.4a. An alternative setup using a tunable narrowband source and polarimeter is shown in Fig. 3.4b.

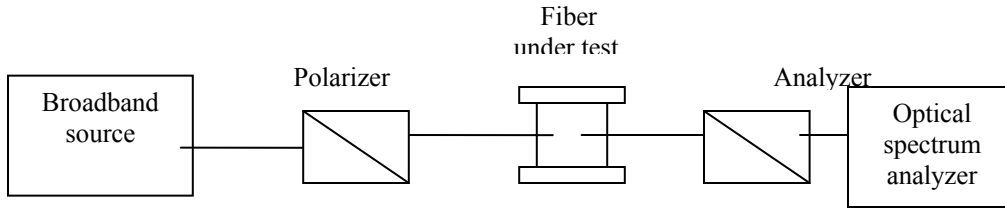


Fig. 3.4a. PMD measurement using the fixed analyzer method [3].

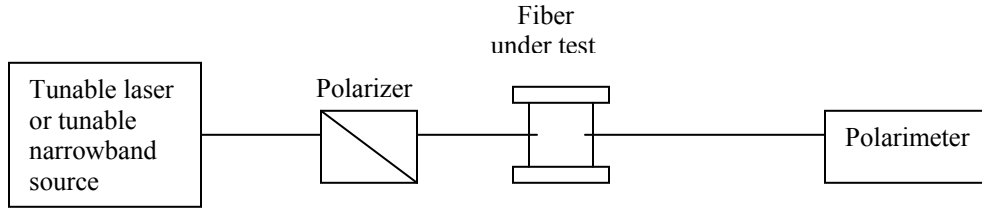


Fig. 3.4b. Alternate setup for the fixed analyzer PMD measurement [3].

Light with a fixed polarization is transmitted through a test fiber and then through the analyzer. The normalized transmission through the analyzer is measured as a function of wavelength. The transmitted spectrum shows a number of extrema (peaks and valleys) resulting from the variation of the polarization incident on the analyzer caused by PMD in the test fiber. These extrema indicate the rate at which the output SOP changes as the wavelength changes. The larger the PMD, the more rapidly the output SOP changes with wavelength and thus, the more densely spaced extrema in the spectrum [2].

Several methods can be used to determine the average DGD of the test fiber from the captured transmission spectrum. One method is to count the number of times the normalized transmission curve crosses the mean transmission level (i.e., 0.5) per unit frequency interval. The mean DGD,  $\langle \Delta \tau \rangle$  is related to the mean-level crossing

density as [2]

$$\langle \Delta \tau \rangle = k_1 \frac{N_m}{\Delta \omega}; N_m \rightarrow \infty, \quad (3.4)$$

where  $N_m$  is the number of mean-level crossings in the frequency interval  $\Delta\omega$ , and  $k_1$  is a constant.  $k_1$  is  $\pi$  for short fibers and 4 for long fibers. Another method is to count the number of extrema in the transmission spectrum per unit frequency interval. The mean DGD is determined from this extrema density using [2]

$$\langle \Delta\tau \rangle = k_2 \frac{N_e}{\Delta\omega}; N_e \rightarrow \infty, \quad (3.5)$$

where  $N_e$  is the number of extrema in the frequency interval  $\Delta\omega$  and  $k_2$  is a constant. The value of  $k_2$  is  $\pi$  for short fibers and  $0.82\pi$  for long fibers. The number of extrema or mean-level crossings is finite in practice and so the above expressions are used as approximations. Another method to obtain mean DGD is to determine the Fourier transform of the transmission spectrum, the width of which is proportional to the mean DGD in the test fiber [2].

The advantages of fixed analyzer method are simple experimental setup and easy data analysis. Also, it does not require coordination between transmitter and receiver when a broadband source is used and so it can be used for field tests. The disadvantages are that it cannot measure instantaneous DGD and it requires a stable fiber during measurement [2].

### **3.6 The Jones Matrix Eigenanalysis (JME) method**

The JME method is similar to the Poincare sphere method in that the output SOP of a test fiber is measured as a function of wavelength. However, the main difference between these two methods is that the JME method makes use of Jones

matrices and Jones calculus in determining the PMD vector [2]. This method makes no assumptions about the device or network under test except that it must be linear and its polarization transformation must be constant over a period of several seconds [23].

According to Jones calculus, a polarized signal can be expressed as a complex two-element Jones vector that completely describes the amplitude and polarization state of the signal. The transmission path can be represented by a complex two-by-two Jones matrix, which relates the input and output Jones vectors. The Jones matrix describes the polarization-transforming characteristic of the two-port device to a complex constant that represents the absolute propagation delay, which is not required to determine DGD. Measurement of the Jones matrix requires the application of three known states of linearly polarized light (typically oriented at 0, 45 and 90 degrees to the device under test). The Jones matrix is determined from the relationship of the measured output states to the known input states [3].

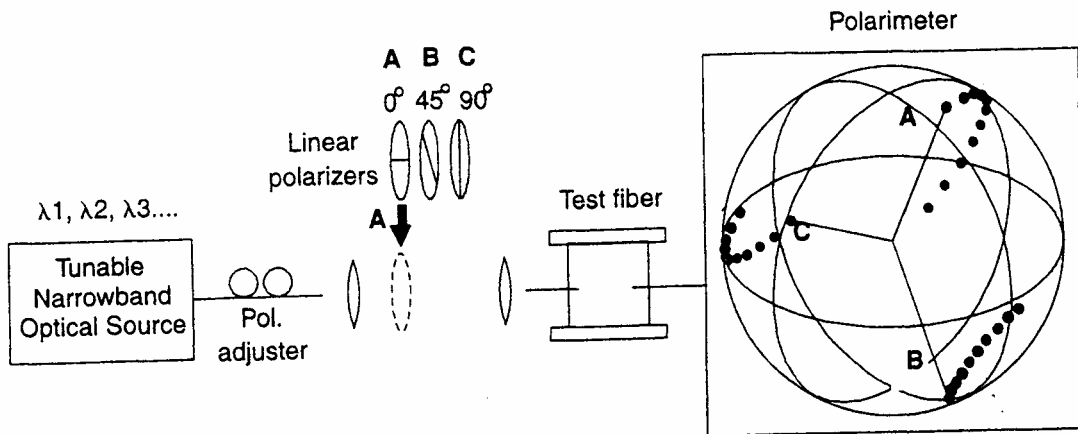


Fig. 3.5. PMD measurement by the JME method [3].



The JME measurement setup, illustrated in Fig. 3.5, has a tunable narrowband optical source, an adjustable polarizer for generating three linear polarization states, a fast polarimeter and a computer for processing the measured data. The source polarization is adjusted to a circular state to allow transmission through each polarizer. To determine the DGD at a particular wavelength,  $\lambda$ , the Jones matrices of the path from the polarizers to the polarimeter at two different wavelengths equally spaced about  $\lambda$ , are measured. Then the DGD,  $\Delta\tau$ , is computed using the expression [3]

$$\Delta\tau = \left| \frac{\text{Arg}\left(\frac{\rho_1}{\rho_2}\right)}{\Delta\omega} \right| \quad (3.6)$$

where  $\Delta\omega$  is the change in optical frequency corresponding to the wavelength interval.  $\rho_1$  and  $\rho_2$  are the eigen values of the expression  $T(\omega+\Delta\omega)T^{-1}(\omega)$  involving the Jones matrices  $T$ . The eigen vectors of  $T(\omega+\Delta\omega)T^{-1}(\omega)$  locate the output PSP as function of frequency [23].

The advantage of the JME method is that, unlike the other methods, this method can be readily automated to determine PMD vectors over a large wavelength range [1]. The drawbacks of this method are the need for sophisticated algorithms for computing DGD and the need to have a stable test fiber during the measurement [2]. This method requires coordination of measurement setup at transmitter and receiver ends. Therefore loop back is used and so it is not always practical in field tests.

To conclude, time domain measurements are generally not suitable for field measurements, as they require lots of stability in both the instrumentation and the fiber under test. Also, time domain measurements are slow because of the need to experimentally determine the PSPs for each test [24]. Of all the frequency domain measurement methods, JME method is the most popular method and this is the method used to measure DGD data in our research work. Table. 3.1 summarize all the aspects of different PMD measurement methods.

Table. 3.1. Summary of different PMD measurement methods [2][3].

Measurement name	Pulse delay	Interferometric	RF response (Modulation phase shift)	Poincaré arc (State of polarization)	Jones matrix	Fixed analyzer
<b>Determines DGD from ...</b>	a sampling scope measurement of the different time of flight between pulses in the two PSPs	an interferogram obtained by placing device in low-coherence interferometer	the phase change of an intensity modulation envelope between two the PSPs	the rate of rotation of the output SOP about the PSP axis	changes in Jones matrix across wavelength intervals	random evolution of the output SOP as wavelength is scanned
<b>Light source</b>	chirp-free laser	broadband	chirp-free laser	tunable laser	tunable laser	broadband or tunable laser
<b>Other equipment involved</b>	polarization controller, high-speed photodiode & sampling scope	Michaelson interferometer, polarizers	Network analyzer	polarization analyzer	linear polarizers, polarimeter	OSA
<b>Time or frequency domain</b>	Time	Time	Time	Frequency	Frequency	Frequency
<b>DGD vs. 1 ?</b>	No	No	Yes	Yes	Yes	No
<b>Measurement sensitive to fiber motion?</b>	Yes	No	Yes	Yes	Yes	Yes
<b>Industry Standard</b>		TIA-FOTP-124			TIA-FOTP-122	TIA-FOTP-113
<b>Sensitive to launch SOP?</b>	Yes	Yes	Yes	Yes	No	No
<b>Measures</b>	$\Delta\tau$	$\langle\Delta\tau\rangle$	$\Delta\tau, \langle\Delta\tau\rangle$	$\Delta\tau, \langle\Delta\tau\rangle$	$\Delta\tau, \langle\Delta\tau\rangle$	$\langle\Delta\tau\rangle$
<b>Measurement range (ps)</b>	~ 10 to >1000	~0.002 to 100	~25 to >100	~0.002 to >1000	~0.002 to >1000	~0.1 to 100
<b>Measurement accuracy (ps)</b>	> ~15 ps	> ~0.003 ps		> ~0.05 ps	> ~0.025 ps	> ~0.05 ps
<b>Higher order dispersion?</b>	No	No	No	Yes	Yes	No

## 4. MESUREMENT SETUP

This chapter gives a description of the measurement setup used to make automated DGD measurements across a given wavelength band and over time using the Agilent lightwave polarization analyzer (PA). Jones Matrix Eigenanalysis (JME) method is used for making DGD measurements.

### 4.1. Measurement Setup

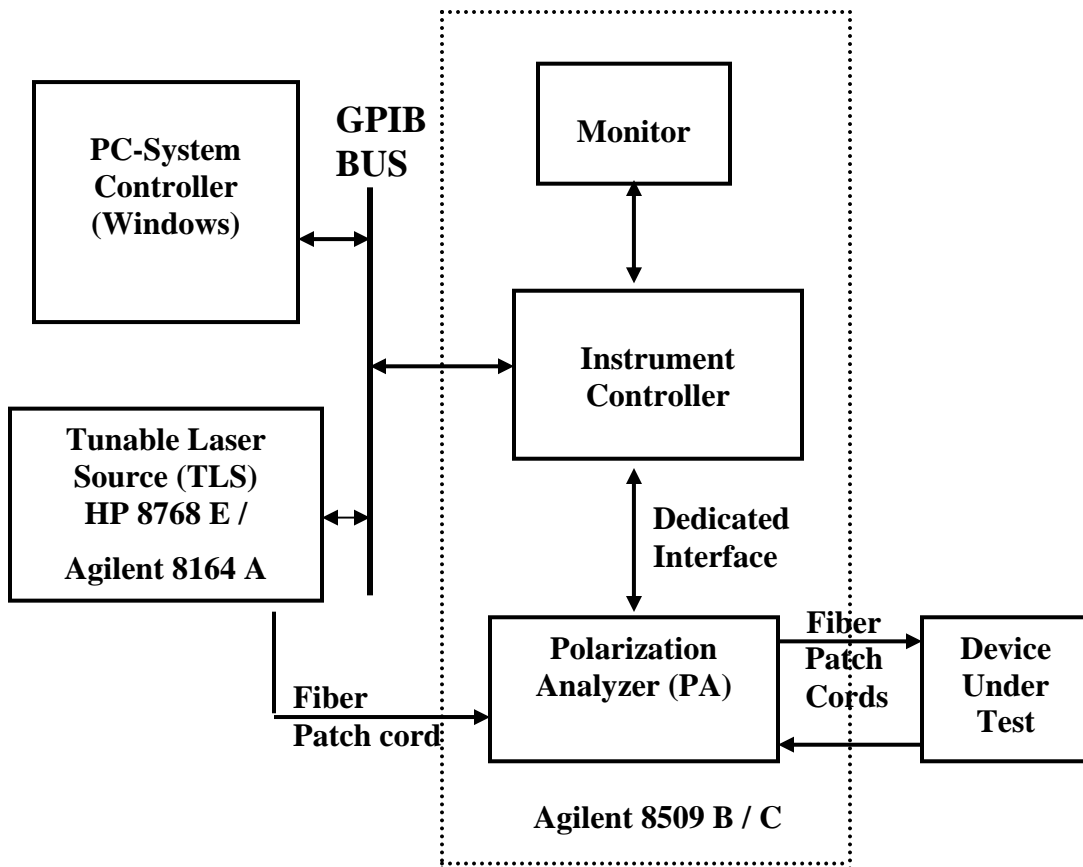


Fig. 4.1. Measurement setup used for making automated DGD measurements.

The measurement setup shown in Fig. 4.1 is controlled by the visual basic (VB) software running on the system controller PC. This setup can be used to

measure DGD as well as polarization-dependent loss (PDL). For measuring DGD it makes use of the JME application in the polarization analyzer.

One measurement at a specific wavelength and at a specific time takes about 4 seconds. The measurement time for an across-the-band measurement is a function of the range of wavelength band and the wavelength step size used. Typically, one measurement across the 35 nm EDFA band with a step size of 0.1 nm takes about 30 minutes and while one measurement across 1510 nm – 1625 nm band with a 0.1 nm step size takes about 90 minutes. The maximum measurable DGD using the JME method varies with the wavelength step and the band of operation. In the 1550 nm band, the maximum measurable DGD is about 40 ps with a 0.1 nm step size and it is 4 ps with a 1 nm step size. The uncertainty in measuring DGD using JME method is also a function of step size. The uncertainty is about  $\pm 310$  fs for a 0.1 nm step size and  $\pm 90$  fs for a 1 nm step size [37].

The measured data are automatically stored into text files. The size of these files depends on the number of measurement points and they are about 8 kB to 30 kB.

The measurement system shown in Fig. 4.1 is usually very reliable and the measurements are stable. However, occasionally (once in a month or so) any of the instruments might become frozen and the measurements are stopped. The best thing to do to avoid loss of data due to such errors is to check the measurements often (several times a day) and then restart the measurement system when such errors occur. To avoid losing data due to unintended power failures, we use uninterruptible power supplies (UPS).

A detailed description of measurement procedure, VB software and other possible errors during the measurements are given in Appendix A.

## **5. MEASUREMENT RESULTS AND DATA ANALYSIS**

In this section the results obtained from the measurements and the data analysis are presented. Experiments were conducted to measure the instantaneous DGD on three different 95-km fibers (1, 2, and 3) within a slotted-core, direct buried, standard single-mode fiber-optic cable made available by Sprint. Two different configurations of the three fibers were used, individual fibers and two fibers concatenated together. Different tests and plots have been used to present the data. In this section, the plots used and the tests performed on the data are explained first, followed by the actual plots and the analyses on the data obtained using the two fiber configurations.

**Note:** All the measured DGD data presented in this chapter were normalized by the mean DGD value for that configuration.

### **5.1 Tests & Plots**

#### **5.1.1 DGD color maps**

Color maps of the normalized DGD data are two-dimensional plots showing three-dimensional data. The two axes represents two dimensions and the color shade represents the third dimension. These plots are used to represent normalized DGD value vs. wavelength and time. The variation of the normalized DGD with wavelength is represented by the change in the color and shade along the horizontal axis and the variation with time is represented by the change in the color and shade along the vertical axis.

### 5.1.2 DGD histograms

To determine the statistical distribution of DGD, a histogram of the normalized DGD data was plotted. The frequency scale (vertical axis) is normalized by the maximum value implying that the stress is on the shape of the histogram. It has been reported before that DGD follows a Maxwellian distribution [1] and so a curve representing a Maxwellian distribution for a 1-ps mean DGD is also plotted, using (5.1), for comparison.

$$f_{\Delta\tau}(\Delta\tau) = \sqrt{\frac{2}{\pi}} \frac{\Delta\tau^2}{\sigma^3} e^{\left(\frac{-\Delta\tau^2}{2\sigma^2}\right)} \quad \text{where } \sigma = \langle\Delta\tau\rangle\sqrt{\pi/8} \quad \text{and } \langle\Delta\tau\rangle = 1; \Delta\tau \geq 0 \quad (5.1)$$

### 5.1.3 Temporal autocorrelation

To determine the DGD rate of change, an autocorrelation analysis was performed on the DGD time histories. The normalized temporal autocorrelation of DGD is plotted and a theoretical curve is fit to it representing the temporal autocorrelation function (ACF) obtained using [8]

$$ACF(\Delta t) = \frac{1 - \exp(-|\Delta t|/t_d)}{|\Delta t|/t_d} \quad (5.2)$$

$t_d$  is the average drift time of the DGD that indicates the timescale over which the DGD changes. The value of  $t_d$  is adjusted to obtain a good fit.

### 5.1.4 Frequency autocorrelation

To determine the DGD bandwidth, spectral autocorrelation analysis was performed on the normalized DGD spectral data. The normalized spectral autocorrelation of

DGD is plotted and a theoretical curve is fit to it representing the spectral autocorrelation function (ACF) obtained using [30]

$$ACF(\Delta\omega) = 3 \frac{1 - \exp\left(-\langle\Delta\tau^2\rangle\Delta\omega^2/3\right)}{\Delta\omega^2} \quad (5.3)$$

where  $\Delta\omega$  is the radian bandwidth and  $\langle\Delta\tau^2\rangle$  represents the DGD variance.

### 5.1.5 System outage analysis

The impact of PMD on a communication system is often expressed in terms of the outage probability, which is defined in different ways. Some define the outage probability as the probability that the power penalty due to PMD exceeds 1 dB while some others define it as the probability that the DGD exceeds a threshold value. The later definition is used in this report.

An outage event occurs when the instantaneous DGD exceeds the given threshold value of DGD,  $\Delta\tau_{th}$ . The outage probability  $P_{out}$  can be calculated from the Maxwellian probability distribution function (pdf),  $f_{\Delta\tau}(\cdot)$  as

$$P(\Delta\tau \geq \Delta\tau_{th}) = 1 - \int_0^{\Delta\tau_{th}} f_{\Delta\tau}(\Delta\tau) d\Delta\tau \quad (5.4)$$

$P_{out}$  is often expressed in minutes/year by multiplying  $P(\Delta\tau \geq \Delta\tau_{th})$  by the number of minutes in a year. As  $P_{out}$  is based on the Maxwellian pdf, it may be expressed as a function of just one independent variable DGD margin (M) defined as  $M = \Delta\tau_{th}/\langle\Delta\tau\rangle$ , as  $P_{out}(M)$ .  $P_{out}$  is fiber independent and will be the same for all installations [33]. If the probability of an outage is quite small,  $P_{out}$  represents the annualized outage probability based on long time records. Accurate estimation of the



impact of PMD on network availability requires statistical analysis of DGD variability. Caponi et al. [31] showed how the mean time between PMD-related outages could be estimated from the temporal characteristics of DGD variations and the Maxwellian probability density function. The mean outage rate,  $R_{out}$ , which is defined as the mean number of outage events per unit time (with units of 1/year), is found using [31]

$$R_{out} = \frac{1}{2} f_{\Delta\tau}(\Delta\tau_{th}) \int_{-\infty}^{\infty} f_{\Delta\tau'}(\Delta\tau') |\Delta\tau'| d\Delta\tau' \quad (5.5)$$

where  $\Delta\tau'$  is the time derivative of the DGD, and  $f_{\Delta\tau'}(\cdot)$  is the pdf of  $\Delta\tau'$ . The calculation of  $R_{out}$  is a simple application of the ‘Level Crossing’ problem and its derivation is given in Sec 5.1.6. The mean duration of DGD-induced outages can be determined using statistical analysis as well. Caponi et al. [31] showed that the mean outage duration,  $T_{out}$ , is

$$T_{out} = P_{out} / R_{out} \quad (5.6)$$

which has units of minutes. Since  $T_{out}$  is found using  $R_{out}$ , which is cable and installation dependent,  $T_{out}$  will also be cable and installation dependent.

### 5.1.6 Derivation of the expression for $R_{out}$

As mentioned above, the calculation of  $R_{out}$  is an application of ‘Level Crossing’ problem. Let  $\Delta\tau(t)$  represent DGD as a function of time.  $\Delta\tau(t)$  is assumed to be stationary. Let us denote the threshold value of DGD as  $\Delta\tau_{th}$  and define a function

$$\phi(t) \text{ as } \phi(t) = \Delta\tau(t) - \Delta\tau_{th} \quad (5.7)$$

$$\Rightarrow \phi'(t) = \Delta\tau'(t) \quad (5.8)$$

where ' denotes the first order derivative with respect to time.

Then, the zeros of the function  $\phi(t)$  are the  $\Delta\tau_{th}$  crossings of  $\Delta\tau(t)$ . If  $t_i$  are all the real zeros of  $\phi(t)$  then from the properties of impulse function [34],

$$\delta[\phi(t)] = \sum_i \frac{\delta(t-t_i)}{|\phi'(t_i)|} = \frac{1}{|\phi'(t)|} \sum_i \delta(t-t_i) \quad (5.9)$$

$$\Rightarrow \sum_i \delta(t-t_i) = |\phi'(t)| \delta[\phi(t)] \quad (5.10)$$

Substituting for  $\phi(t)$  and  $\phi'(t)$  using (5.7) and (5.8),

$$\sum_i \delta(t-t_i) = |\Delta\tau'(t)| \delta[\Delta\tau(t) - \Delta\tau_{th}] \quad (5.11)$$

Let  $S(t) = \sum_i \delta(t-t_i)$  and  $n(T)$  be the number of  $\Delta\tau_{th}$  crossings in an interval of

length  $T$ . Then  $n(T)$  can be expressed as

$$n(T) = \int_t^{t+T} s(\alpha) d\alpha \quad (5.12)$$

and

$$E\{n(T)\} = T \cdot E\{S(t)\} \quad (5.13)$$

$R_{out}$  is defined as the number of times DGD exceeds  $\Delta\tau_{th}$  per unit time and is expressed as

$$R_{out} = \frac{1}{2} \frac{E\{n(T)\}}{T} = \frac{1}{2} E\{S(t)\} \quad (5.14)$$

From (5.11) it is clear that the random variable  $S(t)$  is a function of random variables  $\Delta\tau(t)$  and  $\Delta\tau'(t)$ . Denoting the joint density of  $\Delta\tau(t)$  and  $\Delta\tau'(t)$  by  $f_{\Delta\tau, \Delta\tau'}(\Delta\tau, \Delta\tau')$ ,  $E\{S(t)\}$  can be expressed as [31],

$$E\{S(t)\} = \int_{-\infty}^{\infty} \int_{-\infty}^{\infty} |\Delta\tau| \delta(\Delta\tau - \Delta\tau_{th}) f_{\Delta\tau, \Delta\tau'}(\Delta\tau, \Delta\tau') \cdot d\Delta\tau \cdot d\Delta\tau' \quad (5.15)$$

But from the properties of impulse function [34],

$$\begin{aligned} \int_{-\infty}^{\infty} \delta(\Delta\tau - \Delta\tau_{th}) f_{\Delta\tau, \Delta\tau'}(\Delta\tau, \Delta\tau') \cdot d\Delta\tau &= f_{\Delta\tau, \Delta\tau'}(\Delta\tau, \Delta\tau') \Big|_{\text{Evaluated at } \Delta\tau = \Delta\tau_{th}} \\ &= f_{\Delta\tau}(\Delta\tau_{th}) \cdot f_{\Delta\tau'/\Delta\tau}(\Delta\tau'/\Delta\tau) \end{aligned} \quad (5.16)$$

$$\Rightarrow R_{out} = \frac{1}{2} E\{S(t)\} = \frac{1}{2} f_{\Delta\tau}(\Delta\tau_{th}) \int_{-\infty}^{\infty} |\Delta\tau'| f_{\Delta\tau'/\Delta\tau}(\Delta\tau'/\Delta\tau) \cdot d\Delta\tau' \quad (5.17)$$

Caponi et al. [31] observed  $\Delta\tau$  and  $\Delta\tau'$  to be statistically independent and so (5.17) can be expressed as

$$R_{out} = \frac{1}{2} f_{\Delta\tau}(\Delta\tau_{th}) \int_{-\infty}^{\infty} f_{\Delta\tau'}(\Delta\tau') \cdot |\Delta\tau'| \cdot d\Delta\tau' \quad (5.18)$$

where  $f_{\Delta\tau}$  is the pdf of the DGD and  $f_{\Delta\tau'}$  is the pdf of the first derivative of the DGD.

The integral in (5.18) is evaluated numerically using measured DGD data.

## 5.2 Long-term measurements of individual buried fiber spans

### 5.2.1 Measurement setup

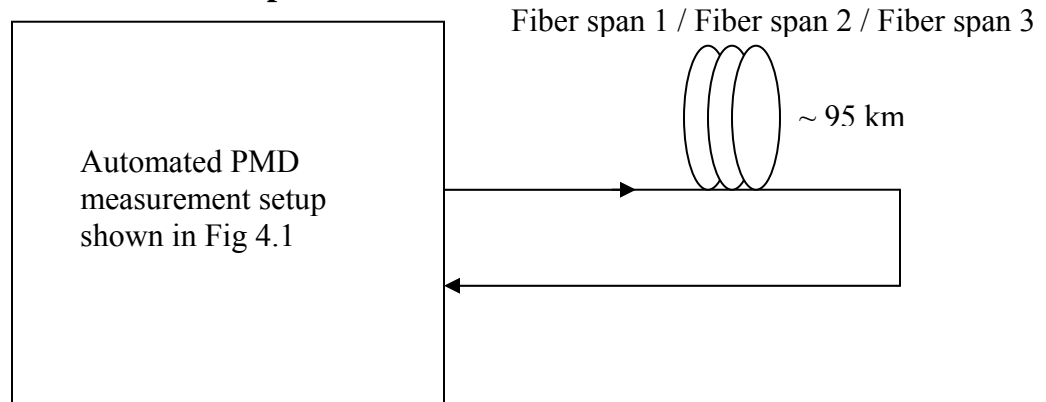


Fig. 5.1. Measurement setup for characterizing individual buried fiber spans.

### **5.2.2 Plots of DGD vs. wavelength and time**

Given the dynamic nature of PMD and the low probability of excursions to intolerable levels, measurements of  $\Delta\tau(\lambda, t)$  on the three buried fiber spans were made over long periods to enable prediction of the potential impact of PMD on network availability. Of particular interest are the frequency and duration of these rare events. On fiber span 1, the DGD was measured roughly every 3 hours for 86 days (692 measurements from November 9, 2001 through February 2, 2002) at wavelengths from 1510 nm to 1625 nm with a spectral resolution of 0.1 nm (about 12.5 GHz). The DGD on fiber span 2 was measured about every 1½ hrs for 14 days (236 measurements from May 4, 2002 through May 18, 2002) over the same spectral band and with the same resolution as fiber span 1. The DGD measurements on fiber span 3 were repeated roughly every 1½ hrs and they were carried out for about 64 days (1072 measurements from May 29, 2002 through Aug. 1, 2002) over the same spectral band with the same resolution. Figs. 5.2, 5.3 and 5.4 show in a color-coded format the normalized DGD measured on these three fiber spans.

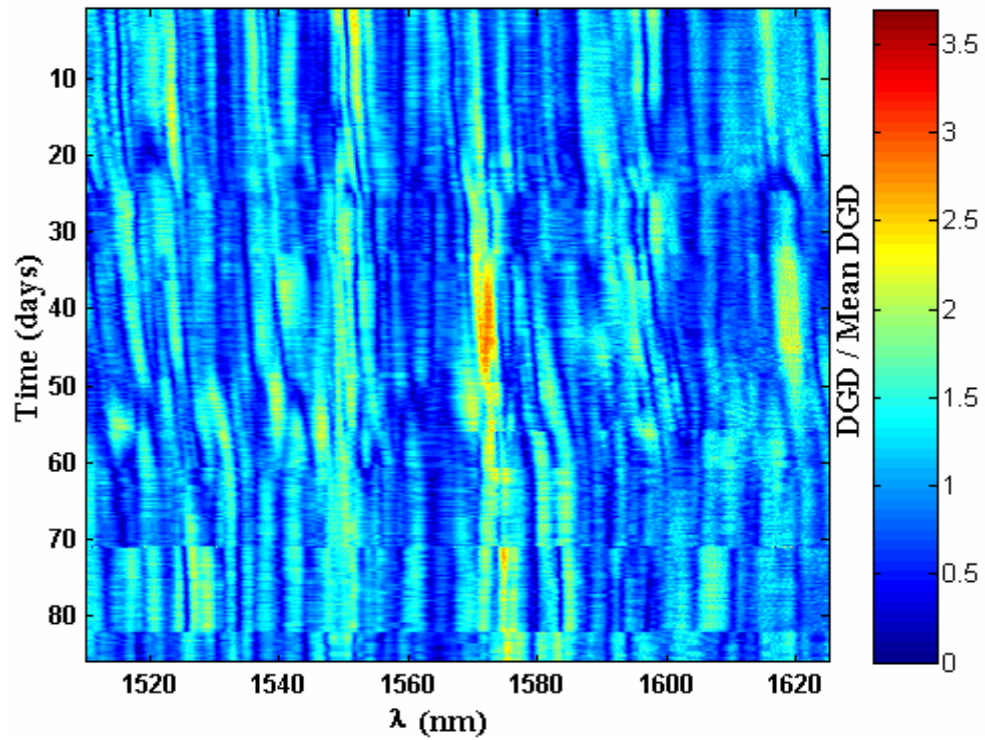


Fig. 5.2. Measured, normalized DGD vs. wavelength and time for fiber span 1 (86 days).

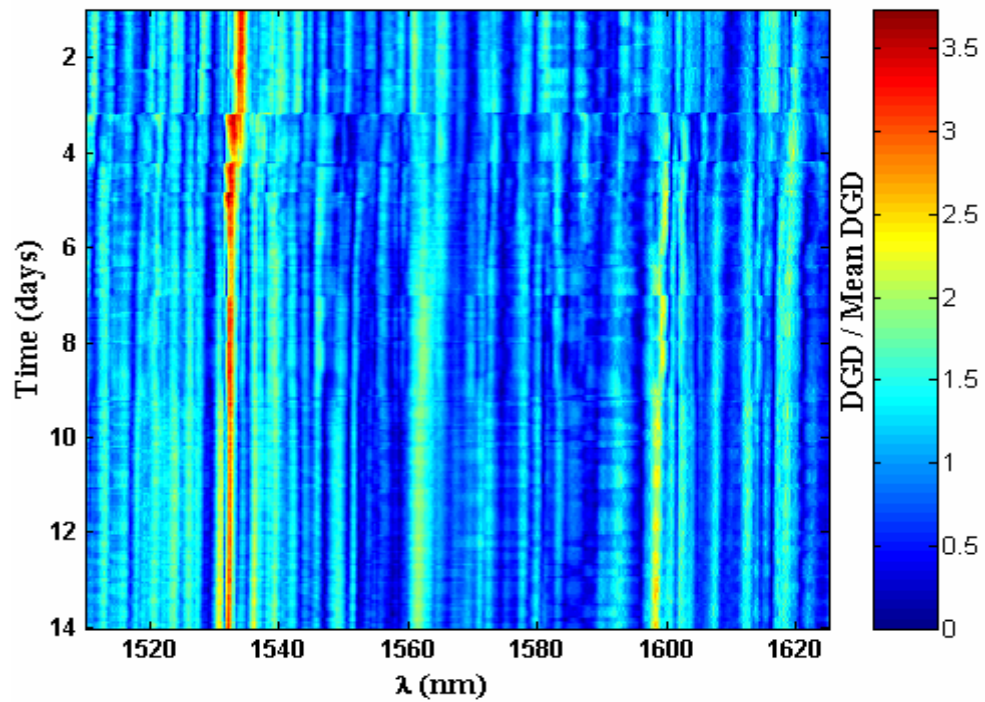


Fig. 5.3. Measured, normalized DGD vs. wavelength and time for fiber span 2 (14 days).

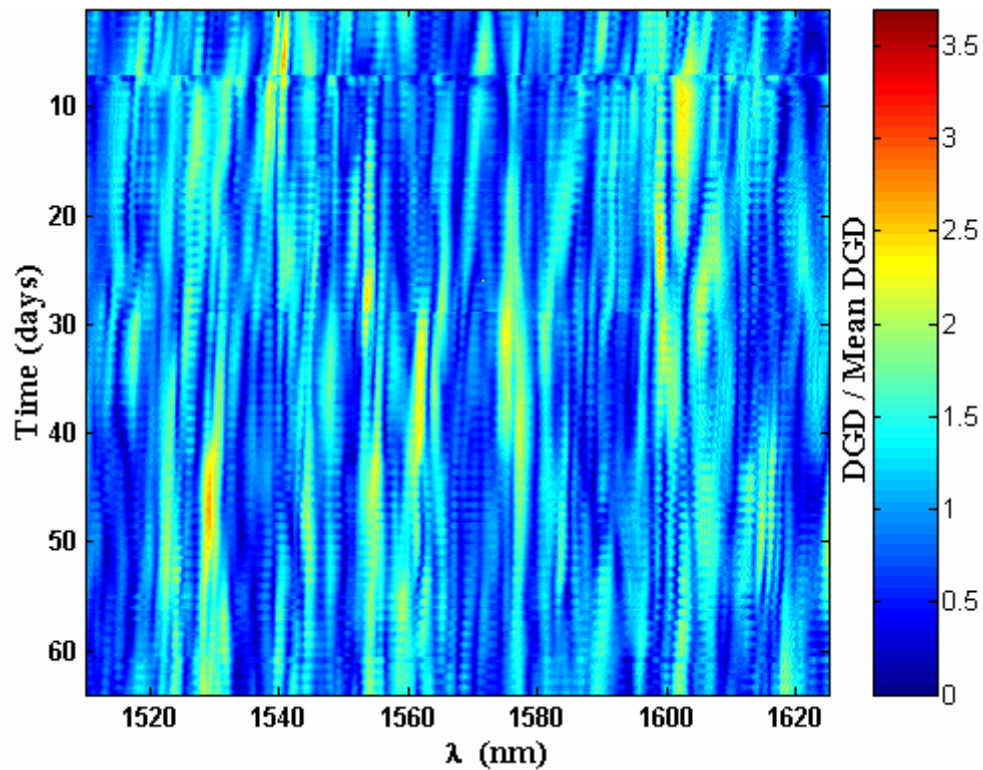


Fig. 5.4. Measured, normalized DGD vs. wavelength and time for fiber span 3 (64 days).

It is clear from Figs. 5.2, 5.3 and 5.4 that for buried fibers, DGD changes with time. This variation is random and differs from fiber to fiber, but is very slow. This is evident by comparing Fig. 5.3 with Figs. 5.2 and 5.4. Fig. 5.3 corresponds to 14 days of DGD data on fiber span 2 and no appreciable change in DGD can be observed over time in that figure, whereas in Figs 5.2 and 5.4, which show DGD data over a longer period on fiber spans 1 and 3, a significant change in DGD over time can be observed. Also, it is evident that DGD varies significantly with wavelength and relatively high-DGD events are spectrally localized.

### 5.2.3 Histograms of measured DGD data

Histograms of the normalized DGD data on all the three fiber spans are shown in Figs. 5.5, 5.6 and 5.7. It can be observed that these histograms have shapes consistent with a Maxwellian distribution, as expected. Curves representing a Maxwellian distribution for a 1-ps mean DGD is also plotted for comparison. These curves fit very well to the measured data, particularly for fiber spans 1 and 3, as there is large amount of data from these fiber spans.

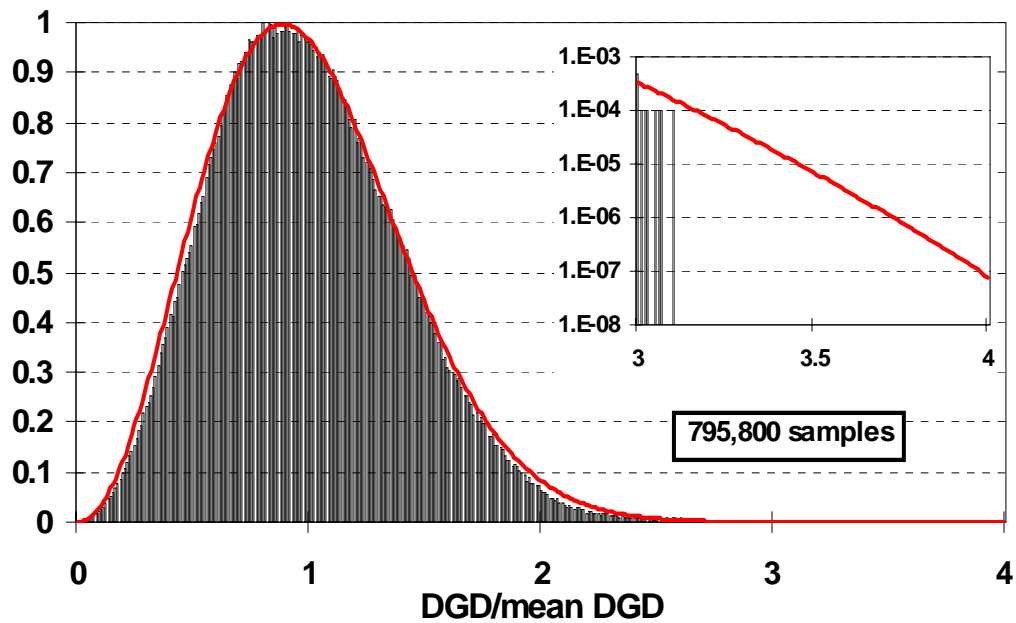


Fig. 5.5. Histogram of measured, normalized DGD data on fiber span 1.

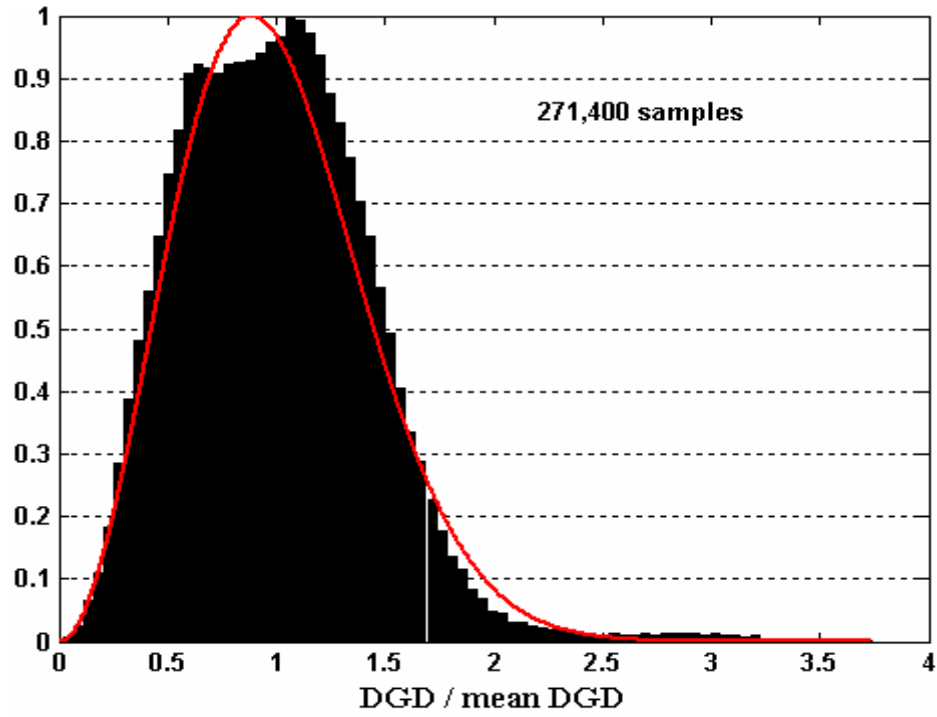


Fig. 5.6. Histogram of measured, normalized DGD data on fiber span 2.

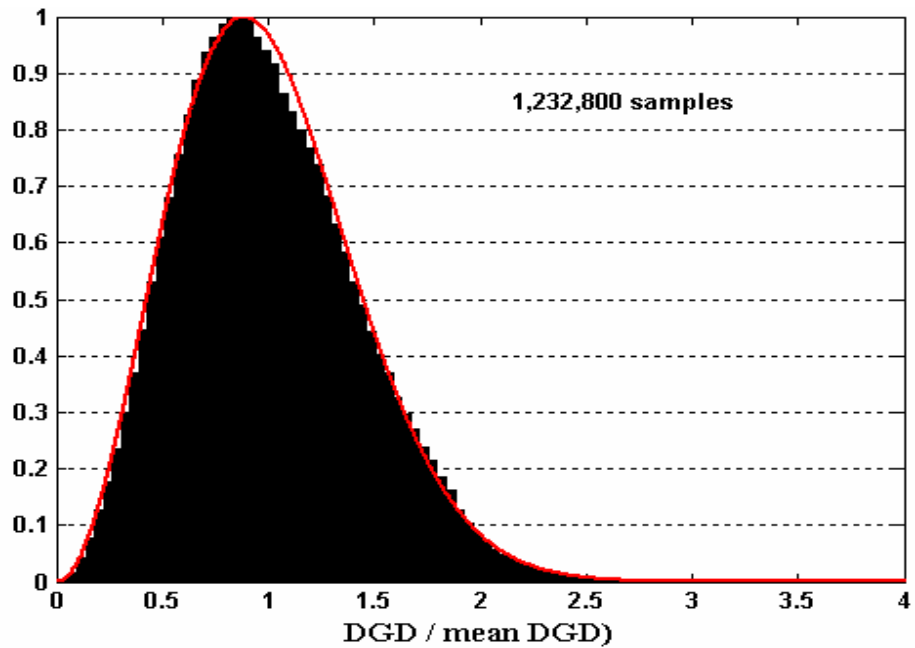


Fig. 5.7. Histogram of measured, normalized DGD data on fiber span 3.



### 5.2.4 Mean DGD variation with time

To observe the time-dependent nature of DGD more closely, 1150 measurements of DGD over all wavelengths were averaged together to obtain frequency-averaged DGD data, denoted as  $\langle \text{DGD} \rangle_\lambda$  normalized by the overall mean DGD, denoted as  $\langle \langle \text{DGD} \rangle_\lambda \rangle_t$ . Since temperature is a known driver of DGD variation [8], hourly air temperature data for the region were collected as well. The variation of normalized frequency-averaged DGD and temperature with time on the three fiber spans is shown in Figs. 5.8, 5.9 and 5.10. From those plots it can be observed that the variation in frequency-averaged DGD is less than 10 % over the measurement period. Since the entire length of the fiber is buried, the diurnal temperature variations do not represent the actual fiber temperature. However it is apparent (see Fig. 5.8) that longer-term temperature variations do correlate with variations in the frequency-averaged mean DGD.

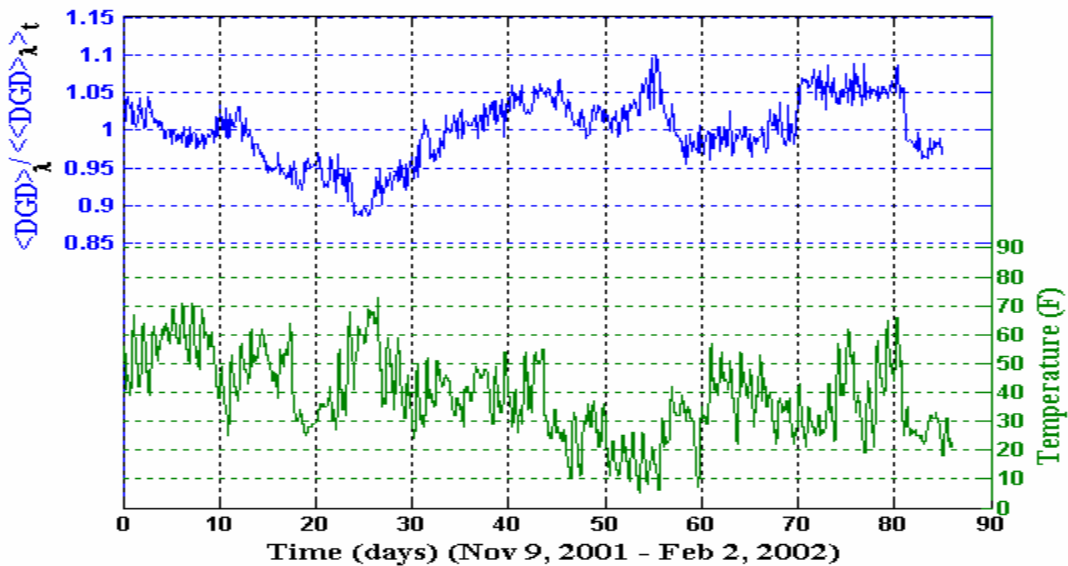


Fig. 5.8. Frequency-averaged DGD and temperature vs. time for fiber span 1.

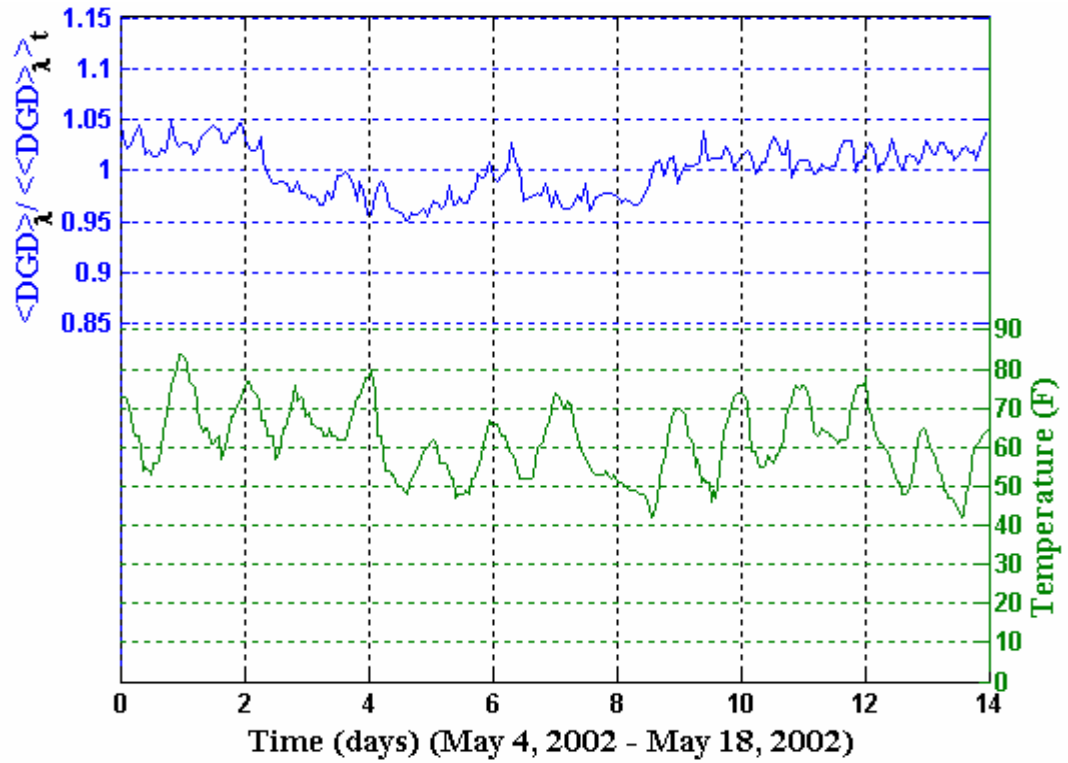


Fig. 5.9. Frequency-averaged DGD and temperature vs. time for fiber span 2.

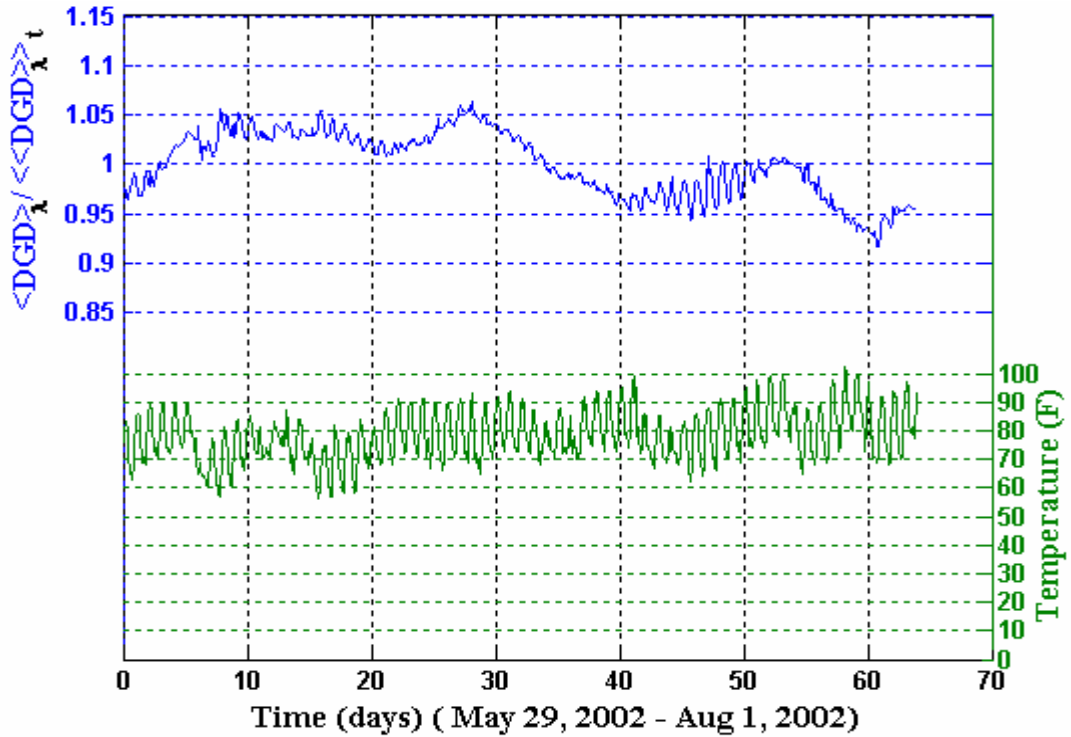


Fig. 5.10. Frequency-averaged DGD and temperature vs. time for fiber span 3.

### 5.2.5 Temporal drift properties of DGD

The drift time indicates the timescale over which the DGD changes. Furthermore, when outages occur, the outage duration will be related to the drift time. The drift time cannot be predicted or estimated from the known fiber parameters, since it depends on installation-specific data such as the amount of environmental perturbations and disturbances. The drift time is an important, individual characteristic parameter that should be measured together with the PMD for all fibers [8]. From a mathematical point of view, it is convenient to treat the drift in terms of autocorrelation function (ACF) [8] and so autocorrelation analysis was performed on the DGD time histories of the three fiber spans. Figs. 5.11, 5.12 and 5.13 show the normalized temporal ACFs of the frequency-averaged DGD data on the three fiber spans and their curve-fits using (5.2).

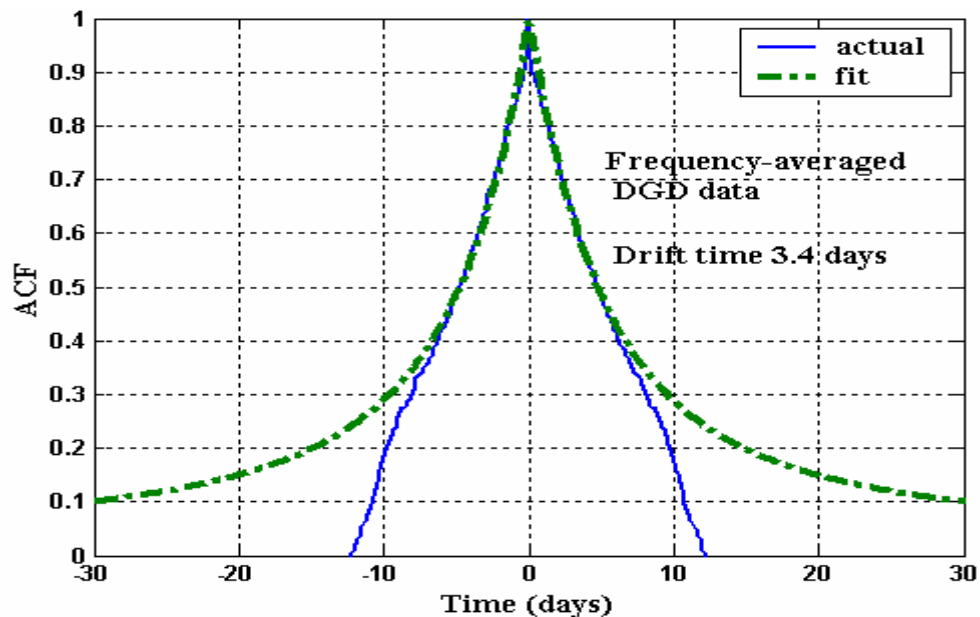


Fig. 5.11. Normalized temporal ACF of frequency-averaged DGD data on fiber span 1 and its theoretical curve-fit.

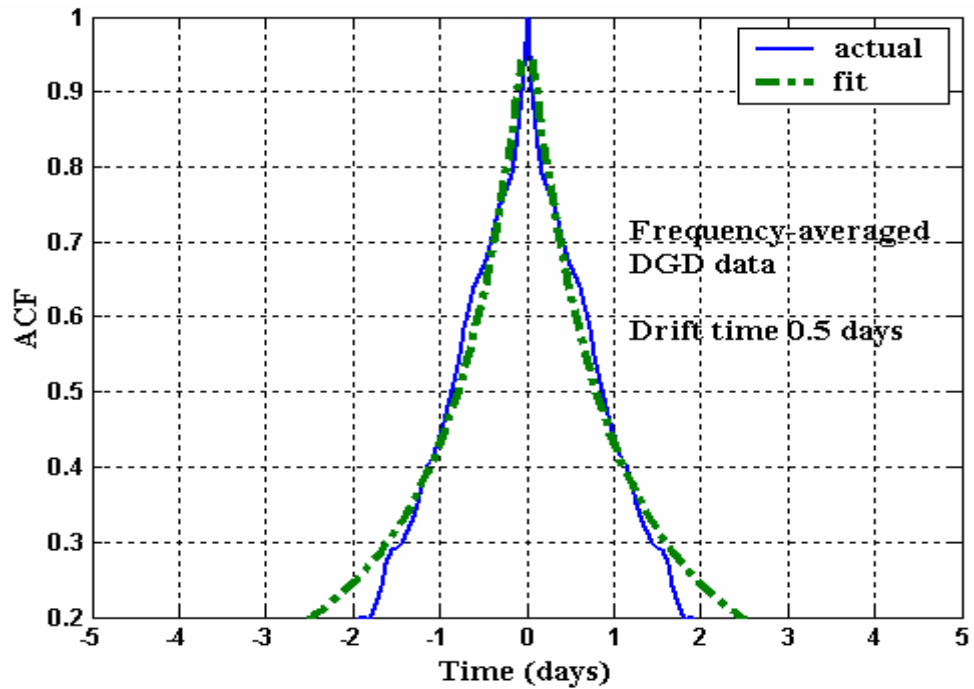


Fig. 5.12. Normalized temporal ACF of frequency-averaged DGD data on fiber span 2 and its theoretical curve-fit.

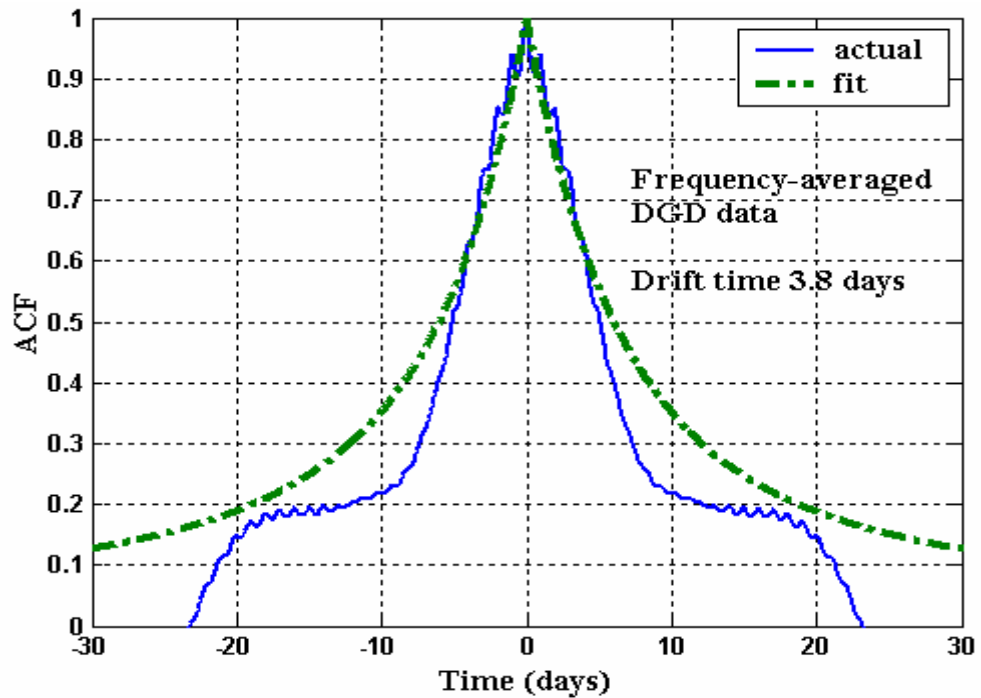


Fig. 5.13. Normalized temporal ACF of frequency-averaged DGD data on fiber span 3 and its theoretical curve-fit.

The drift times are obtained as 3.4 days for fiber span1, 3.8 days for fiber span 3, but only 0.5 days for fiber span 2, which seems to be a discrepancy. To verify this, we have repeated the autocorrelation analysis with fewer days of data from fiber spans 1 and 3. From that analysis we found that the drift time varied with the observation period, but we could not come up with proper reasoning for such type of behavior. This is one of the issues identified for future work.

### 5.2.6 Spectral behavior of DGD

To determine the DGD bandwidth, spectral autocorrelation analysis was performed on the normalized DGD spectral data. Figs. 5.14, 5.15, 5.17 show the resulting normalized spectral ACFs for the time-averaged DGD data (averaged over all the measurements) on the three fiber spans and also the curves representing theoretical spectral ACFs for DGD, with the form given by (5.3). However, to get the best theoretical fit for the actual data, the DGD variance term in (5.3) has been multiplied by a factor between 2.7 and 7.7.

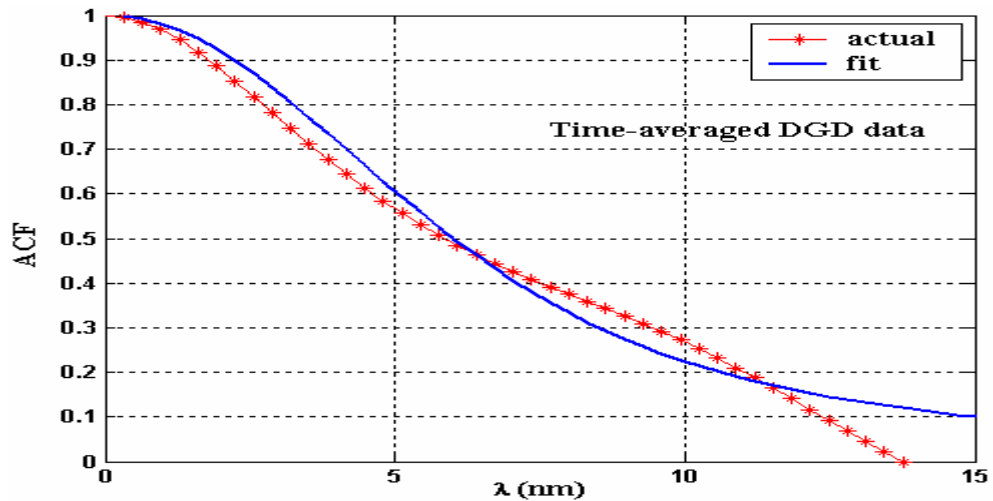


Fig. 5.14. Normalized spectral ACF of time-averaged DGD data from fiber span 1 and its adjusted theoretical curve-fit.

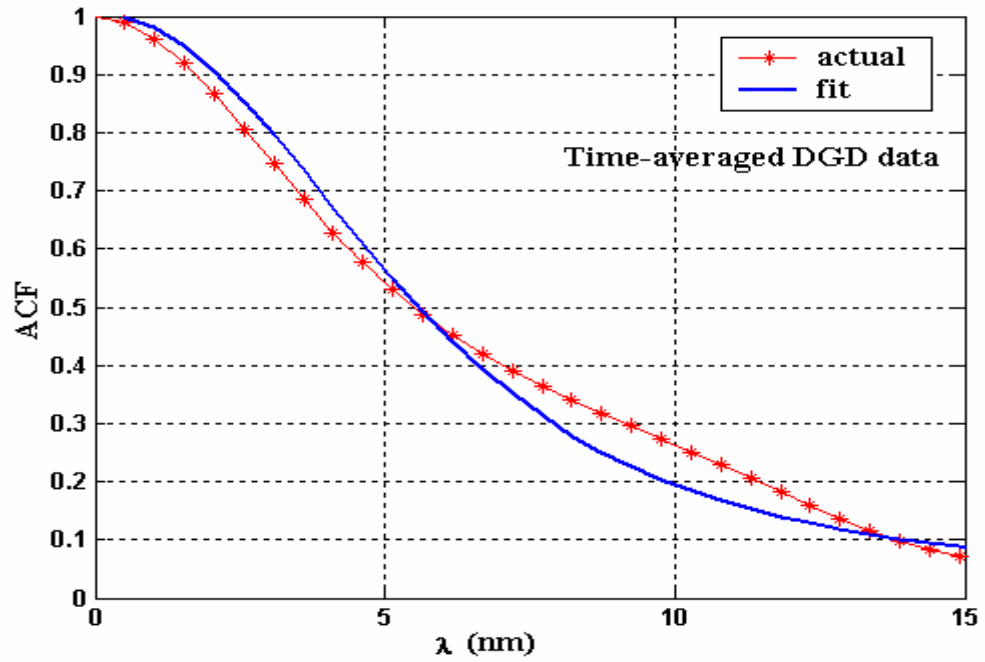


Fig. 5.15. Normalized spectral ACF of time-averaged DGD data from fiber span 2 and its adjusted theoretical curve-fit.

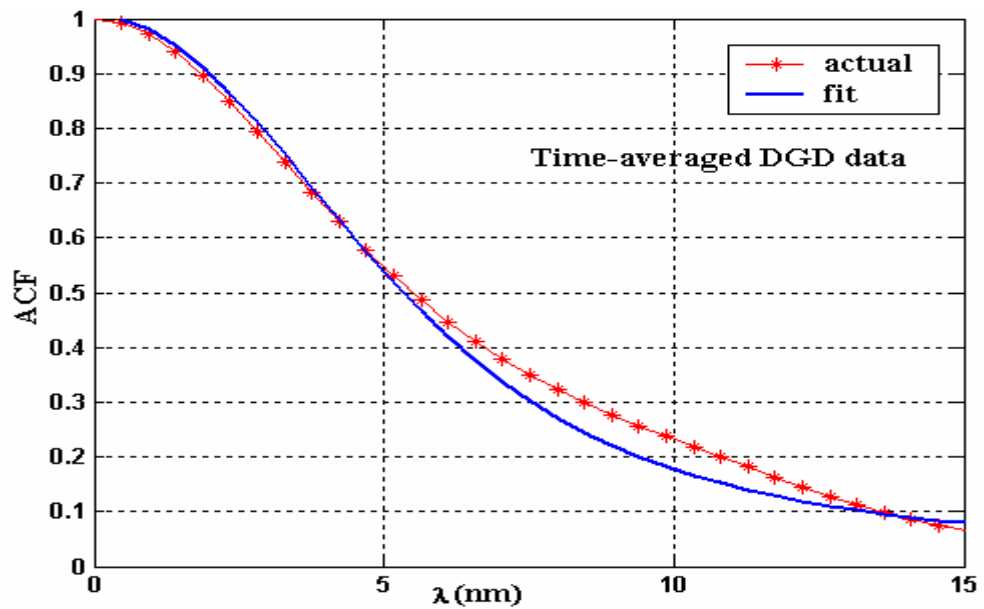


Fig. 5.16. Normalized spectral ACF of time-averaged DGD data from fiber span 3 and its adjusted theoretical curve-fit.

The importance of DGD bandwidth is that if an optical channel is affected by significant DGD, nearby channels within the DGD bandwidth may also experience the same effect. Theory and experiments [30] have demonstrated that the DGD bandwidth is inversely proportional to the mean DGD.

$$\omega_c = 4\sqrt{2} / \langle \Delta\tau \rangle \quad (5.19)$$

Thus fibers with a high mean DGD have a narrower DGD bandwidth than fibers with a low mean DGD. In Figs. 5.14, 5.15, and 5.16, the actual DGD bandwidth is masked and all those figures show a DGD bandwidth corresponding to a mean DGD of 1 ps. Thus for a fiber with a mean DGD of 1 ps, the predicted DGD bandwidth is 900 GHz which agrees well with bandwidth found using the spectral ACF fit in the above-mentioned figures.

### 5.2.7 System outage analysis

A detailed discussion of theoretical concepts of system outage analysis was presented in Sec. 5.1.5 and 5.1.6. Following that discussion, the outage probability  $P_{\text{out}}$ , is determined using the Maxwellian distribution, the mean outage rate  $R_{\text{out}}$  and the mean outage duration  $T_{\text{out}}$  are determined from the measured DGD data on all the three fibers.

Fig. 5.17. shows the calculated outage probability,  $P_{\text{out}}$ , and the mean outage rate,  $R_{\text{out}}$ , for a given system threshold relative to the mean DGD on the three fiber spans. Fig. 5.18. shows the calculated mean outage duration,  $T_{\text{out}}$ , as a function of system threshold relative to the mean DGD on the three fiber spans.

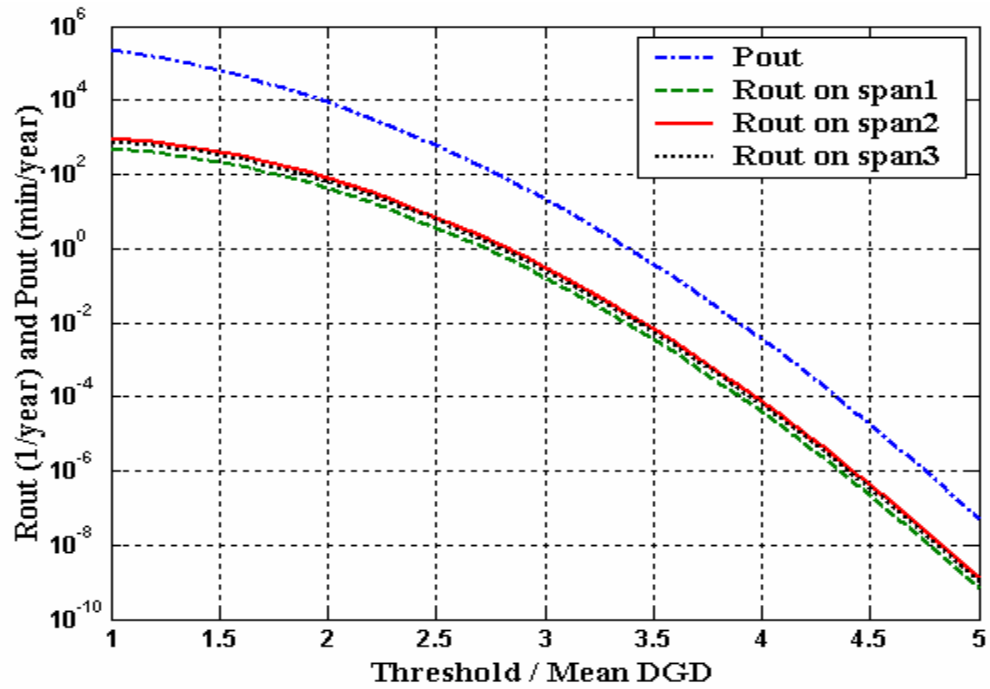


Fig. 5.17. Calculated outage probability,  $P_{out}$ , and mean outage rate  $R_{out}$ , versus threshold/mean DGD for the three fiber spans.

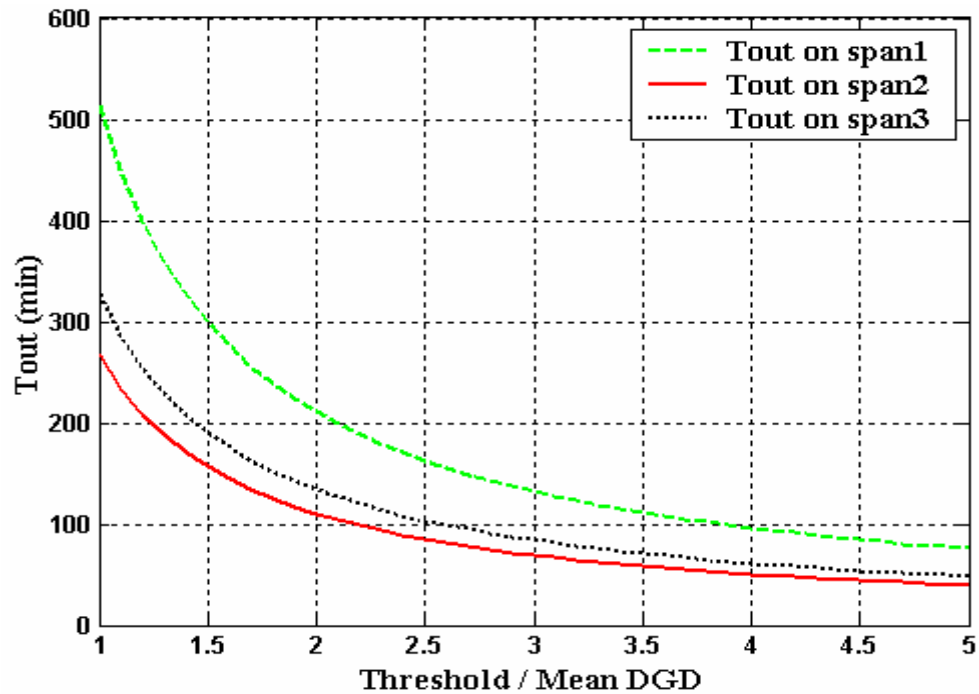


Fig. 5.18. Calculated mean outage duration,  $T_{out}$ , as a function of threshold/mean DGD for the three fiber spans.



From the above analysis, we have can estimate the mean time between outages (MTBOs) and mean outage durations for various DGD tolerances for these fiber spans. Table 5.1. lists these values for system thresholds of 3 and 3.7 times the mean DGD. Table 5.2 shows the values of  $P_{out}$ ,  $R_{out}$  and  $T_{out}$  for different values of threshold/mean DGD on fiber span1.

Table. 5.1. Predicted mean time between outages (MTBOs) and mean outage durations for different DGD tolerances.

	<b>3*<math>\langle</math>DGD<math>\rangle</math></b>	<b>3.7*<math>\langle</math>DGD<math>\rangle</math></b>
Span 1 MTBO Outage duration	6.39 years 136 min	1648 years 108 min
Span 2 MTBO Outage duration	3.25 years 69 min	833 years 55 min
Span 3 MTBO Outage duration	3.96 years 84 min	1021 years 67 min

For comparison, Nagel et al. [35] predicted that for the 114-km buried link they studied, the DGD will exceed three times its mean value once every 3.5 years and estimated mean outage duration of between 10 and 20 minutes for their link. From data measured on 37-km of buried cable, Caponi [31] predicted the DGD would exceed three times the mean DGD once every 2.5 years with mean outage duration of 56 minutes.

Table. 5.2. Values of  $P_{out}$ ,  $R_{out}$  and  $T_{out}$  for different values of threshold / mean DGD on fiber span 1.

DGD Margin, M	Outage Probability Threshold/ $\langle$ DGD $\rangle P_{out}$ (min/year)	Mean Rate $R_{out}$ (1/year)	Outage Mean Duration $T_{out}$ (min)	Outage
1.0	243046	461	527.0	
1.1	197138	427	461.6	
1.2	155591	379	410.3	
1.3	119480	324	369.1	
1.4	89268	266	335.3	
1.5	64893	211	307.2	
1.6	45901	162	283.4	
1.7	31594	120	263.0	
1.8	21162	86.2	245.4	
1.9	13796	60.0	229.9	
2.0	8754	40.5	216.4	
2.1	5407	26.5	204.3	
2.2	3251	16.8	193.5	
2.3	1903	10.4	183.8	
2.4	1084	6.20	175.0	
2.5	602	3.60	167.0	
2.6	325	2.04	159.7	
2.7	171	1.12	153.1	
2.8	87.7	0.597	146.9	
2.9	43.8	0.310	141.2	
3.0	21.3	0.156	136.0	
3.1	10.1	0.0768	131.1	
3.2	4.65	0.0367	126.5	
3.3	2.09	0.0171	122.3	
3.4	0.913	0.00772	118.3	
3.5	0.389	0.00340	114.6	
3.6	0.162	0.00146	111.1	
3.7	0.0654	6.07E-04	107.8	
3.8	0.0258	2.46E-04	104.6	
3.9	0.00990	9.74E-05	101.7	
4.0	0.00370	3.75E-05	98.9	
4.1	0.00135	1.40E-05	96.3	
4.2	4.80E-04	5.12E-06	93.7	
4.3	1.66E-04	1.82E-06	91.4	
4.4	5.60E-05	6.29E-07	89.1	
4.5	1.84E-05	2.12E-07	86.9	
4.6	5.89E-06	6.94E-08	84.9	
4.7	1.84E-06	2.22E-08	82.9	
4.8	5.59E-07	6.90E-09	81.0	
4.9	1.66E-07	2.09E-09	79.3	
5.0	4.82E-08	6.18E-10	78.0	

### 5.3 Long-term measurements of concatenated fiber spans

To study the behavior of PMD on fiber spans of greater length, experiments were conducted to measure the instantaneous DGD on two fiber spans concatenated with an EDFA in between, with an effective length of about 190 km. Three different combinations of the three individual fibers were used in the experiments. The measurement setup for these experiments is shown in Fig. 5.19.

Measurements of concatenated fiber spans were made at wavelengths from 1535 nm to 1565 nm and were repeated once every 23 minutes. Since EDFAs were used in the loop, the  $\lambda$ -band had been reduced to the EDFA band. Measurements were carried on for 18 days on fiber spans 1 and 2 concatenated together (Aug. 22, 2002-Sept. 9, 2002), for 21 days on fiber spans 2 and 3 concatenated together (Aug. 1, 2002-Aug. 22, 2002) and for 16 days on fiber spans 1 and 3 concatenated together (Sept. 27, 2002-Oct. 13, 2002).

#### 5.3.1 Measurement setup

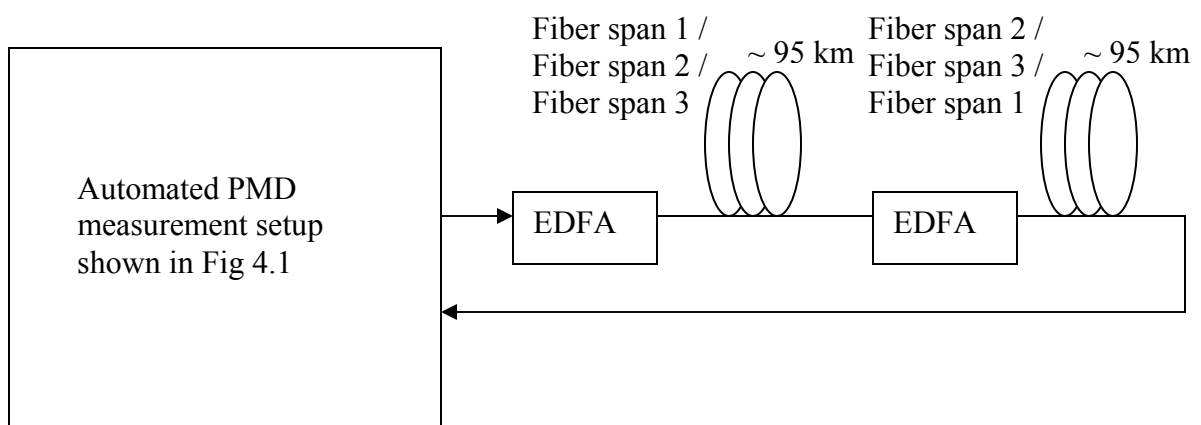


Fig. 5.19. Measurement setup for characterizing the concatenated fiber spans.

### 5.3.2. Plots of DGD vs. wavelength and time

Figs. 5.20, 5.21 and 5.22 show in color-coded format the normalized DGD measured on the three configurations of concatenated fibers respectively.

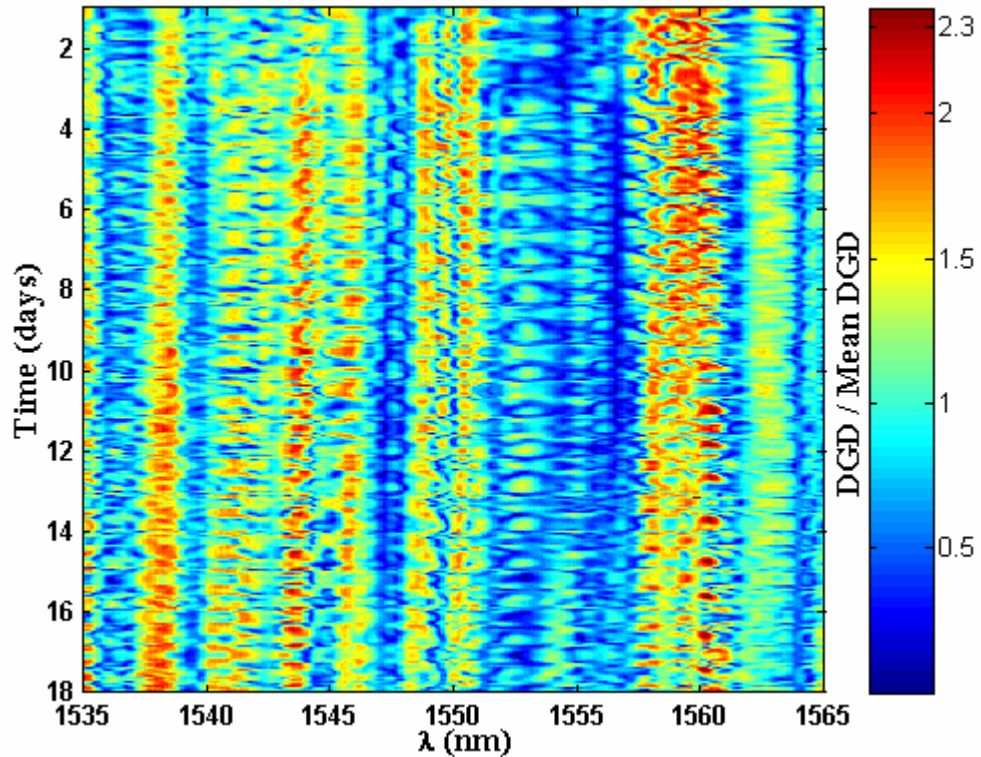


Fig. 5.20. Measured, normalized DGD vs. wavelength and time for fiber spans 1 and 2 concatenated (18 days).

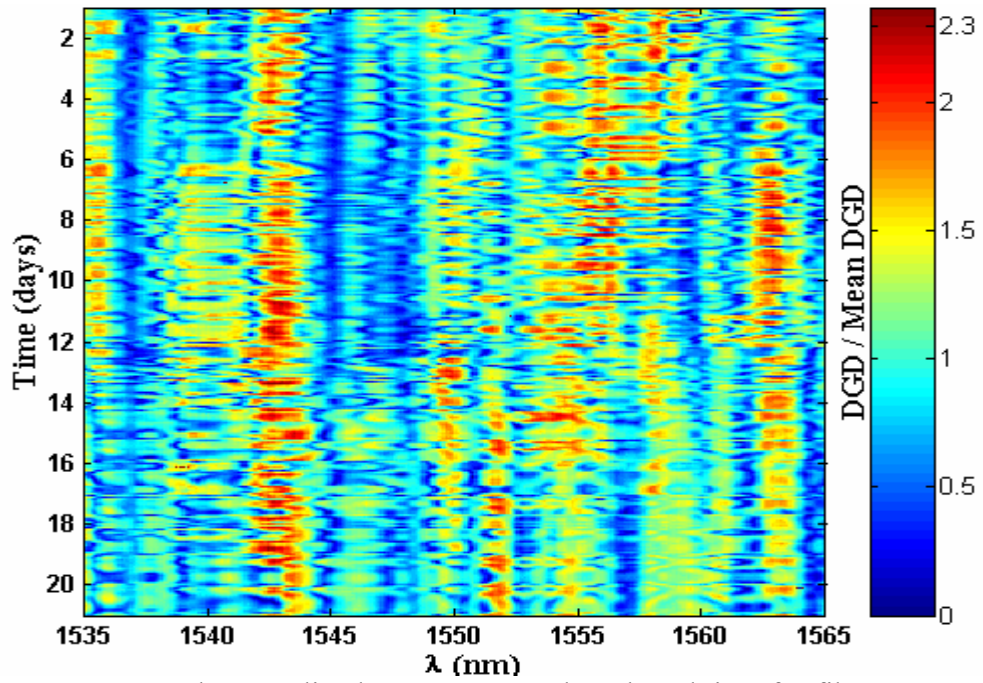


Fig. 5.21. Measured, normalized DGD vs. wavelength and time for fiber spans 2 and 3 concatenated (21 days).

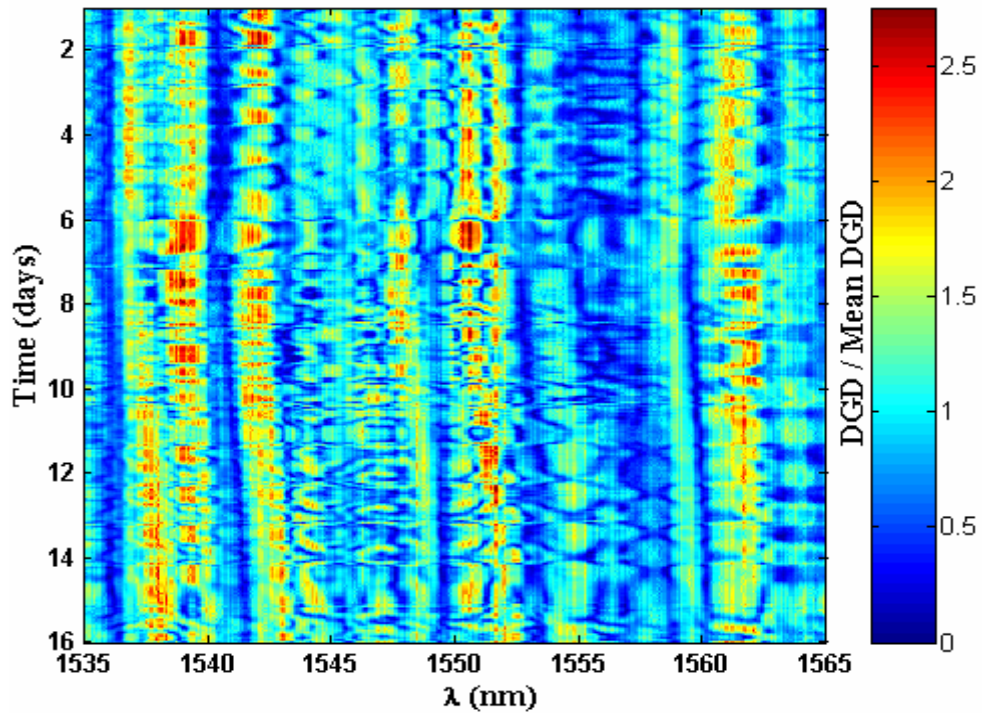


Fig. 5.22. Measured, normalized DGD vs. wavelength and time for fiber spans 1 and 3 concatenated (16 days).

It can be observed from the above color maps that the DGD on concatenated fiber spans changes with time and wavelength. However, unlike the individual fiber spans, the variation of DGD with time on concatenated fiber spans is more rapid. This might be due to the fact that on concatenated fibers, light is transmitted through the first buried fiber span, amplified at the end of first fiber span in the laboratory and then retransmitted through the second buried fiber span. The temperature of the laboratory was not maintained at a constant value and so it varied during the day. To observe any periodic variations in the DGD a discrete Fourier transform (DFT) of the DGD data is obtained and examined. Fig. 5.23 shows normalized DGD variations with time at 1560 nm wavelength on fiber spans 1 and 2 concatenated together. Fig. 5.24 shows the DFT of the DGD data (with mean value subtracted). It can be observed from Fig 5.24 that there are many periodic components, however, the 1-day component is the most dominant followed by the  $\frac{1}{2}$  day component. Even though the mean value is subtracted from the data, the DC component in Fig 5.24 is still relatively strong. This might be because of the variation of mean DGD over time. Similar observations were made at other wavelengths as well which showed similar results.

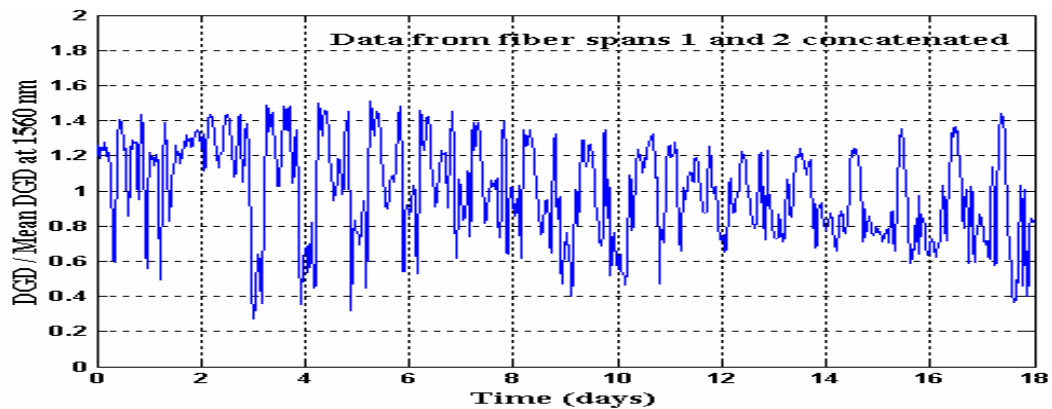


Fig. 5.23. DGD/Mean DGD vs. Time at 1560 nm on fiber spans 1 and 2 concatenated.

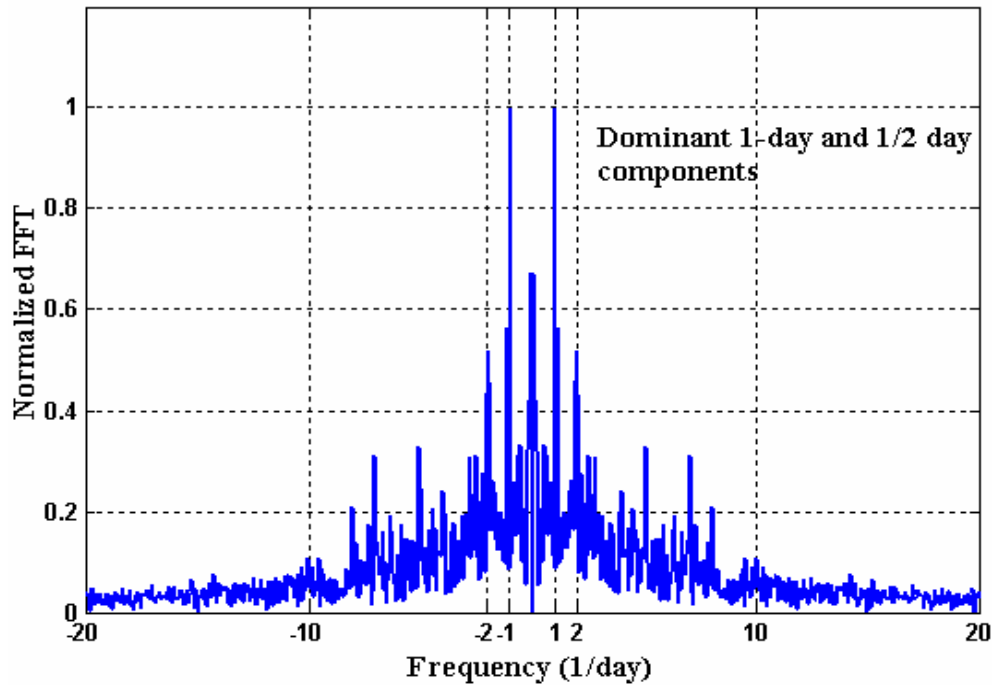


Fig. 5.24. DFT of DGD at 1560 nm with mean value subtracted from DGD data.

### 5.3.3 Histograms of measured DGD data

To verify the Maxwellian nature of the measured DGD, histograms of the normalized DGD data measured on the three configurations of concatenated fiber spans are obtained and are shown in Figs. 5.25, 5.26 and 5.27. Curves representing a Maxwellian distribution for a 1-ps mean DGD are also plotted for comparison. It can be observed from the figures that the histograms show a good agreement with the theoretical Maxwellian curve-fits.

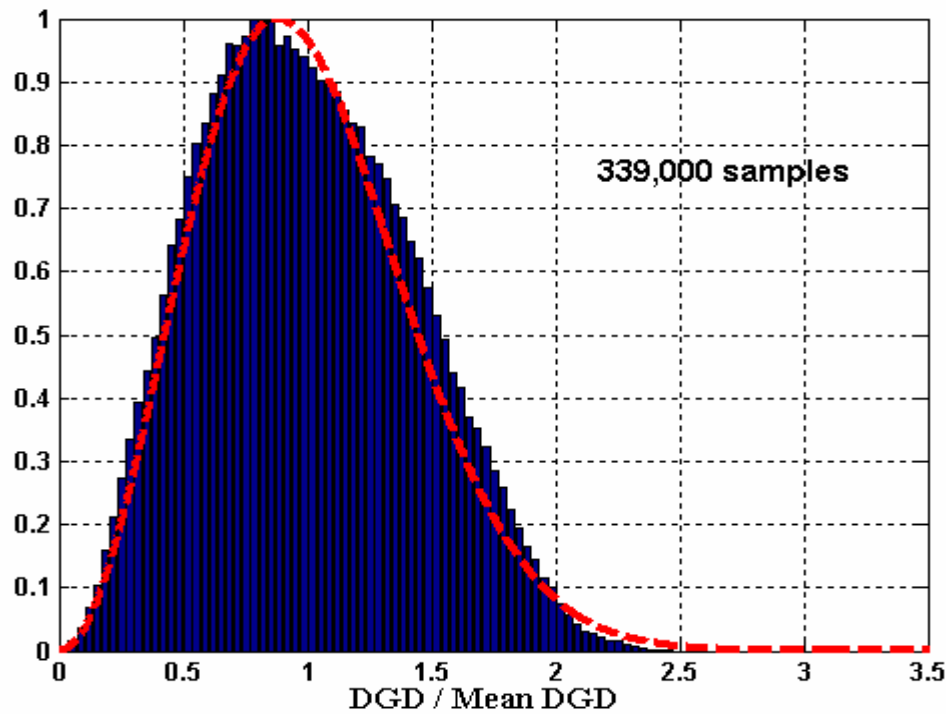


Fig. 5.25. Histogram of measured, normalized DGD data on fibers 1 and 2 concatenated.

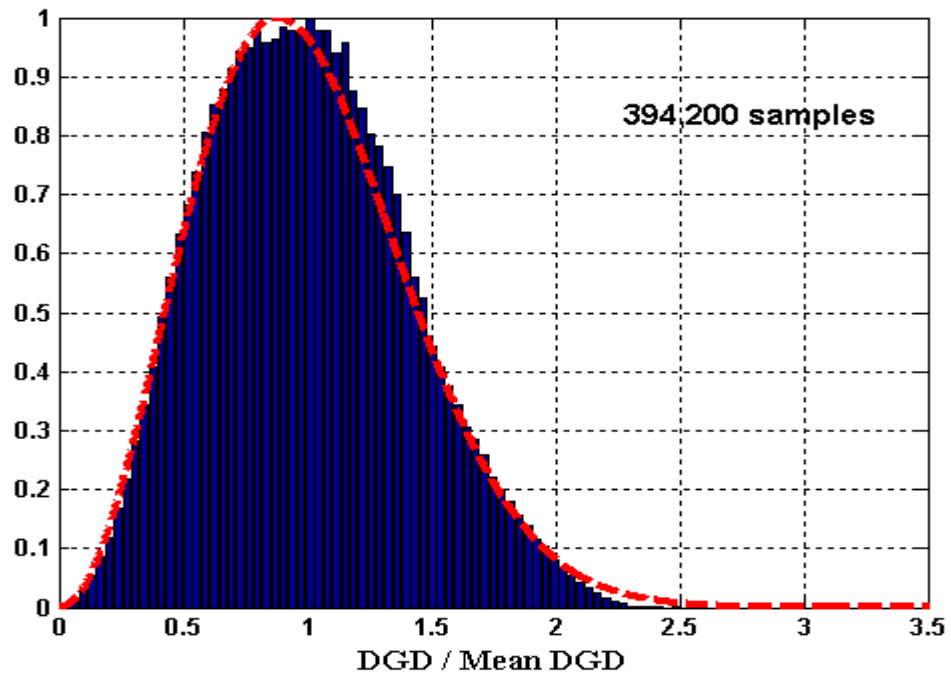


Fig. 5.26. Histogram of measured, normalized DGD data on fibers 2 and 3 concatenated.



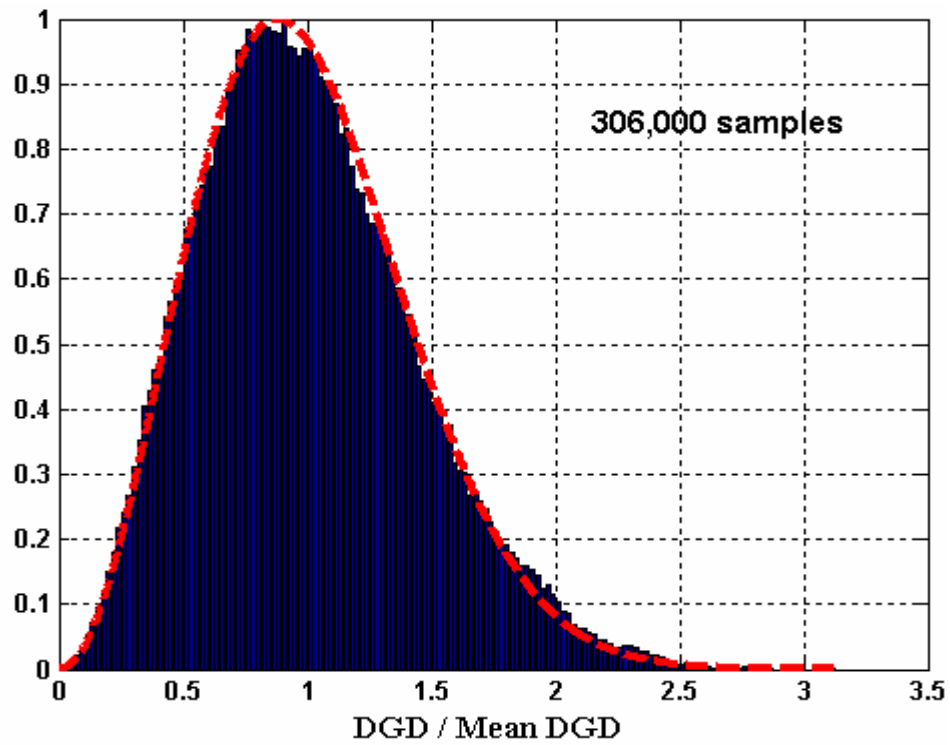


Fig. 5.27. Histogram of measured, normalized DGD data on fibers 1 and 3 concatenated.

### 5.3.4 Mean DGD variation with time

The variation of frequency-averaged DGD data, denoted as  $\langle \text{DGD} \rangle_\lambda$  normalized by the overall mean DGD, denoted as  $\langle \langle \text{DGD} \rangle_\lambda \rangle_t$  and temperature with time on the three concatenated fiber spans is shown in Figures 5.28, 5.29 and 5.30. The temperature shown in these plots is the hourly air temperature data for the region and not the laboratory temperature. It can be observed from the above-mentioned plots that the variation in frequency-averaged DGD on the fiber spans 1 & 2 and 1 & 3 concatenated is less than 10 % over the measurement period and is less than 20 % on the fiber spans 2 and 3 concatenated.

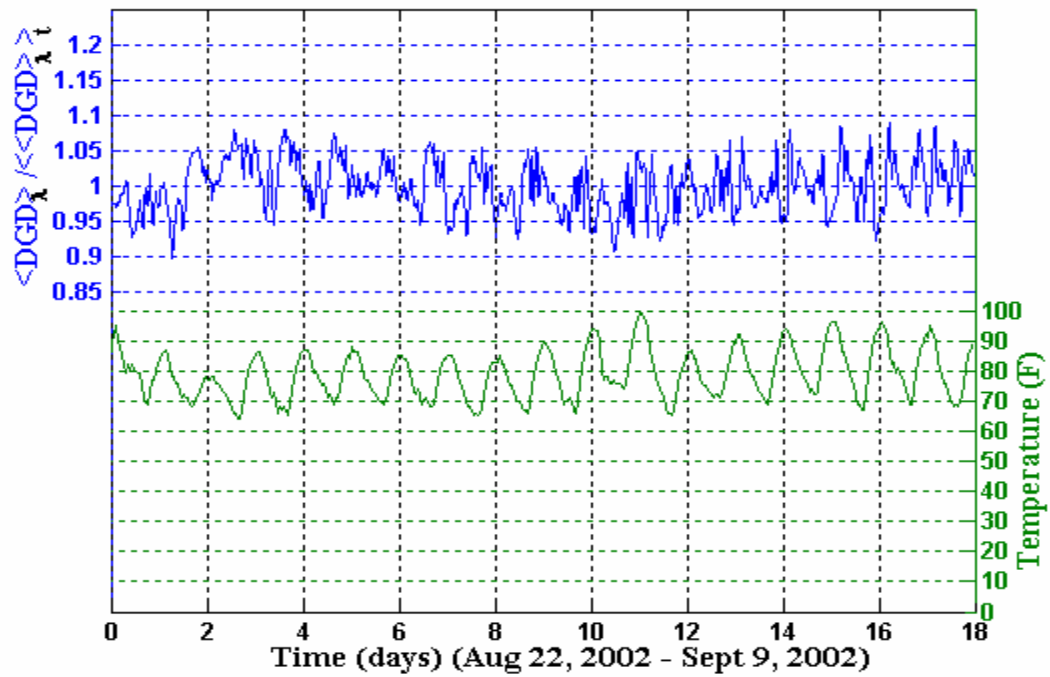


Fig. 5.28. Frequency-averaged DGD and temperature vs. time for fiber spans 1 and 2 concatenated.

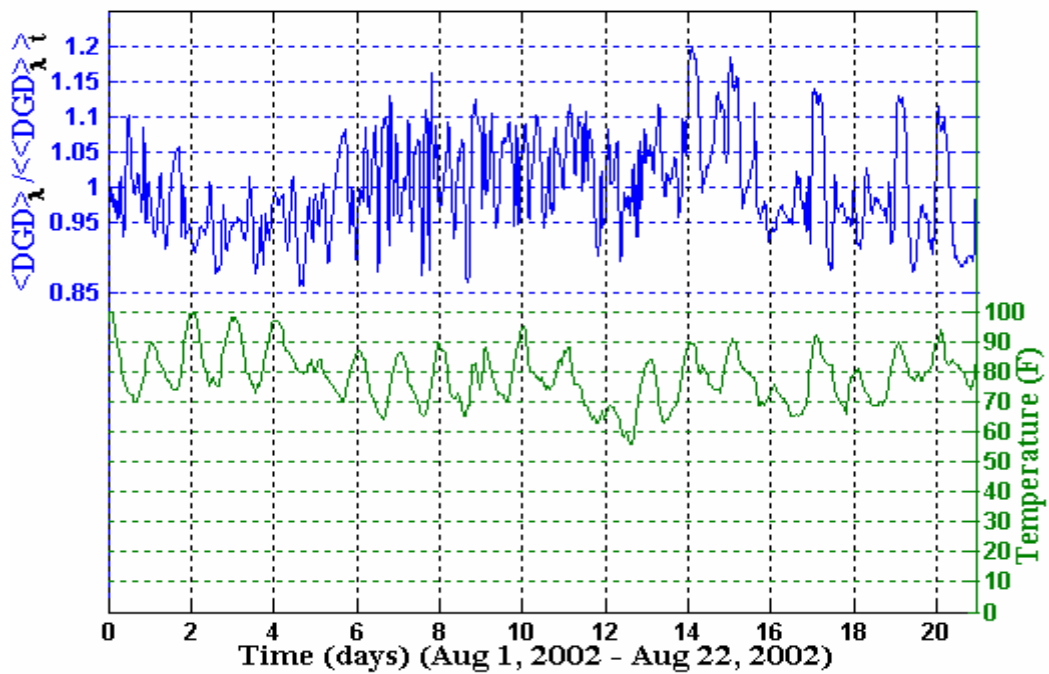


Fig. 5.29. Frequency-averaged DGD and temperature vs. time for fiber spans 2 and 3 concatenated.

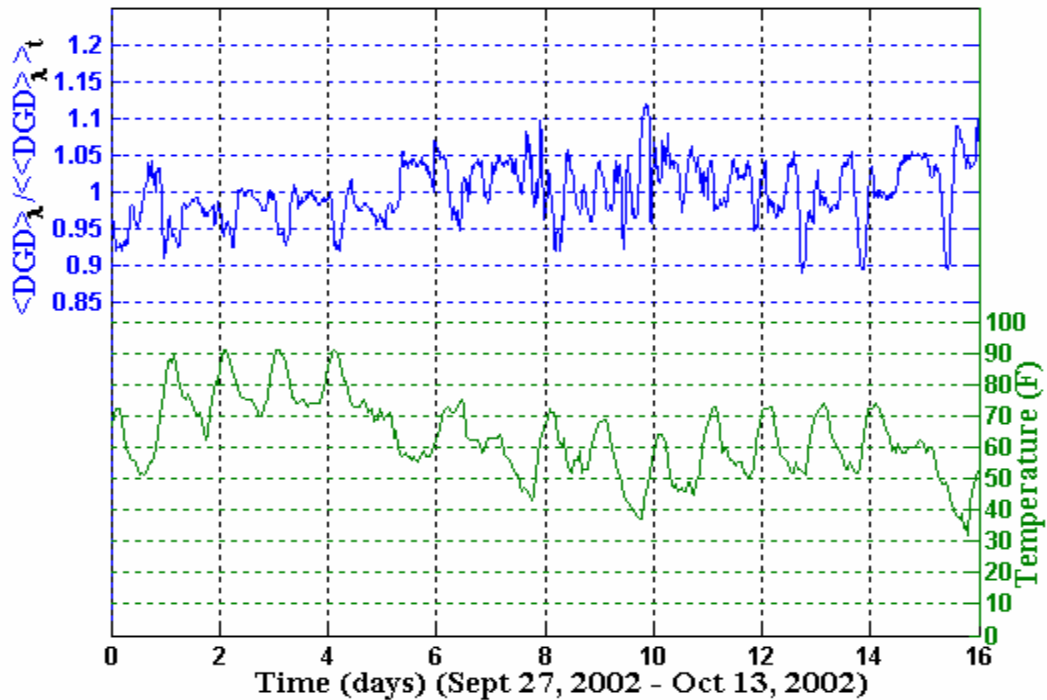


Fig. 5.30. Frequency-averaged DGD and temperature vs. time for fiber spans 1 and 3 concatenated.

### 5.3.5. Temporal drift properties of DGD

The DGD color maps on the concatenated fiber spans, shown in Sec. 5.3.2, indicate that the DGD is changing at a much faster rate than the case for individual fiber spans discussed in Sec. 5.2. This implies a much lower drift time for DGD on concatenated fiber spans. Temporal autocorrelation analysis similar to the one described in Sec. 5.2.5 was done on the DGD data from the concatenated links and the resulting ACFs are shown in Figs. 5.31, 5.32 and 5.33. As expected, the drift time on the concatenated links is observed to be low, however, the exact values shown in the figures may not be accurate owing to our observation that the drift times varied with the observation period. As mentioned before, this is one of the issues recommended for future work.

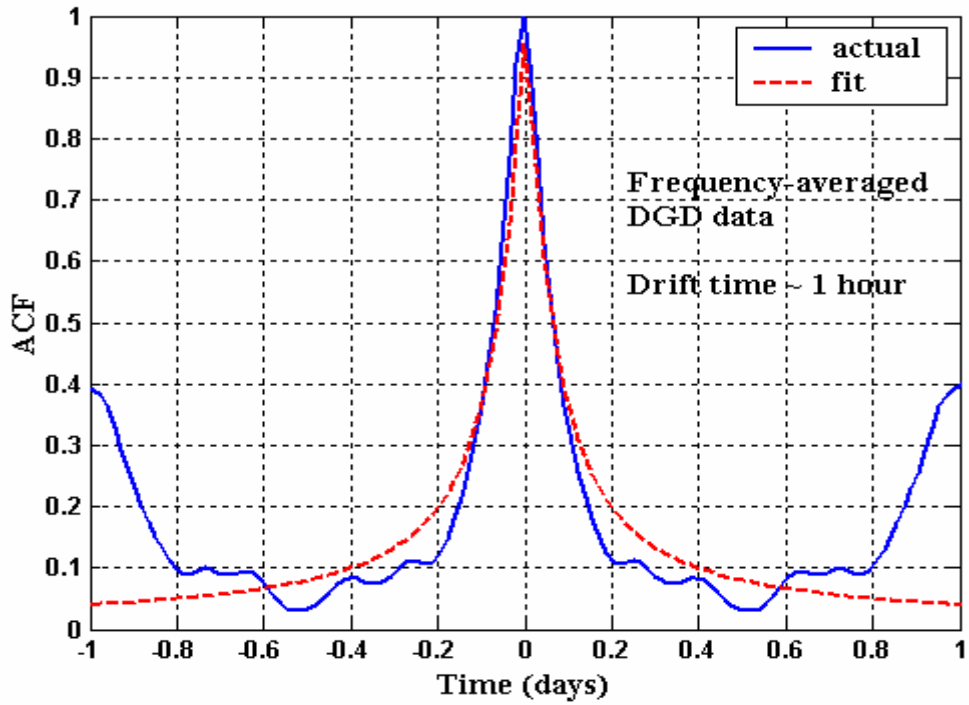


Fig. 5.31. Normalized temporal ACF of frequency-averaged DGD data on fiber spans 1 and 2 concatenated and its theoretical curve-fit.

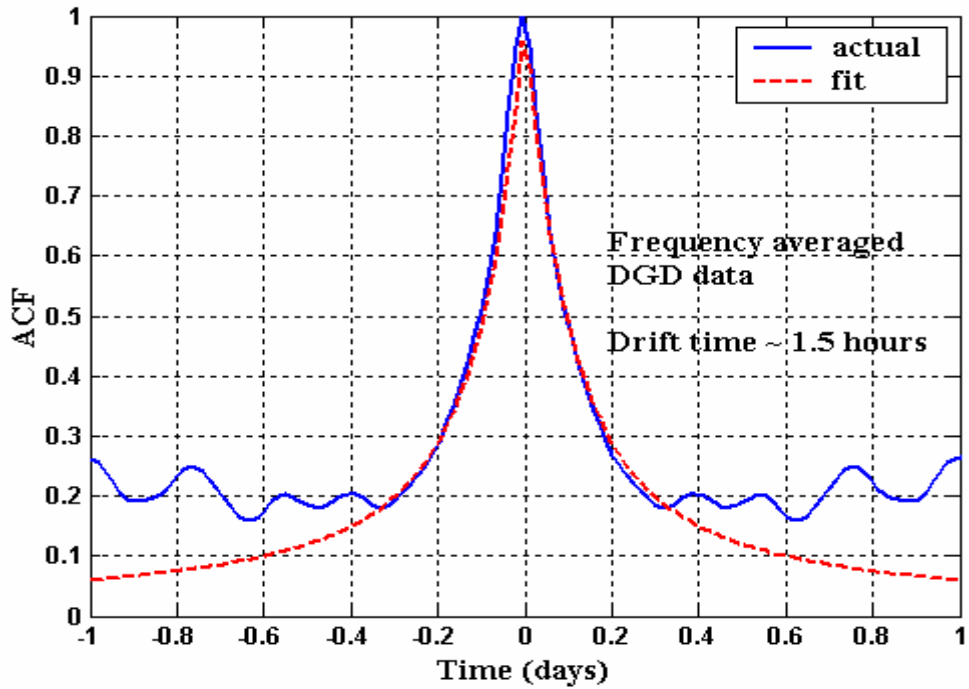


Fig. 5.32. Normalized temporal ACF of frequency-averaged DGD data on fiber spans 2 and 3 concatenated and its theoretical curve-fit.

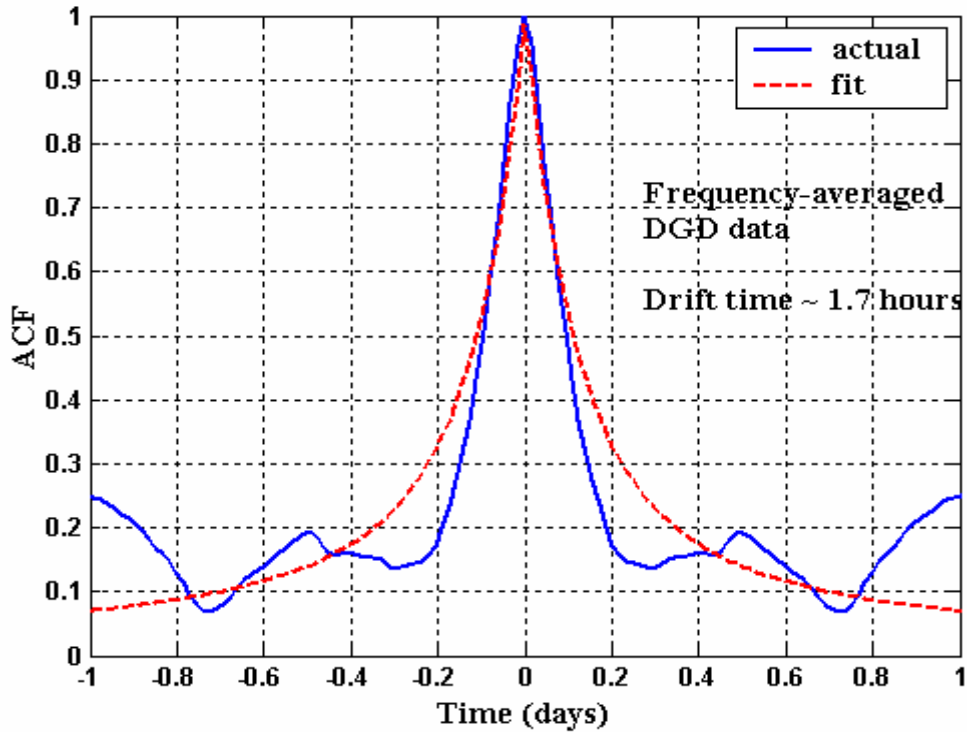


Fig. 5.33. Normalized temporal ACF of frequency-averaged DGD data on fiber spans 2 and 3 concatenated and its theoretical curve-fit.

### 5.3.6 Spectral behavior of DGD

Spectral autocorrelation analysis, described in Sec. 5.2.6, is repeated with the time-averaged DGD from the concatenated links. The ACFs obtained from the analysis are shown in Figs. 5.34, 5.35 and 5.36 along with their theoretical curve-fits with the form given by (5.3). However, to get the best theoretical fit for the actual data, the DGD variance term in (5.3) has been multiplied by a factor between 3.5 and 11.4. The actual values of the DGD bandwidth on all the concatenated fiber spans are masked so as to not to reveal the mean DGD of the fiber spans and so all the plots show a DGD bandwidth corresponding to a mean DGD of 1-ps.

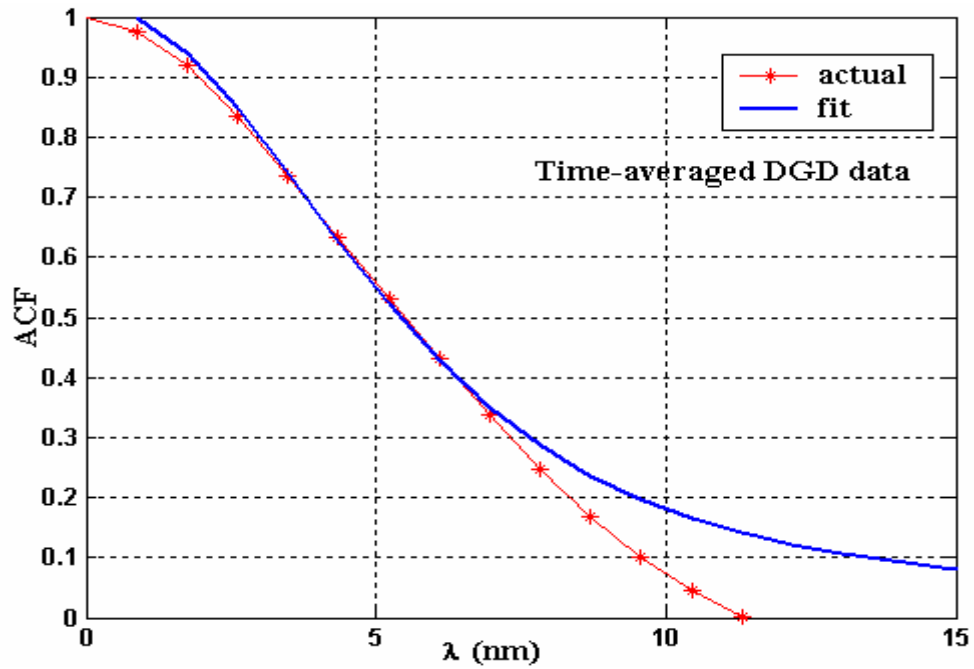


Fig. 5.34. Normalized spectral ACF of time-averaged DGD data on fiber spans 1 and 2 and its adjusted theoretical curve-fit.

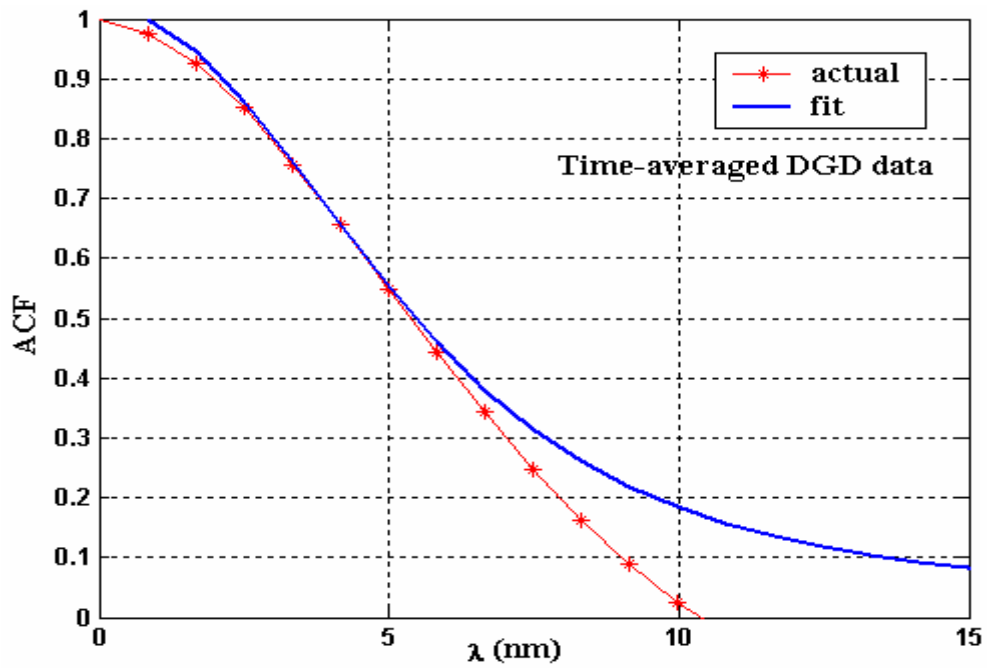


Fig. 5.35. Normalized spectral ACF of time-averaged DGD data on fiber spans 2 and 3 and its adjusted theoretical curve-fit.

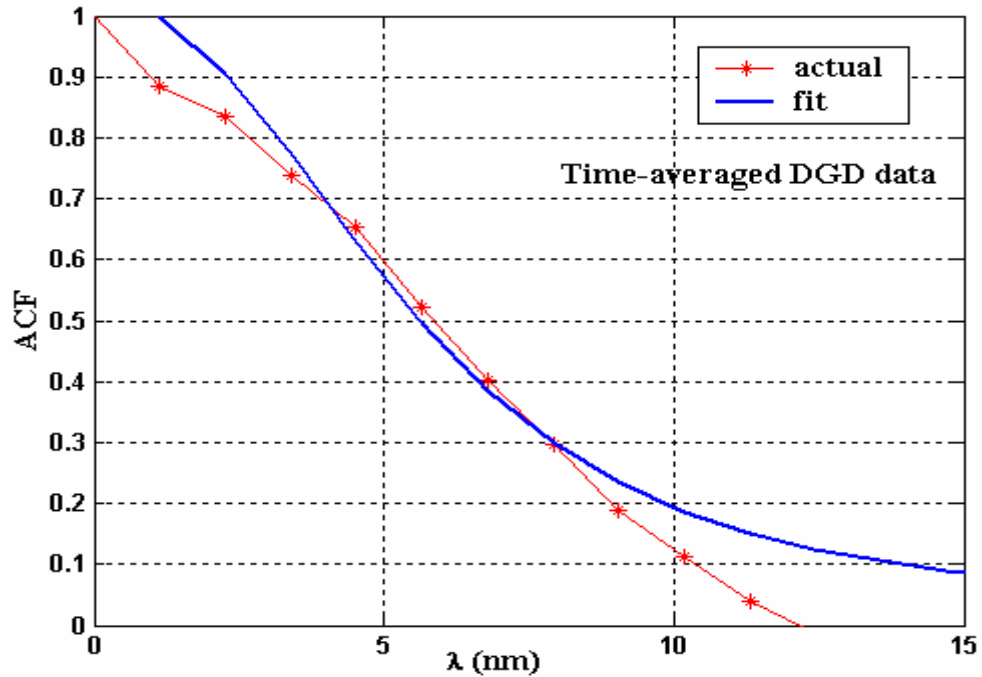


Fig. 5.36. Normalized spectral ACF of time-averaged DGD data on fiber spans 1 and 3 and it's adjusted theoretical curve-fit.

### 5.3.7 System outage analysis

The outage probability,  $P_{out}$ , for different threshold values is calculated from the Maxwellian distribution using (5.4). The mean outage rate,  $R_{out}$ , and the mean outage duration,  $T_{out}$ , for different threshold values are calculated from the DGD data measured on the concatenated fiber spans using (5.5) and (5.6) respectively. The calculated  $P_{out}$ ,  $R_{out}$  and  $T_{out}$  values as a function of normalized threshold are shown in Figs. 5.37 and 5.38. Table 3 lists the values of mean time between outages (MTBOs) and mean outage durations for system thresholds of 3 and 3.7 times the mean DGD.

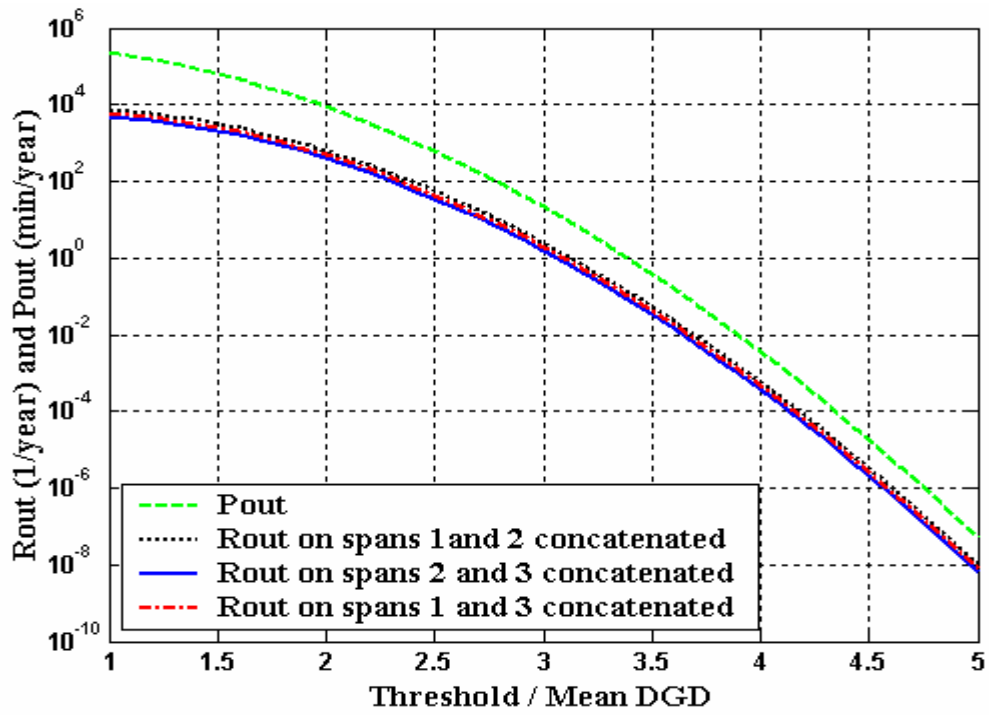


Fig. 5.37. Calculated outage probability,  $P_{out}$ , and mean outage rate  $R_{out}$ , versus threshold/mean DGD for the concatenated fiber spans.

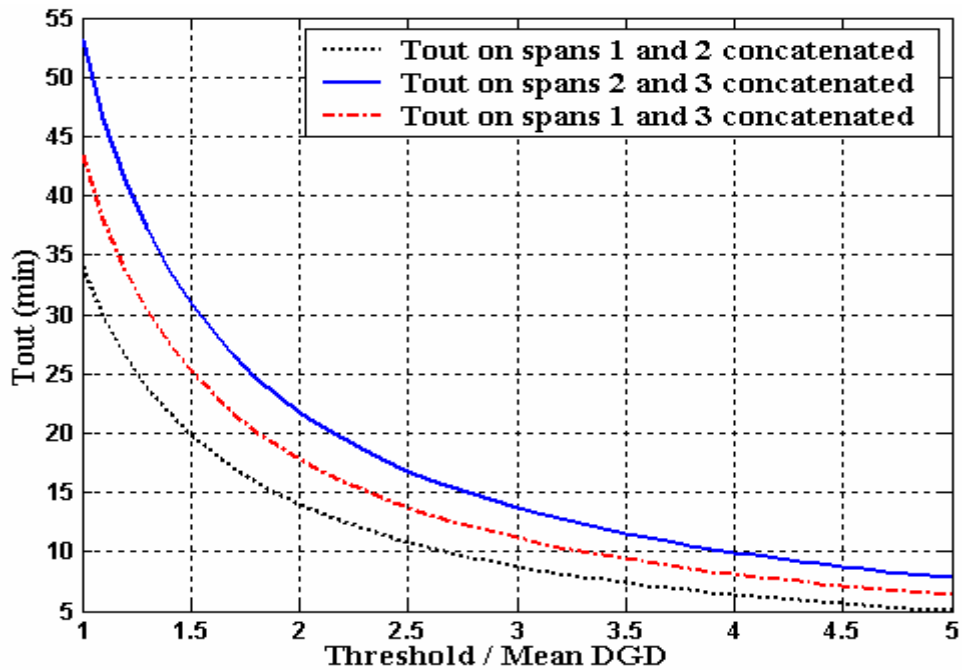


Fig. 5.38. Calculated mean outage duration,  $T_{out}$ , as a function of threshold/mean DGD for the concatenated fiber spans.



Table. 5.3. Predicted mean time between outages (MTBOs) and mean outage durations for different DGD tolerances.

	<b>3*⟨DGD⟩</b>	<b>3.7*⟨DGD⟩</b>
Span 1 and Span 2 MTBO Outage duration	0.413 years 9 min	106 years 7 min
Span 2 and Span 3 MTBO Outage duration	0.644 years 14 min	167 years 11 min
Span 1 and Span 3 MTBO Outage duration	0.525 years 11 min	135 years 9 min

A comparison of values from Table 5.3 with those of Table 5.1 shows that the outage rates are much higher for concatenated fiber spans than for individual spans and since outage probability is constant in both cases, the outage durations are correspondingly lower for the concatenated spans. In Sec. 5.3.2, from the color maps of the DGD we observed that the DGD varied at a much faster rate with time on concatenated fiber spans compared to the individual spans. As a result the chances of an outage occurrence also increases. On individual fiber spans, for example span 1, DGD drifted at a very slow rate and so it takes years to observe a high-DGD outage event (like 3.7 times the mean). On the other hand, since DGD drifted at a much higher rate on the concatenated fiber spans the rate occurrence of a high-DGD outage event is higher but the outage event lasts for a much shorter duration.

## 5.4. Design rules based on DGD margin

Based on the observations and analyses presented in this chapter, certain rules may be developed. An important parameter in making decisions regarding PMD in a network is the DGD margin, which is defined as the ratio between the receiver's DGD tolerance,  $\Delta\tau_{RX}$ , and the link mean DGD.

$$M_{\tau} = \frac{\Delta\tau_{RX}}{\langle\Delta\tau\rangle} \quad (5.20)$$

For cases where  $M_{\tau} > 3$  on single-span fibers, the frequency of PMD-induced outages will be low, and their duration may be brief. In these cases the approach proposed by Särkimukka [36] (in which some channels in a wavelength-division multiplexed (WDM) system are reserved for protection and when traffic on a channel starts to be distorted it can be redirected through those protection channels) may be viable. The instances when switching this traffic may be required will likely be infrequent (spanning years), and may only be required for several minutes or a couple of hours.

For cases where  $2 < M_{\tau} < 3$  on single-span fibers, PMD-induced outages may occur with a maximum frequency of one event every few days and a mean outage duration of 2 to 4 hours. For cases where  $M_{\tau} < 2$  on single-span fibers, chronic PMD-induced outages will result with durations of several hours. In these instances the option of applying PMD compensation, interrupting the link with a back-to-back terminal regenerator, or even replacing particular fiber segments may be appropriate.

## 5.5. Example scenarios (Single-span only)

### 1) 10-Gb/s, $\langle \Delta\tau \rangle = 10$ ps, receiver's DGD tolerance 40 ps

In this scenario the DGD margin,  $M_\tau$ , is 4. The probability of the DGD exceeding the receiver's DGD tolerance level is about  $7.4 \times 10^{-9}$ , or effectively zero. In this case it is quite unlikely a PMD-induced outage will ever be observed, and if one does occur its mean duration will be 100 minutes. The DGD bandwidth will be about 90 GHz or about 0.72 nm.

### 2) 10-Gb/s, $\langle \Delta\tau \rangle = 10$ ps, receiver's DGD tolerance 23 ps

In this case the margin,  $M_\tau$ , will be 2.3 meaning that the probability of the DGD exceeding the receiver's limit is about 0.37%. For our buried cable, PMD-induced outages typically will occur about once a month and with a mean duration of about three hours. The DGD bandwidth will again be about 90 GHz.

### 3) 40-Gb/s, $\langle \Delta\tau \rangle = 3.2$ ps, receiver's DGD tolerance 5.7 ps

The DGD margin,  $M_\tau$ , in this case is 1.8 so the probability of the DGD exceeding the receiver's limit is 4.4%. In this scenario PMD-induced outages typically will occur about every six days. The mean duration will be about 4 hours, however outages persisting for a day may occur. The DGD bandwidth is about 2.2 nm or 280 GHz so in a DWDM application with 100 GHz channel spacing, two or three channels may be affected during each outage.

## **6. Conclusions and Future work**

### **6.1 Conclusions**

An automated, long-term PMD measurement system, using a polarization analyzer, a tunable laser source and a PC, was configured, which measures DGD using the Jones Matrix Eigenanalysis (JME) method. Using this measurement system, measurements were made on three different 95-km fibers within a slotted-core, direct buried, standard single-mode fiber-optic cable. Through analysis of the measured DGD data, the statistical behavior of DGD was examined and predictions were made regarding the probability, frequency and duration of high-DGD occurrences. The color maps of DGD showed that DGD changes with time randomly and that high-DGD events are spectrally localized. The measured DGD data showed good agreement with Maxwellian distribution. The frequency-averaged mean DGD, in most cases, varied by about 10 % or less during the measurements. The drift times obtained from the DGD data measured for a very long time agreed well with those reported by others, however, it needs to be studied why the drift times varied with observation period. The DGD bandwidths estimated on different fiber spans agreed well with the bandwidths found using the theoretical spectral ACF fits.

For outages characterized by high DGD episodes (DGD more than three times the mean DGD), the mean time between outages and mean outage durations are similar for the three individual fibers. These values for concatenated fibers are different from those of the individual fibers but are similar to each other. Reports by others confirm our observation that DGD excursions of three or more times the mean

DGD are infrequent and relatively short lived. This finding is significant for network operators who must assess the impact of PMD on network reliability. A new parameter called, DGD margin (the ratio of the receiver's maximum tolerable DGD to the link's mean DGD) was defined and based on this parameter, different PMD mitigation approaches were suggested for different values of the parameter.

Also, this report presented a detailed discussion of various aspects of polarization-mode dispersion including its causes, behavior in short and long fibers, principal states model, the statistical nature and its impact on system performance. A brief description of different PMD emulation, simulation and mitigation techniques were presented. Further, various time-domain and frequency-domain PMD measurement methods were described.

## **6.2 Future work**

The research work presented in this report can be further extended to completely characterize DGD on buried fibers. First, the discrepancy in time autocorrelation analysis, i.e., the variation of drift time with observation period, should be studied. The variation of DGD with the fiber length can be studied by making measurements on buried fibers of different lengths. In our measurements on concatenated fiber spans, we amplified the optical signals using EDFAs in the lab and we observed some diurnal changes in DGD. It would be interesting to see whether the same behavior repeats using EDFAs buried in the ground along with the fiber spans. Also, it might take years and years to track changes in DGD on buried fibers over a

wide temperature range, instead, these experiments can be accelerated using a temperature chamber that can change the temperature over a wide range at a much faster rate. In this report we have presented the variation of DGD with wavelength, but our work did not include extensive study of second-order PMD. A detailed study of statistical nature of second-order PMD will be extremely useful. Also, the outage analysis can be repeated by including the second-order PMD data.

## REFERENCES

1. H. Kogelnik, R.M. Jopson, and L.E. Nelson, "Polarization-mode dispersion", *Optical fiber telecommunications: Systems and impairments*, Eds. I.P. Kaminov, and T. Li, San Diego: Academic press, vol. IV B, 2002.
2. C.D. Poole, and J. Nagel, "Polarization effects in lightwave systems," in *Optical Fiber Telecommunications*, Eds. I.P. Kaminov, and T.L. Koch, San Diego: Academic Press, vol. III A, 1997.
3. P. Hernday, "Dispersion measurements", *Fiber optic test and measurement*, Eds. D. Derickson, New Jersey: Prentice Hall PTR, 1998.
4. G.P. Agrawal, *Fiber optic communication systems*, New York: John Wiley & Sons, 1997.
5. G. Keiser, *Optical fiber communications*, Boston: McGraw-Hill Inc, 1999.
6. F. Kapron, A. Dori, J. Peters, and H. Knehr, "Polarization-mode dispersion: should you be concerned?" *NFOEC'96*, Denver, pp. 757-768, 1996.
7. J.P. Gordon, and H. Kogelnik, "PMD fundamentals: Polarization mode dispersion in optical fibers," *Proceedings of the National Academy of Science*, 97(9), pp. 4541-4550, 2000.
8. M. Karlsson, J. Brentel, and P.A. Andrekson, "Long-term measurement of PMD and polarization drift in installed fibers," *Journal of Lightwave Technology*, 18(7), pp. 941-951, 2000.
9. G.J. Foschini, L.E. Nelson, R.M. Jopson, and H. Kogelnik, "Probability densities of second-order polarization mode dispersion including polarization dependent

- chromatic-fiber dispersion,” *IEEE Photonics Technology Letters*, 12(3), pp. 293-295, 2000.
10. N. Gisin, and B. Huttner, “Combined effects of polarization mode dispersion and polarization dependent losses in optical fibers,” *Optics Communications*, 142, pp. 119-125, 1997.
  11. P. Lu, L. Chen, and X. Bao, “Polarization mode dispersion and polarization dependent loss for a pulse in single-mode fiber,” *Journal of Lightwave Technology*, 19(6), pp. 856-860, 2001.
  12. R. Khosravani, I.T. Lima Jr, P. Ebrahimi, E. Ibragimov, A.E. Willner, and C.R. Menyuk, “Time and frequency domain characteristics of polarization-mode dispersion emulators,” *IEEE Photonics Technology Letters*, 13(2), pp. 127-129, 2001.
  13. M.C. Hauer, Q. Yu, A.E. Willner, E.R. Lyons, C.H. Lin, A.A. Au, and H.P. Lee, “Compact, all-fiber PMD emulator using an integrated series of thin-film micro-heaters,” *OFC '02*, Anaheim, CA, ThA3, pp. 374-375, 2002.
  14. J.H. Lee, and Y.C. Chung, “Statistical PMD emulator using variable DGD elements,” *OFC '02*, Anaheim, CA, ThA4, pp. 375-376, 2002.
  15. I.T. Lima Jr., R. Khosravani, P. Ebrahimi, E. Ibragimov, A. E. Willner, and C. R. Menyuk, "Polarization mode dispersion emulator," *Proc. OFC 2000*, Baltimore, paper ThB4, pp. 31-33, 2000.
  16. I.T. Lima Jr., R. Khosravani, P. Ebrahimi, E. Ibragimov, C. R. Menyuk, and A. E. Wilner, “Comparison of polarization mode dispersion emulators,” *Journal of Lightwave Technology*, 19(12), pp. 1872-1881, 2001.



17. A.O. Dal Forno, A. Paradisi, R. Passy, and J.P.von der Weid, "Experimental and theoretical modeling of polarization-mode dispersion in single-mode fibers," *IEEE Photonics Technology Letters*, 12(3), pp. 296-298, 2000.
18. R.M. Jopson, L. E. Nelson, G. J. Pendock, and A. H. Gnauck, "PMD impairment in return-to-zero and nonreturn-to-zero systems," *Proc. OFC'99*, San Diego, CA, paper WE3, pp. 80-82, 1999.
19. R. Khosravani, and A. E. Willner, "Comparison of different modulation formats in terrestrial systems with high polarization mode dispersion," *Proc. OFC 2000*, Baltimore, paper WL5, pp. 201-203, 2000.
20. C. Xie, M. Karlsson, and P.A. Andrekson, "Soliton robustness to the polarization-mode dispersion in optical fibers," *IEEE Photonics Technology Letters*, 12(7), pp. 801-803, 2000.
21. C. Xie, M. Karlsson, P.A. Andrekson, and H. Sunnerud, "Robustness of dispersion-managed solitons to the polarization-mode dispersion in optical fibers," *IEEE Photonics Technology Letters*, 13(2), pp. 121-123, 2001.
22. A. Galtarossa, G. Gianello, C. G. Someda, and M. Schiano, "In-field comparison among polarization mode dispersion measurement techniques," *Journal of Lightwave Technology*, 14(1), pp. 42-49, 1996.
23. B.L. Heffner, "Automated measurement of polarization mode dispersion using Jones matrix eigenanalysis," *IEEE Photonics Technology Letters*, 4(9), pp. 1066-1069, 1992.
24. Tektronix tutorial on polarization mode dispersion available at <http://www.tektronix.com/Measurement/commtest/pmd/guide>

25. M.W. Chbat, "Mitigation of polarization mode dispersion," *LEOS'99*, San Francisco, paper TuB3, pp. 151-152, 1999.
26. M. Karlsson, "Polarization mode dispersion mitigation-performance of various approaches," *OFC '02*, Anaheim, CA, WI1, pp. 231-233, 2002.
27. D. Penninckx, and S. Lanne, "Reducing PMD impairments," *Proc. OFC'2001*, Los Angeles, CA, paper TuP1, 2001.
28. H. Sunnerud, C. Xie, M. Karlsson, R. Samuelsson, and P.A. Andrekson, "A comparison between different PMD compensation techniques," *Journal of Lightwave Technology*, 20(3), pp. 368-378, 2002.
29. H.Y. Pua, K. Peddanarappagari, B. Zhu, C. Allen, K. Demarest, and R. Hui, "An adaptive first-order polarization-mode dispersion compensation system aided by polarization scrambling: theory and demonstration," *Journal of Lightwave Technology*, 18(6), pp. 832-841, 2000.
30. M. Karlsson and J. Brentel, "Autocorrelation function of the polarization-mode dispersion vector," *Optics Letters*, 24(14), pp. 939-941, 1999.
31. R. Caponi, B. Riposati, A. Rossaro, and M. Schiano, "WDM design issues with highly correlated PMD spectra of buried optical fibers," *OFC '02*, Anaheim, CA, ThI5, pp. 453-455, 2002.
32. C. Allen, P.K. Kondamuri, D.L. Richards, and D.C. Hague, "Measured temporal and spectral PMD characteristics and their implications for network level mitigation approaches", *Proceedings of the IASTED International Conference on Wireless and Optical Communications*, Canada, pp. 713-720, July 2002 [Refer: Appendix B].

33. C. Allen, P.K. Kondamuri, D.L. Richards, and D.C. Hague, "Analysis and comparison of measured DGD data on buried single-mode fibers", *Symposium on Optical Fiber Measurements, NIST conference, USA*, pp. 195-198, Sept. 2002  
[Refer: Appendix. C].
34. A. Papoulis, *Probability, random variables, and stochastic processes*, New York: McGraw-Hill Inc, 1984.
35. J.A. Nagel, M. W. Chbat, L. D. Garrett, J. P. Soigné, N. A. Weaver, B. M. Desthieux, H. Bülow, A. R. McCormick, and R. M. Derosier, "Long-term PMD mitigation at 10 Gb/s and time dynamics over high-PMD installed fiber," *Proc. ECOC 2000*, Munich, Germany Vol. II (4.2.1), pp. 31-32, 2000.
36. S. Särkimukka, A. Djupsjöbacka, A. Gavler, and G. Jacobsen, "Mitigation of polarization-mode dispersion in optical multichannel systems," *J. Lightwave Technology*, 18(10), pp. 1374-1380, 2000.
37. "PMD specifications, JME method", *User's guide*, Agilent 8509C, pp. 9-4, 9-5, Agilent Technologies.
38. H.K. Pua, C. Allen, K. Demarest, R. Hui, K.V. Peddanarappagari, Sprint Communications Company, L.P., *Method and apparatus to compensate for polarization mode dispersion*, U.S. Patent 6,459,830 October 1, 2002.

# AUTOMATED DGD MEASUREMENTS USING POLARIZATION ANALYZER

## 1. Introduction

This report gives a detailed description of the measurement setup and the procedure used to make automated DGD measurements across a given wavelength band and over time using the Agilent lightwave polarization analyzer (PA). Jones Matrix Eigenanalysis (JME) method is used for making DGD measurements. This report assumes that the user knows how to use the Agilent PA. [If not the user is advised to go through the manual of PA first]. Also, the user should know how to compile and run Visual basic files.

## 2. Measurement Setup

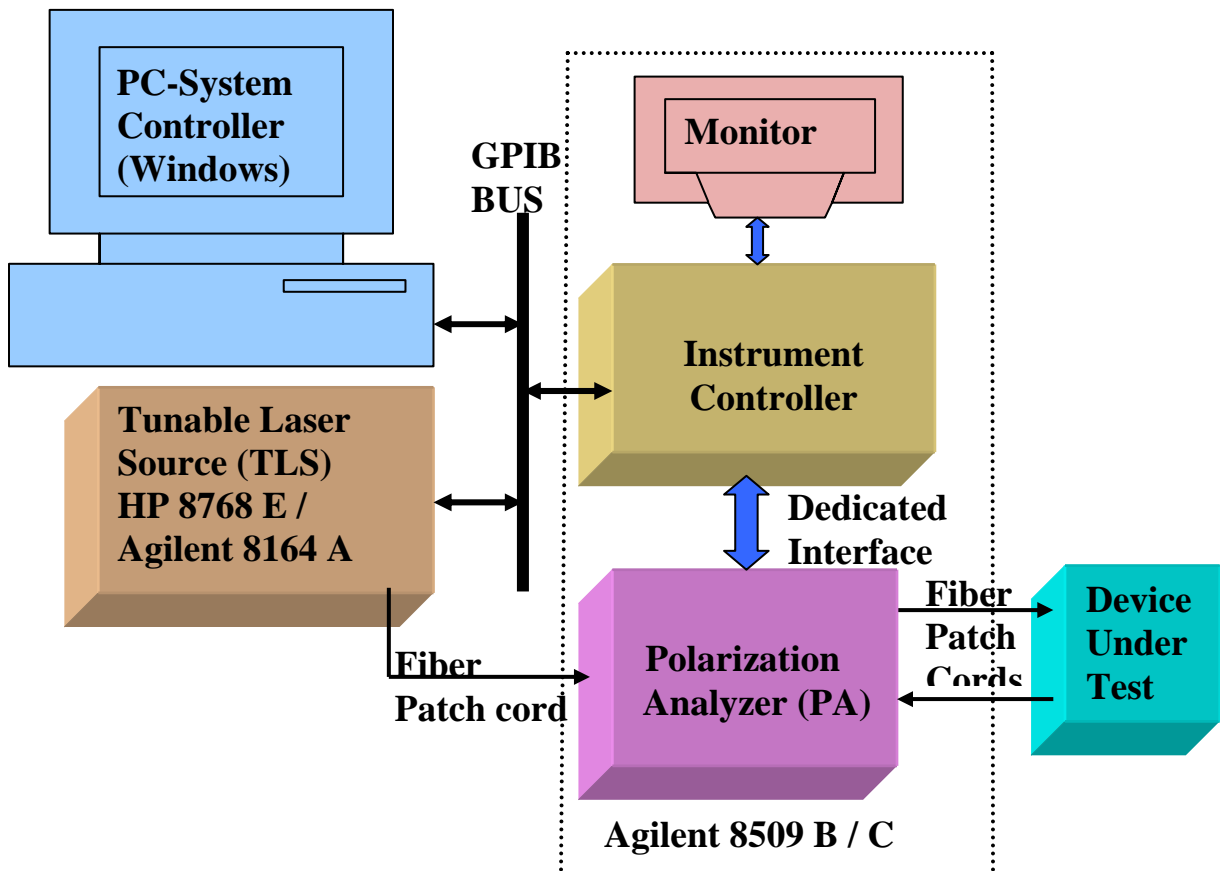


Fig 1. Measurement setup used for making automated DGD measurements.

## 2.1 Description

The Agilent PA shown in Fig 1 comes with an instrument controller, monitor, keyboard and a mouse. The PA and the instrument controller are connected using the dedicated interface cable provided by the vendor. The monitor, keyboard and the mouse are connected to the instrument controller using their respective cables. An external Tunable Laser Source (TLS) operating in the desired wavelength band, the instrument controller and the system controller PC (a Windows machine) used for automating the measurements are connected together using a common GPIB bus. Optical output from the TLS is fed into the 'external source input' of the PA and the input and output ends of the Device Under Test (DUT) are connected to the 'optical output' and 'optical input' of the PA using fiber patch cords.

The Agilent PA provides two methods to measure the DGD, namely JME method and Wavelength Scanning (WS) method. Using JME application of Agilent PA one DGD measurement in time across the specified wavelength band can be made. To repeat the measurements in time automatically another PC is used as a system controller. A Visual Basic (VB) application running on the system controller PC communicates with the instrument controller by sending device specific commands (refer PA manual) thereby controlling the operation of the PA. Using the system controller PC, after each across-the-band measurement (one full measurement across the specified wavelength band) in time the PA sits idle for a certain period (specified by the user at the start of the measurements, usually 1 minute or so) providing the user an option to exit the application. If the user does not exit the

application within the specified time interval the PA restarts the across-the-band measurement again. This process keeps repeating until the user stops the measurements. However, the user does not have the option of stopping the measurements when an across-the-band measurement is in progress (can only be stopped forcibly). The user has to wait until that particular measurement across the specified band is completed to stop the measurements.

## **2.2 Saving data**

When the measurements are in progress, the VB application running on the system controller PC will automatically open a text file for each across-the-band measurement in the current folder of the system controller PC with a file name 'JME -'date' -'time' and records the measured data. These text files can be opened using 'Notepad' or 'WordPad' applications. Each file has three columns separated by commas, first column is the wavelength in nm, second column is the instantaneous DGD in ps and the third column is the average DGD in ps up to that point in that particular across-the-band measurement. [The data in the third column is rarely used; it is the data in the second column that is of interest to the user.]

## **3. Measurement procedure**

*Step 1:* Connect the instruments as shown in Fig 1 and power up the instruments.

*Step 2:* Before starting the measurements, follow the method described in the Agilent PA (8509 B/C) user's manual to perform one-time adjustment of external source polarization. This step is important as the vendor recommends it for enhanced accuracy.

**Step 3:** Open the Agilent 8509B/C and HPIB2DDE applications by double clicking on the icons on the monitor screen that comes with the PA.

**Step 4:** On the systems controller PC, open a new folder [this is recommended so that all the data files will be saved in that folder] and copy the executable file of the VB application into that folder.

**Step 5:** Start the VB application by double clicking on the executable file. This will open a window showing a few instructions that the user should follow before starting the measurements.

Clicking 'OK' will open an input dialog box showing the fields: start wavelength (nm), stop wavelength (nm), delta (step size in nm), power level (dBm) and the time interval (minutes) between the measurements (explained in Sec 2.1) and their default values. It also shows two icons namely, 'start measurement' and 'exit'.

**Step 6:** The user should provide the required values in the fields and click on the 'start measurement' icon. After that the system controller PC will start communicating with the instrument controller and the measurements will start in a few seconds.

**Step 7:** While the measurements are in progress, a plot between the instantaneous DGD (ps) and wavelength (nm) is displayed on the monitor screen that comes with the PA. This plot is refreshed after each across-the-band measurement. Both the monitors can be switched off to save power.

**Step 8:** To stop the measurements the user has to wait until the current across-the-band measurement is completed after which the VB application running the systems

controller PC will provide an option for the user to exit the application. In case the user wants to stop the measurements in the middle, it can be done using the task manager (not recommended). The data collected till that moment will be saved in the file.

**Note:** Refer to the PA manual for the details about the uncertainty in the measurements using the JME method.

#### **4. Possible errors during measurements**

The following errors are observed rarely which will stop the measurements.

- a. Error writing to the polarization analyzer – This message will appear on the system controller PC monitor. When this occurs the measurements are stopped abruptly. The user has to restart the measurements.
- b. Power under range – This message appears on the monitor that comes with the PA usually at the start of the measurements. This implies the power input to the PA from the DUT is below the sensitivity of the PA. The user has to take necessary action (such as increasing power from TLS or using an optical amplifier etc.) and restart the measurements.

It's better to check often whether the measurements are running or stopped due to some error. That way the measurements can be restarted soon in case of an error without missing much data.

#### **5. Details about using VB software**

Two zipped folders, namely, 'PMD installer.zip' and 'Sourcecode.zip' are attached to this report.



The following are required to use the above software:

- a. National instruments GPIB board installed.
- b. NI-488.2 software installed (It comes with the GPIB board).
- c. Visual basic 6.0 compiler [Only if the source code is modified].

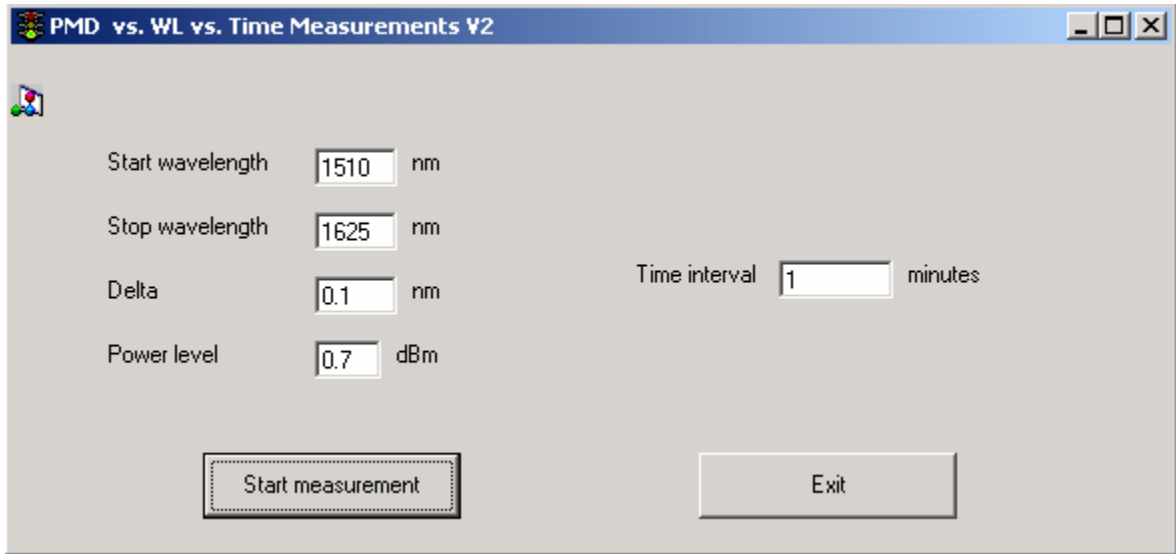
If the PMD installer folder is unzipped, it has a setup file in that. First the GPIB address of the PA has to be set to 29 and that of TLS to 24 (these are the values used in the code). Then if the setup file is run, it will install an executable file of the current version of the code. Now the user is ready to start the measurements with the specifications used in the code, namely, start wavelength is greater than 1510 nm, stop wavelength is less than or equal to 1635 nm, power level is between  $-20$  dBm and 6 dBm. If the user wants to use values within the above-mentioned ranges of wavelength and power he/she can straight away start the measurements and mention the desired values at the start of the measurements while prompted.

If the user wants to extend or change the above-mentioned ranges, modifications has to be made to the source code file (PMD-WL-Timev2.VPB, a visual basic project file which is located in the Sourcecode folder) and compile it again to get the executable file.

## 6. Sample measurement

A sample window of specifications and sample plot and data files of the measurements in lab are shown below.

### *Sample Specifications*

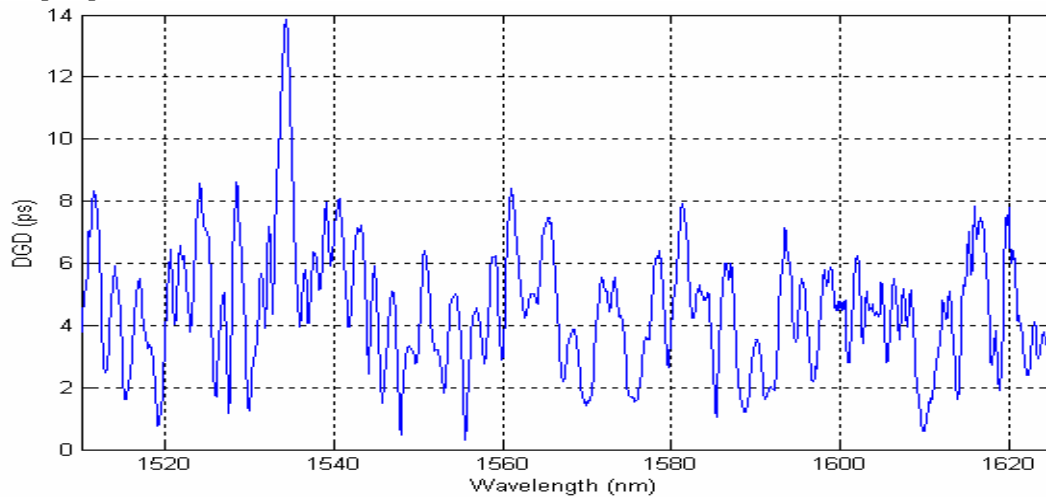


The screenshot shows a software window titled "PMD vs. WL vs. Time Measurements V2". It features a light gray background and a blue title bar. The window contains several input fields for measurement parameters:

- Start wavelength:  nm
- Stop wavelength:  nm
- Delta:  nm
- Time interval:  minutes
- Power level:  dBm

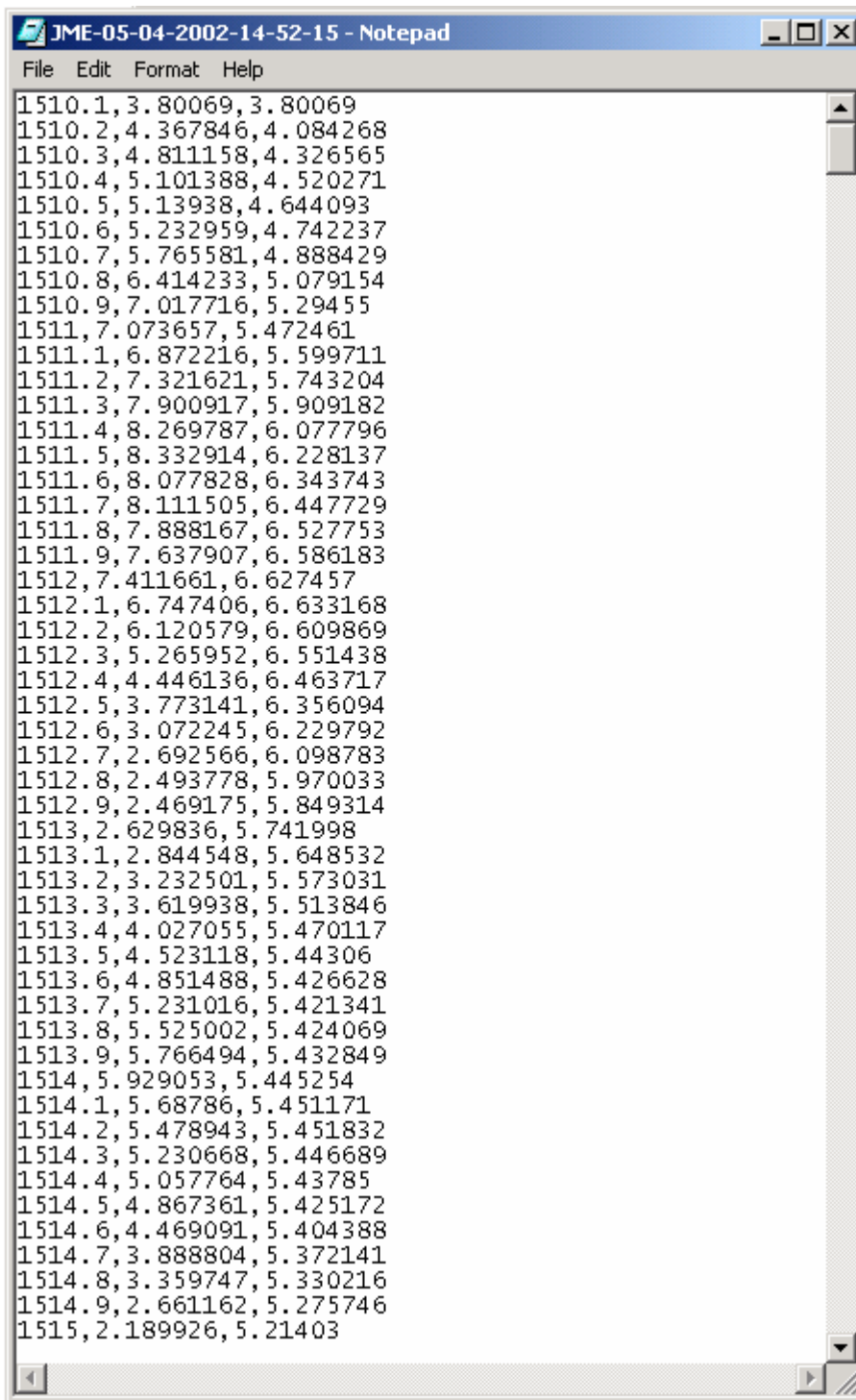
At the bottom of the window, there are two buttons: "Start measurement" (highlighted with a dashed border) and "Exit".

### *Sample plot*



The data corresponding to this plot is taken from the data file shown in the next page.

*Sample data file*



```
JME-05-04-2002-14-52-15 - Notepad
File Edit Format Help
1510.1,3.80069,3.80069
1510.2,4.367846,4.084268
1510.3,4.811158,4.326565
1510.4,5.101388,4.520271
1510.5,5.13938,4.644093
1510.6,5.232959,4.742237
1510.7,5.765581,4.888429
1510.8,6.414233,5.079154
1510.9,7.017716,5.29455
1511,7.073657,5.472461
1511.1,6.872216,5.599711
1511.2,7.321621,5.743204
1511.3,7.900917,5.909182
1511.4,8.269787,6.077796
1511.5,8.332914,6.228137
1511.6,8.077828,6.343743
1511.7,8.111505,6.447729
1511.8,7.888167,6.527753
1511.9,7.637907,6.586183
1512,7.411661,6.627457
1512.1,6.747406,6.633168
1512.2,6.120579,6.609869
1512.3,5.265952,6.551438
1512.4,4.446136,6.463717
1512.5,3.773141,6.356094
1512.6,3.072245,6.229792
1512.7,2.692566,6.098783
1512.8,2.493778,5.970033
1512.9,2.469175,5.849314
1513,2.629836,5.741998
1513.1,2.844548,5.648532
1513.2,3.232501,5.573031
1513.3,3.619938,5.513846
1513.4,4.027055,5.470117
1513.5,4.523118,5.44306
1513.6,4.851488,5.426628
1513.7,5.231016,5.421341
1513.8,5.525002,5.424069
1513.9,5.766494,5.432849
1514,5.929053,5.445254
1514.1,5.68786,5.451171
1514.2,5.478943,5.451832
1514.3,5.230668,5.446689
1514.4,5.057764,5.43785
1514.5,4.867361,5.425172
1514.6,4.469091,5.404388
1514.7,3.888804,5.372141
1514.8,3.359747,5.330216
1514.9,2.661162,5.275746
1515,2.189926,5.21403
```

# Measured temporal and spectral PMD characteristics and their implications for network-level mitigation approaches

Christopher Allen<sup>1</sup>, Pradeep Kumar Kondamuri<sup>1</sup>, Douglas L. Richards<sup>2</sup>, Douglas C. Hogue<sup>2</sup>

<sup>1</sup>Lightwave Communication Systems Laboratory, Information and Telecommunications Technology Center (ITTC)  
The University of Kansas, Lawrence, Kansas 66045  
voice 785-864-3017 fax 785-864-7789 callen@eecs.ukans.edu

<sup>2</sup>Sprint Corporation, Overland Park, Kansas

**Abstract**— Signal degradation due to polarization-mode dispersion (PMD) effects may become significant for signaling rates of 10 Gb/s, 40 Gb/s, and beyond. As expected, statistical analysis of variations in differential group delay (DGD) indicate that excursions from the mean DGD by factors of 3.7 or higher have very low probability. Temporal and spectral measurements of DGD were made on 95 km of buried standard SMF over an 86 day period to determine the distribution and rate of change of high DGD events. A drift time of about 3.4 days was found. The DGD data agree well with results of similar experiments reported in the literature. Coupling the drift time characteristic with the statistical behavior of DGD, we conclude that high-DGD episodes will be exceedingly rare and short lived. The impact of PMD on network operators is explored. Approaches are reviewed for network operators tasked with transporting high bit-rate channels over fiber links with known PMD characteristics.

## INTRODUCTION

In the phenomenon called polarization-mode dispersion (PMD), birefringence in the optical fiber provides two polarization-dependent group velocities for optical signals. In the high-coherence model of PMD (which assumes the coherence time of the light source is greater than the PMD-induced delays and no polarization-dependent loss) an input pulse will result in two orthogonally polarized pulses that preserve the shape of the original input pulse. The relative amplitudes of these two pulses is determined by the state of polarization (SOP) of the input pulse relative to the fiber's input principal states of polarization (PSPs). Thus for each pulse input, two pulses arrive at the receiver with different arrival times, called the differential group delay (DGD),  $\Delta\tau$ . This first-order model is frequency independent and is only valid over limited bandwidths. For wider bandwidths higher order effects must be considered resulting in frequency dependent polarization and dispersion [1], [2]. The bandwidth over which the PSPs can be assumed constant depend on the properties of the fiber and has been shown to vary inversely with the mean DGD,  $\langle\Delta\tau\rangle$  [3]. While the minimum bandwidth of the PSPs in single-mode fibers was found to be always over 50 GHz [3], this bandwidth for standard single-mode fiber is of the order of 100 GHz [1].

PMD may become a major impediment for network operators seeking to increase the per channel data rate on long-haul fiber-optic links. While the DGD in buried fiber had negligible impact at 2.5-Gb/s signaling rates, upgrades to

10 Gb/s, 40 Gb/s and beyond will require increasingly more attention. While there are PMD challenges facing carriers at 10 Gb/s, these challenges are not as severe as originally feared. Major carriers are successfully deploying 10 Gb/s dense-wavelength division multiplexed (DWDM) links across the core of their networks. A marked improvement in the DGD tolerance of 10 Gb/s long-reach receivers (to about 40 ps) will likely satisfy most length demands, obviating the need for PMD compensation (PMDC). Signaling rates of 40 Gb/s and beyond will most likely require some form of mitigation in long-haul applications, such as robust modulation schemes or PMDC.

To ensure signal quality on their fiber at higher bit rates, network engineers must anticipate the impact of PMD on the various fiber routes. Design of a reliable network requires a good model of the PMD characteristics on each link. An understanding of the variability of both the DGD and the PSPs is required to specify appropriate transmission parameters. Factors such as the mean DGD, PMD correlation time and bandwidth, as well as second-order effects together with performance prediction models can provide this understanding.

While PMD is a vector quantity, with a magnitude (DGD) and a direction (PSP), we are deliberately focusing exclusively on DGD as this is a readily measured parameter on installed optical networks. The statistical distribution and behavior of PSPs has been extensively studied and reported elsewhere.

## PMD STATISTICS

### Mean DGD

For long optical fibers, the PMD figure of merit typically specified is its mean DGD,  $\langle\Delta\tau\rangle$ , (having units of ps) or its PMD coefficient,  $\langle\Delta\tau\rangle/\sqrt{L}$ , (having units of ps/ $\sqrt{\text{km}}$ ) where  $L$  is the fiber length. The PMD for an installed (buried) fiber-optic cable is dominated by the inherent PMD of the bare fiber; however, the level of relaxation provided by the cabling and installation techniques also affect PMD. While the PMD in bare fiber is determined largely by the core-cladding concentricity achieved during manufacture, we have found that loose-tube cabling results in a lower PMD than other cabling methods, such as slotted core cabling. In addition, mechanical stresses introduced during cable installation (burial) also contribute to the PMD and will be affected by the installation practices used and whether the cable is in a protective conduit.

The mean DGD for a given fiber is a constant that represents both the average of DGD values at one time across a broad spectral bandwidth

$$\langle \Delta\tau \rangle = \frac{1}{N_\lambda} \sum_{i=1}^{N_\lambda} \Delta\tau(\lambda_i, t) \quad (1)$$

and the average of DGD values for a single wavelength over a long time period

$$\langle \Delta\tau \rangle = \frac{1}{N_t} \sum_{i=1}^{N_t} \Delta\tau(\lambda, t_i) \quad (2)$$

where  $\Delta\tau(\lambda, t)$  is the DGD value at wavelength  $\lambda$  and time  $t$ . Although the mean DGD for an installed fiber is constant, changing environmental factors (e.g., temperature) cause the instantaneous DGD at a given wavelength,  $\Delta\tau(\lambda, t)$ , to vary randomly about that mean.

When various fiber segments are concatenated to form a single long fiber, the mean DGD of the overall fiber is found by

$$\langle \Delta\tau_{\text{total}} \rangle = \sqrt{\sum_{i=1}^N \langle \Delta\tau_i^2 \rangle} \quad (3)$$

where  $N$  is the number of segments.

### Maxwellian distribution

The DGD for a given wavelength at any moment in time,  $\Delta\tau(\lambda, t)$ , is a random variable with a Maxwellian probability density function [4,5]

$$p(\Delta\tau) = \sqrt{\frac{2}{\pi}} \frac{\Delta\tau^2}{\sigma^3} e^{\left(\frac{-\Delta\tau^2}{2\sigma^2}\right)} \quad (4)$$

for  $0 < \Delta\tau < +\infty$ , where

$$\langle \Delta\tau \rangle = \sigma \sqrt{8/\pi} \quad (5)$$

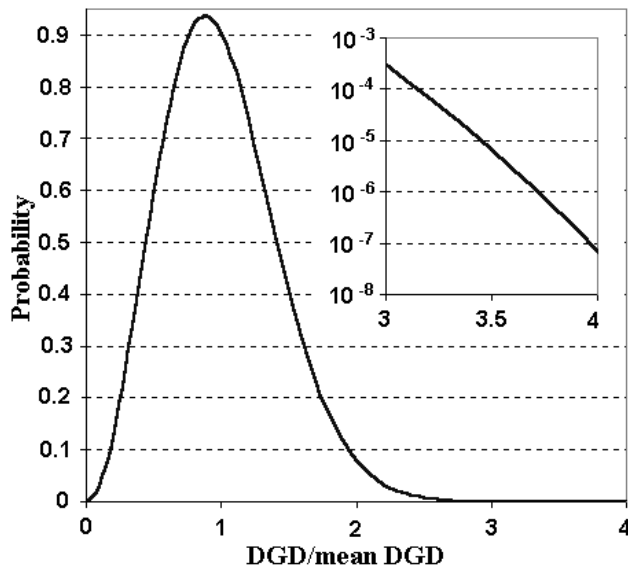


Figure 1. Maxwellian probability density function.

Therefore the single parameter  $\langle \Delta\tau \rangle$  fully specifies the distribution. Figure 1 shows the Maxwellian probability density function normalized by the mean DGD.

Using this distribution, the probability of  $\Delta\tau$  exceeding a particular value can be found using

$$P(\Delta\tau \geq X) = 1 - \int_0^X p(\Delta\tau) d\Delta\tau \quad (6)$$

For example, the probability of  $\Delta\tau/\langle \Delta\tau \rangle$  exceeding 3.7 is  $1.3 \times 10^{-7}$ . Expressed another way, if the mean DGD of a fiber link is 10 ps, 99.99999% of the time the DGD will be less than 37 ps.

### NETWORK DESIGN CONSIDERATIONS

In the design of a robust, long-haul fiber-optic network, the relationship between the maximum achievable link length and bit rate must be considered. For link designs where the maximum tolerable DGD is exceeded, techniques for coping with the effects of PMD must be explored.

#### Receiver DGD tolerance

The maximum link DGD that a receiver can tolerate before the signal degradation becomes unacceptable depends on a variety of factors, including modulation format, optical signal-to-noise ratio, and receiver design. For intensity-modulated, direct-detected (IM-DD) systems, Iannone et al. [6] found that when the transmitted signal excites both PSPs equally (a worst case condition), a 1-dB receiver sensitivity penalty results when the instantaneous DGD is about 23% of the signaling time period,  $T_{\text{bit}}$ . For a 2.5-Gb/s NRZ signal ( $T_{\text{bit}}$  is 400 ps), this corresponds to a tolerable DGD value of about 92 ps; at 10-Gb/s, about 23 ps is tolerable; and for a 40-Gb/s NRZ signal, this corresponds to about 5.7 ps. This maximum tolerable DGD level is representative of the NRZ IM-DD case; receiver DGD tolerance can be improved through careful receiver design, use of PMD-tolerant signaling formats, and the use of forward-correction codes (FEC). Khosravani and Willner [7] showed that RZ, chirped RZ, and dispersion-managed soliton signaling formats are much more tolerant of PMD effects compared to NRZ formats. Shieh et al. [8] and Xie et al. [9] have demonstrated a substantial increase in receiver tolerance of DGD when FEC is used. Modern long-haul, 10-Gb/s receivers using FEC or RZ modulation can tolerate about 40 ps of DGD with a 1-dB power penalty.

#### Probability of signal outage

For occurrences of high instantaneous DGD, signal quality may be intolerable resulting in a PMD-induced outage. Such outages may significantly affect network availability for higher bit rates (10 Gb/s, 40 Gb/s, and higher). For a network to operate with an overall availability of “five nines” (i.e., 99.999% of availability), the desired PMD-related availability factor may be “seven nines” (i.e., 99.99999%) which corresponds to a maximum tolerable DGD 3.7 times the mean DGD. For a 2.5-Gb/s IM-DD NRZ system with a DGD tolerance of 92 ps, this results in an acceptable mean DGD value of 25 ps; for a 10-Gb/s system with a DGD tolerance of 23 ps, the acceptable mean DGD is 6.2 ps; and for 40-Gb/s with a tolerable DGD of 5.7 ps, the acceptable mean DGD

level is 1.5 ps. For DGD-tolerant receivers (40 ps at 10 Gb/s) this results in an acceptable mean DGD of 10.8 ps.

### Coping with PMD

For network operators faced with the challenge of upgrading the channel data rate on a high-PMD link in the network, a handful of solutions exist that will preserve the signal quality at increased data rates.

One alternative cost solution is to selectively replace those fiber segments in the link known to be the dominant contributors to the overall link DGD, if they can be identified.

Another alternative cost solution is to regenerate the optical signal by placing a back-to-back terminals at the point in the link where the DGD affects approach an intolerable level, thus effectively reducing the optical link length.

Still another approach is to introduce error correction codes, such as FEC. In this approach the optical data payload is reduced incrementally in exchange for a marginal gain in PMD tolerance.

Yet another solution is to incorporate an adaptive PMD compensation system [8, 9, 10, 11, 12], typically located at the receiver. Typical PMD compensation systems are effective at minimizing the effects of first-order PMD, and, in some cases, second-order PMD. However both first- and second-order PMD compensation systems suffer the drawback that they reduce the effects of signal degradation over a very narrow optical bandwidth. This is a significant drawback for dense wavelength-division multiplexing (DWDM) systems. For a long-haul fiber-optic link carrying 100s of wavelengths, a separate PMD compensation system may be required for each wavelength to provide the desired seven nines availability.

For DWDM systems, another potential solution exists. Särkimukka et al. [13] proposed a method for mitigating PMD effects in a multichannel system by moving traffic off of PMD-impaired channels onto spare channels that are not experiencing PMD degradation.

One may also rely upon more traditional protection techniques (e.g. SONET ring or IP routing at layers 1 & 3, respectively). This protection can easily provide a guard against occasional PMD-induced outages of limited duration. However, for this approach to be viable, the episodes of abnormally high DGD events must be infrequent and spectrally localized. To evaluate the feasibility and limits of this solution, an understanding of the temporal and spectral nature of PMD is required.

Finally, there are also efficient optical networking solutions offering varying degrees of protection by using an optical cross-connect with a DWDM system. Operators may then construct a mesh-protected network and provide managed wavelength services that are protected against a possible PMD induced outages. Similar to the traditional protection methods, these more recent techniques will only be viable with infrequent and spectrally localized outages.

### TEMPORAL BEHAVIOR OF DGD

Given the dynamic nature of PMD and the low probability of excursions to intolerable levels, measurements of  $\Delta\tau(\lambda, t)$

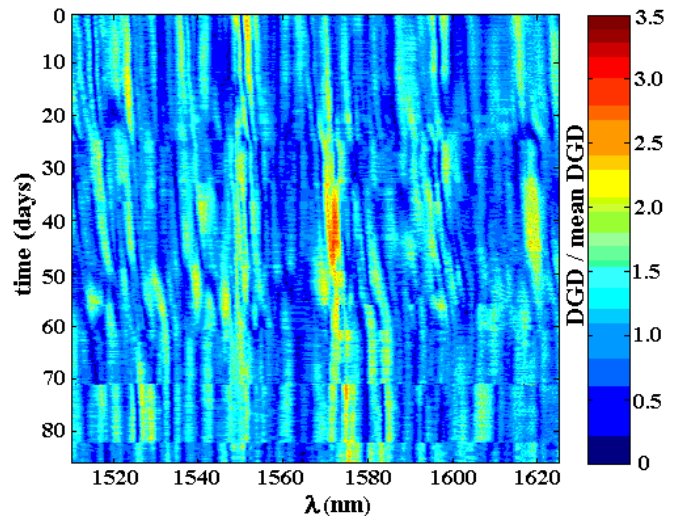


Figure 2. Map of normalized DGD vs. wavelength and time.

on buried fiber spans were made over long periods to enable prediction of the potential impact of PMD on network availability. Of particular interest are the frequency and duration of these rare events. The Jones Matrix Eigenanalysis (JME) technique was used to measure the DGD data on a 95-km span of slotted-core, direct buried fiber-optic cable made available by Sprint.

DGD was measured roughly every 3 hours at wavelengths from 1510 nm to 1625 nm with a spectral resolution of 0.1 nm (about 12.5 GHz). Over 86 days (from November 9, 2001 through February 2, 2002) 692 measurements were made on the 1150 discrete wavelengths. Figure 2 shows in a color-coded format this normalized DGD data (i.e.,  $\Delta\tau/\langle\Delta\tau\rangle$ ) representing 795,800 measured values. Expressed another way, if the 0.1-nm spectral samples and 3-hour time samples are statistically independent, then this data set would represent about 272 years of DGD data.

A histogram of this normalized DGD data is shown in Figure 3, and is seen to have shape consistent with a Maxwellian distribution, as expected. A curve representing a Maxwellian distribution normalized to the mean is also plotted for comparison.

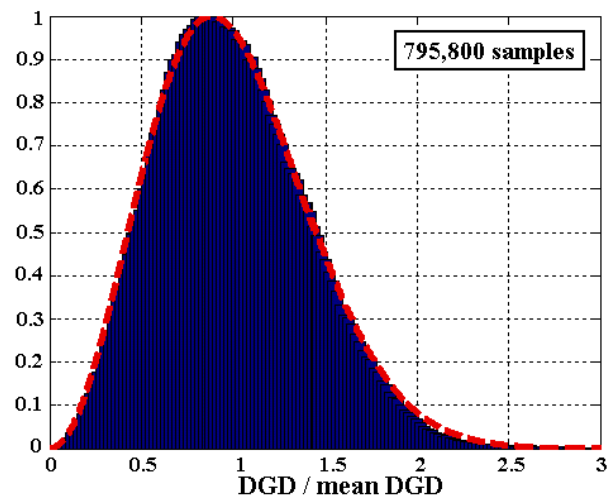
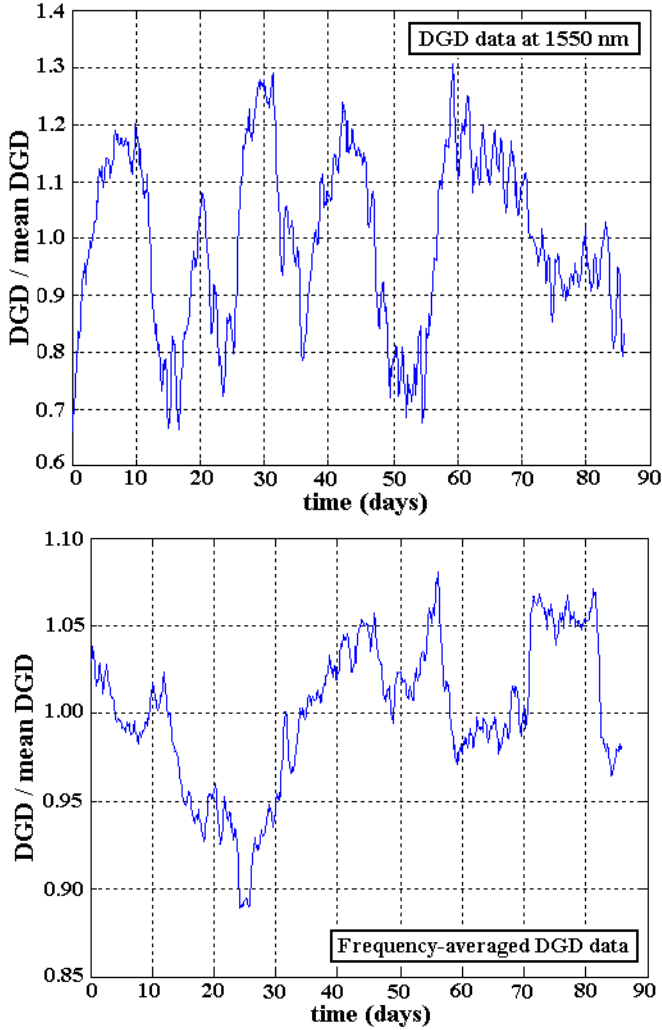


Figure 3. Normalized histogram of measured DGD data.



**Figure 4. Measured temporal variations in normalized DGD over 86 days (top) at 1550 nm and (bottom) averaged over all 1150 frequency measurements.**

From Figure 2 it is apparent that for buried fiber DGD values do not change rapidly. Figure 4 shows time histories of measured DGD data over the 86-day period. The top plot is DGD data at 1550 nm and the bottom plot is frequency-averaged data. While the mean value of the bottom plot is one (by definition), the mean value of the top plot is 1.088. This should not be interpreted to mean that the mean DGD is changing; rather since fewer data were used to estimate the mean, there is more uncertainty in that estimate compared to the estimate using all of the data.

To determine the DGD rate of change, an autocorrelation analysis was performed on the DGD time histories. Figure 5(top) shows the normalized temporal autocorrelation function (ACF) of the DGD data measured at 1550 nm. Figure 5(bottom) shows the ACF for the DGD time history for the frequency-averaged DGD data. Also shown in Figure 5 are curves representing the theoretical temporal autocorrelation function for DGD [14] which has the form

$$AFC(\Delta t) = \frac{1 - \exp(-|\Delta t|/t_d)}{|\Delta t|/t_d} \quad (7)$$

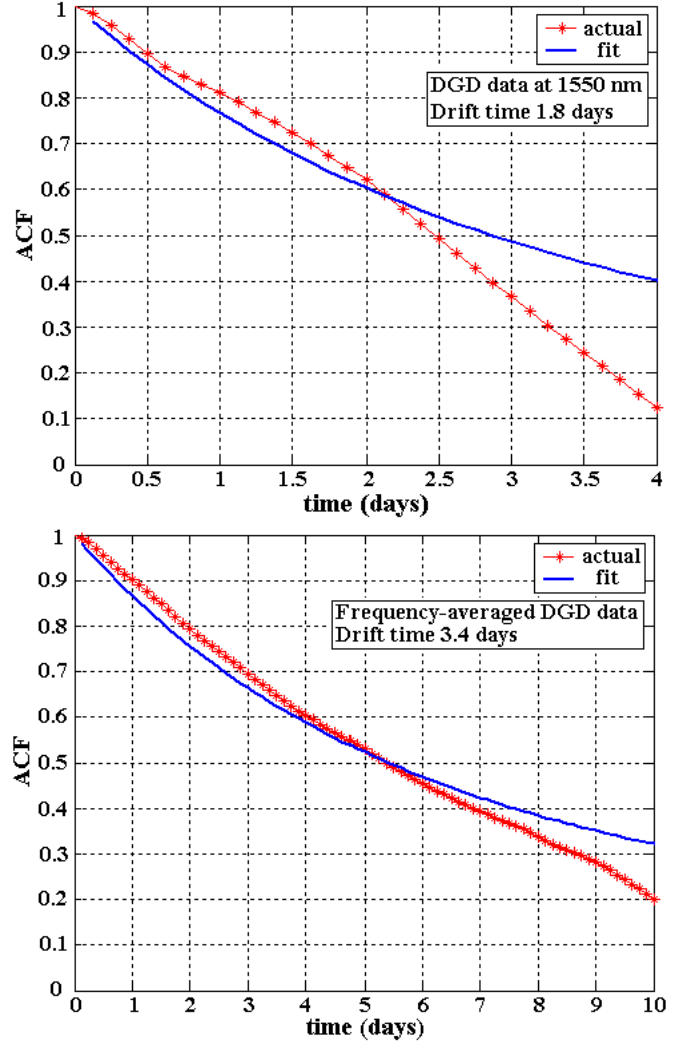


**Figure 5. Normalized temporal autocorrelation functions (ACFs) of normalized DGD data measured (top) at 1550 nm and (bottom) across 1150 frequencies. Theoretical ACF curves are fitted to the measured temporal ACFs.**

where  $t_d$  is the average drift time of DGD. The drift time indicates the timescale over which the DGD changes. Furthermore, when outages occur, the outage duration will be related to the drift time [14,15]. Based on data collected over the 86 days, the drift time for this fiber is estimated to be around 3.4 days. Expressed another way, samples should be collected about once every three days to obtain statistically independent DGD values on a specific wavelength; measurements collected more often are correlated.

For comparison, others have reported a range of DGD correlation times under various fiber conditions. For spools of fiber in a laboratory environment, correlation times of about 30 minutes on 31.6 km of fiber [16] and 3 hours on a 10-km fiber [17] have been reported. DGD variations on a 48-km aerial cable exhibited time scales ranging from 5 to 90 minutes depending the air temperature rate of change [18]. For submarine cables, a DGD correlation time of about an hour was observed on a 119-km cable [19], and [20] observed

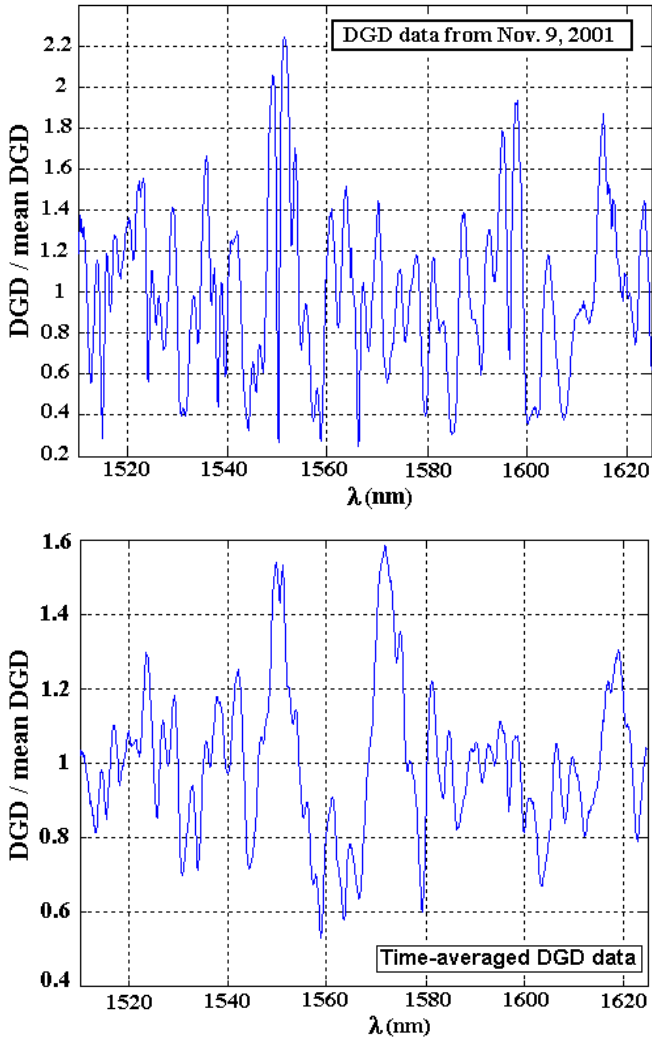


**Figure 6. Spectral variations in normalized DGD over 1150 wavelengths (top) measured on Nov. 9, 2001 and (bottom) time-averaged over all 692 time measurements.**

PMD changes with a period of about two months on a 62-km fiber-optic cable. On buried fibers, correlation times of at least 20 minutes (17 km) [21], 1-2 hours (48.8 km) [18], 3 and 5.7 days (127 km) [14], and 19 hours (114 km) [22] have been reported. Thus our observation of 3.4 days is consistent.

With knowledge gained from the ACF analysis, we can now interpret realistically our DGD data set. Over the 86 days of observation, about 25 independent samples were collected.

#### SPECTRAL BEHAVIOR OF DGD

From Figure 2 we note that the DGD varies significantly with wavelength. Figure 6(top) shows the normalized spectral variation of the first DGD data (measured on Nov. 9,2001) and the bottom plot shows the spectral variation of the time-averaged, normalized DGD data.

To determine the DGD bandwidth, spectral autocorrelation analysis was performed on the normalized DGD spectral data. Figure 7(top) shows the resulting normalized spectral ACF for one spectral measurement (data collected on

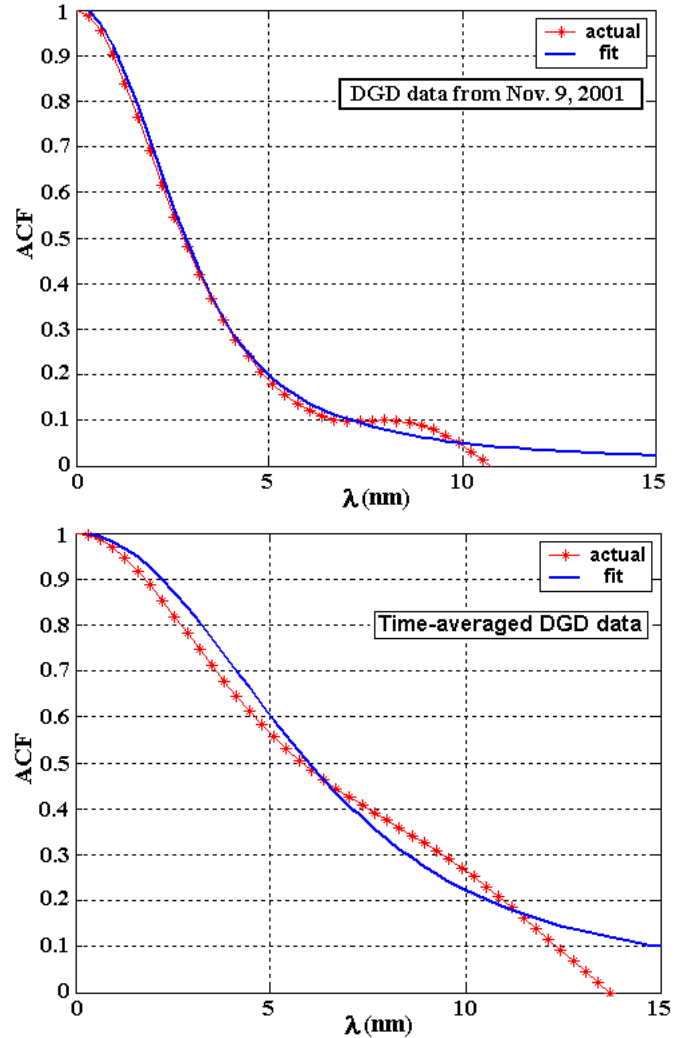


**Figure 7. Normalized spectral autocorrelation functions (ACFs) of normalized DGD data measured (top) on Nov. 9, 2001 and (bottom) time-averaged over all 692 measurements. Theoretical ACF curves are fitted to the measured spectral ACFs.**

Nov. 9,2001) and Figure 7(bottom) shows the normalized spectral ACF for the time-averaged data. Also shown in Figure 7 are curves representing theoretical spectral ACFs for DGD, with the form [23]

$$\text{ACF}(\Delta\omega) = 3 \frac{1 - \exp(-\langle \Delta\tau^2 \rangle \Delta\omega^2 / 3)}{\Delta\omega^2} \quad (8)$$

where  $\Delta\omega$  is the radian frequency and  $\langle \Delta\tau^2 \rangle$  represents the variance of the DGD.

From the measured data the bandwidth for the normalized DGD is estimated to be about 7.5 nm or 936 GHz. Therefore if the mean DGD is 1 ps and an optical channel is affected by significant DGD, nearby channels (within about 7.5 nm) may also experience this effect.

Theory and experiments [23] have demonstrated that the DGD bandwidth is inversely proportional to the mean DGD.

$$\omega_c = 4\sqrt{2}/\langle \Delta\tau \rangle \quad (9)$$



Thus fibers with a high mean DGD have a narrower DGD bandwidth than fibers with a low mean DGD. Thus for a fiber with a mean DGD of 1 ps, the predicted DGD bandwidth is 900 GHz which agrees well with bandwidth found using the spectral ACF fit in Figure 6(bottom). Note that normalized DGD bandwidth in the Figure 6(top) is about 4 nm which is significantly less than the approximately 7.5 nm bandwidth seen in Figure (bottom). This should not be interpreted to mean that the DGD bandwidth is varying; rather the bandwidth estimate obtained using all of the data will be more accurate as it is based on significantly more data points.

#### IMPLICATIONS FOR NETWORK AVAILABILITY

##### Mean time between PMD-related outages

The mean time between PMD-related outages can be estimated from the temporal characteristics of DGD variations and the Maxwellian probability density function. The DGD rate of change is characterized by the DGD drift time,  $t_d$ . This drift time may be thought of as “rolling the dice” every  $t_d$  to obtain a new, statistically independent DGD value. Therefore the mean time between high-DGD events (i.e., DGD exceeding a value X) can be estimated as

$$T_X = t_d / (k \cdot P(\Delta\tau > X)) \quad (10)$$

where k is a proportionality constant.

For example, Nagel et al. [22] observed a DGD correlation time of 19 hours, and predicts that the DGD will exceed three times its mean value once every 3.5 years. Since the probability of the DGD exceeding three times its mean is about  $4.2 \times 10^{-5}$  we can determine a value of 15 for k.

Applying (10) with a drift time of 3.4 days and a threshold of three times the mean DGD, the mean time between high-DGD events is about 14.8 years. For a PMD-induced outage probability of  $1.3 \times 10^{-7}$  (network availability of seven nines) the receiver should tolerate  $3.7 \times \langle \Delta\tau \rangle$ . With a DGD drift time,  $t_d$ , of 3.4 days, the estimated mean time between high-DGD events will be about 4,700 years, making it an extremely rare occurrence!

##### Duration of high-DGD events

Again from the DGD drift time, the Maxwellian probability density function, and the temporal ACF, the average duration of a high-DGD event can be estimated. While the correlation time represents the time delay resulting in a 63% reduction in the normalized ACF, smaller variations in the ACF require significantly shorter times. Again Nagel et al. [22] estimated a mean outage duration between 10 and 20 minutes for their link having a DGD correlation time of 19 hours. Bülow and Veith [15] found that while unusually long duration outages occur, the probability of occurrence decreases almost exponentially with outage duration. In other words, when outages occur, most will be of short duration.

Based on these findings, for the 95-km link we observed, we anticipate the typical duration of an outage to be between 1 and 2 hours with the possibility that a prolonged outage could persist for 1 to 1.5 days.

##### Impact of high-DGD events on adjacent channels

When a high-DGD episode occurs, how many DWDM channels will be affected? For a link with a mean DGD of 5 ps, the DGD bandwidth will be about 180 GHz or 1.44 nm. Therefore for a DWDM system with a 50-GHz channel spacing, during a  $3.7 \times \langle \Delta\tau \rangle$  event, the DGD in adjacent channels may also experience PMD-induced signal degradation, (i.e., only two or three channels will likely be affected by a single high-DGD episode).

##### Design rules

Based on these observations and analyses, certain rules may be developed. An important parameter in making decisions regarding PMD in a network is the ratio between the receiver’s DGD tolerance,  $\Delta\tau_{RX}$ , and the link’s mean DGD.

$$M = \frac{\Delta\tau_{RX}}{\langle \Delta\tau \rangle} \quad (11)$$

For cases where  $M > 3$ , the frequency of PMD-induced outages will be low, and their duration may be brief. In these cases the approach proposed by Särkimukka (or one utilizing new protection techniques) may be viable. The occurrences when switching this traffic may be required will likely be infrequent (spanning years), and may only be required for a few minutes or as long as a day.

For cases where  $2 < M < 3$ , PMD-induced outages may occur about once a month with typical durations measured in 10s of minutes.

For cases where  $M < 2$ , chronic PMD-induced outages will result. In these instances the option of applying PMD compensation, interrupting the link with a back-to-back terminal regenerator, or even replacing particular fiber segments may be appropriate.

##### Example scenarios

*10-Gb/s,  $\langle \Delta\tau \rangle = 10$  ps, receiver’s DGD tolerance 40 ps*

In this scenario the DGD margin, M, is 4. The probability of the DGD exceeding the receiver’s DGD tolerance level is about  $7.4 \times 10^{-9}$ , or effectively zero. In this case it is quite unlikely a PMD-induced outage will ever be observed. The DGD bandwidth will be about 90 GHz or about 0.72 nm.

*10-Gb/s,  $\langle \Delta\tau \rangle = 10$  ps, receiver’s DGD tolerance 23 ps*

In this case the margin will be 2.3 meaning that the probability of the DGD exceeding the receiver’s limit is about 0.37%. For a buried cable with a DGD drift time of about 2 days, PMD-induced outages typically will occur about once a month and last less than an hour. The DGD bandwidth will again be about 90 GHz.

*40-Gb/s,  $\langle \Delta\tau \rangle = 3.2$  ps, receiver’s DGD tolerance 5.7 ps*

The DGD margin in this case is 1.8 so the probability of the DGD exceeding the receiver’s limit is 4.4%. For a link with a drift time of 2 days, PMD-induced outages typically will occur about every third day. The typical duration will be 1 to 2 hours, however outages persisting for a day may occur. The DGD bandwidth is about 2.2 nm or 280 GHz so in a DWDM application with 50 GHz channel spacing, two or three channels may be affected during each outage.

## CONCLUSIONS

By examining the statistical behavior of DGD in an optical fiber, and using measured DGD data on a buried optical cable, predictions regarding the probability, frequency of occurrence, and spectral extent of high-DGD episodes can be made. Reports by others confirm our observation that DGD excursions of three or more times the mean DGD are infrequent and relatively short lived. This finding is significant for network operators who may consider providing a few spare channels in a DWDM environment to ensure high network availability.

For cases where the mean DGD is comparable to the receiver's maximum tolerable DGD, approaches for ensuring network availability include inclusion of PMD compensation systems, shortening the link length by strategically introducing back-to-back terminal regenerators, replacing fiber segments found to have excessively high DGD levels, or by utilizing an optical networking solution whereby traffic may efficiently share protection bandwidth.

## ACKNOWLEDGMENT

This work was funded by Sprint Corporations Company, L. P. A special tribute is paid to Francis Yarkosky, for his leadership and support.

## REFERENCES

- [1] Iannone, E., F. Matera, A. Mecozzi, and M. Settembre, *Nonlinear Optical Communication Networks*, New York: John Wiley & Sons, Inc., pp. 30-35, 1998.
- [2] Poole, C. D. and J. Nagel, Chapter 6: "Polarization effects in lightwave systems," in *Optical Fiber Telecommunications III A*, eds. I. P. Kaminow and T. L. Koch, San Diego: Academic Press, 1997.
- [3] Betti, S., F. Curti, B. Daino, G. De Marchis, E. Iannone, and F. Matera, "Evolution of the bandwidth of the principal states of polarization in single-mode fibers," *Optics Letters*, 16(7), pp. 467-469, 1991.
- [4] Curti, F., B. Daino, G. de Marchis, and F. Matera, "Statistical treatment of the evolution of the principal states of polarization in single-mode fibers," *Journal of Lightwave Technology*, 8, pp. 1162-1166, 1990.
- [5] Gisin, N., R. Passy, J. C. Bishoff, and B. Perry, "Experimental investigation of the statistical properties of polarization mode dispersion in single mode fibers," *IEEE Photonics Technology Letters*, 5(7), pp. 819-821, 1993.
- [6] Iannone, E., F. Matera, A. Galtarossa, G. Gianello, and M. Schiano, "Effect of polarization dispersion on the performance in IM-DD communication systems," *IEEE Photonics Technology Letters*, 5(10), pp. 1247-1249, 1993.
- [7] Khosravani, R. and A. E. Willner, "Comparison of different modulation formats in terrestrial systems with high polarization mode dispersion," *Proc. OFC 2000*, Baltimore, paper WL5, pp. 201-203, 2000.
- [8] Shieh, W., H. Haunstein, B. Mckay, D. Fishman, A. Golubchik, J. Diubaldi, C. Martell, V. Arya, R. Lee, and H. Choudhury, "Dynamic polarization-mode-dispersion compensation in WDM systems," *Proc. ECOC 2000*, Munich, Germany Vol. II(4.2.5), pp. 41-43, 2000.
- [9] Xie, Y., Q. Yu, L.-S. Yan, O. H. Adamczyk, Z. Pan, S. Lee, A. E. Willner, and C. R. Menyuk, "Enhanced PMD mitigation using forward-error-correction coding and a first-order compensator," *Proc. OFC'2001*, Los Angeles, CA, paper WAA2, 2001.
- [10] Rosenfeldt, H., Ch. Knothe, R. Ulrich, E. Brinkmeyer, U. Feiste, C. Schubert, J. Berger, R. Ludwig, H. G. Weber, and A. Ehrhardt, "Automatic PMD compensation at 40 Gbit/s and 80 Gbit/s using a 3-dimensional DOP evaluation for feedback," *Proc. OFC'2001*, Los Angeles, CA, Postdeadline Papers, paper PD27, 2001.
- [11] Kikuchi, N., "Analysis of signal degree of polarization degradation used as control signal for optical polarization mode dispersion compensation," *Journal of Lightwave Technology*, 19(4), pp. 480-486, 2001.
- [12] Pua, H.Y., K. Peddanarappagari, B. Zhu, C. Allen, K. Demarest, and R. Hui, "An adaptive first-order polarization-mode dispersion compensation system aided by polarization scrambling: theory and demonstration," *Journal of Lightwave Technology*, 18(6), pp. 832-841, 2000.
- [13] Särkimukka, S., A. Djupsjöbacka, A. Gavler, and G. Jacobsen, "Mitigation of polarization-mode dispersion in optical multichannel systems," *Journal of Lightwave Technology*, 18(10), pp. 1374-1380, 2000.
- [14] Karlsson, M., J. Brentel, and P. A. Andrekson, "Long-term measurement of PMD and polarization drift in installed fibers," *Journal of Lightwave Technology*, 18(7), pp. 941-951, 2000.
- [15] Bülow, H. and G. Veith, "Temporal dynamics of error-rate degradation induced by polarization mode dispersion of an installed field fiber link," *Proc. ECOC 1997*, vol. 1, Mo3C, Edinburgh, pp. 115-118, 1997.
- [16] Poole, C. D., R. W. Tkach, A. R. Chaplyvy, and D. A. Fishman, "Fading in lightwave systems due to polarization-mode dispersion," *IEEE Photonics Technology Letters*, 3(1), pp. 68-70, 1991.
- [17] Bahsoun, S., J. Nagel, and C. Poole, "Measurements of temporal variations in fiber transfer characteristics to 20 GHz due to polarization-mode dispersion," *Proc. ECOC'90*, Amsterdam, The Netherlands, Postdeadline Paper, pp. 1003-1006, 1990.
- [18] Cameron, J., L. Chen, X. Bao, and J. Stears, "Time evolution of polarization mode dispersion in optical fibers," *IEEE Photonics Technology Letters*, 10(9), pp. 1265-1267, 1998.
- [19] Takahashi, T., T. Imai, and M. Aiki, "Time evolution of polarization mode dispersion in 120 km installed optical submarine cable," *Electronics Letters*, 29(18), pp. 1605-1606, 1993.
- [20] Kawazawa, T. and Y. Namihira, "Long-term polarization-mode-dispersion measurement of installed optical submarine cable," *Proceedings of OFC'94*, pp. 228-229, 1994.

- [21] De Angelis, C., A. Galratossa, G. Gianello, F. Marera, and M. Schiano, "Time evolution of polarization mode dispersion in long terrestrial links," *Journal of Lightwave Technology*, 10(5), pp. 552-555, 1992.
- [22] Nagel, J. A., M. W. Chbat, L. D. Garrett, J. P. Soigné, N. A. Weaver, B. M. Desthieux, H. Bülow, A. R. McCormick, and R. M. Derosier, "Long-term PMD mitigation at 10 Gb/s and time dynamics over high-PMD installed fiber," *Proc. ECOC 2000*, Munich, Germany Vol. II(4.2.1), pp. 31-32, 2000.
- [23] Karlsson, M. and J. Brentel, "Autocorrelation function of the polarization-mode dispersion vector," *Optics Letters*, 24(14), pp. 939-941, 1999.

# Analysis and comparison of measured DGD data on buried single-mode fibers

Christopher Allen<sup>1</sup>, Pradeep Kumar Kondamuri<sup>1</sup>, Douglas L. Richards<sup>2</sup>, and Douglas C. Hogue<sup>2</sup>

<sup>1</sup>Lightwave Communication Systems Laboratory  
Information and Telecommunications Technology Center (ITTC)  
The University of Kansas, Lawrence, Kansas 66045

<sup>2</sup>Sprint Corporation, Overland Park, Kansas

## Abstract

Temporal and spectral measurements were made on three different 95-km fibers within a slotted-core, direct buried, standard single-mode fiber-optic cable over many days to characterize DGD variability. From this data we observed that DGD varies slowly over time but rapidly over wavelength. This data showed good agreement with a Maxwellian distribution. The frequency-averaged mean DGD varied by about 10% or less during the periods that included significant temperature swings. Outage analysis showed that for system tolerances of three times the mean DGD, outages will occur typically every 3 to 8 years with mean outage durations ranging from about one to two hours. From this analysis we conclude that high-DGD episodes are spectrally localized and will be exceedingly rare and short lived.

## Introduction

Polarization-mode dispersion (PMD) may be a major impediment for network operators seeking to increase the per channel data rate on long-haul fiber-optic links. While the differential group delay (DGD, or  $\Delta\tau$ ) in buried fiber had negligible impact at 2.5-Gb/s signaling rates, upgrades to 10 Gb/s, 40 Gb/s and beyond will require increasingly more attention. While there are PMD challenges facing carriers operating at 10 Gb/s, these challenges are not as severe as originally feared. Major carriers are successfully deploying 10-Gb/s dense-wavelength division multiplexed (DWDM) links across the core of their networks. A marked improvement in the DGD tolerance of 10 Gb/s long-reach receivers (to about 40 ps) will likely satisfy most length demands, obviating the need for PMD compensation (PMDC). Signaling rates of 40 Gb/s and beyond will most likely require some form of mitigation in long-haul applications, such as robust modulation schemes or PMDC.

To ensure signal quality on their fiber at higher bit rates, network engineers must anticipate the impact of PMD on the various fiber routes. An understanding of the variability of both the DGD and the principal states of polarization (PSPs) is required to specify appropriate transmission parameters. Factors such as the mean DGD, PMD correlation time and bandwidth, as well as

second-order effects together with performance prediction models can provide this understanding.

The availability of measured PMD data on installed, buried fibers is limited. In this paper we present measured DGD data for buried, standard single-mode fiber to improve our understanding of the variability of PMD. While PMD is a vector quantity, with a magnitude (DGD) and a direction (PSP), we are only focusing on the DGD. The statistical distribution and behavior of PSPs has been extensively studied and is shown to be correlated to DGD behavior [1,2].

## Experimental setup

Experiments were conducted to measure the instantaneous DGD on three different 95-km fibers (1, 2, and 3) within a slotted-core, direct buried, standard single-mode fiber-optic cable made available by Sprint. A polarization analyzer employing the Jones-Matrix-Eigenanalysis (JME) method was used for measurements at wavelengths from 1510 nm to 1625 nm with a spectral resolution of 0.1 nm (about 12.5 GHz). Measurements on fiber span 1 were repeated approximately every 3 hrs and they were carried on for about 86 days whereas on fiber spans 2 and 3 they were repeated approximately every 1½ hours and carried out for about 14 and 9 days, respectively. Over the 86 days (from Nov. 9, 2001 through Feb. 2, 2002) 692 measurements were made on fiber span 1 across the 1150 discrete wavelengths representing 795,800 measured values. For fiber spans 2 and 3 the corresponding number of DGD measurements is about 271,600 and 181,700.

## Plots of DGD vs. wavelength and time

Figures 1, 2, and 3 show in a color-coded format normalized DGD data (i.e., DGD/mean DGD) measured on the three fiber spans, respectively. From the plots it is clear that for buried fibers DGD changes with time but not at a rapid rate. This variation is random and differs from fiber to fiber. It is also evident that the DGD varies significantly with wavelength and relatively high-DGD events are spectrally localized.

A histogram of the normalized DGD data on fiber span 1, shown in Figure 4, is seen to have shape consistent with a Maxwellian distribution, as expected. A curve representing a Maxwellian distribution for a 1-ps mean DGD is also plotted for comparison.

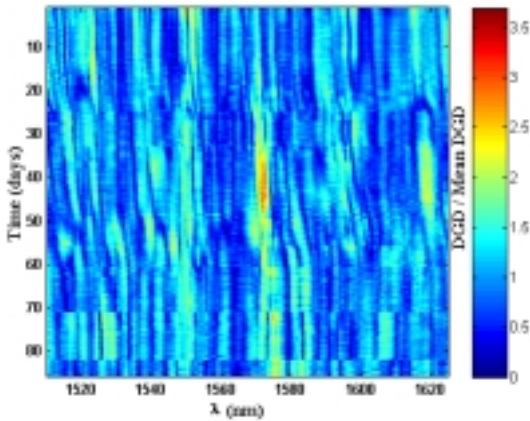


Figure 1. Measured, normalized DGD vs. wavelength and time for fiber span 1 (86 days of data).

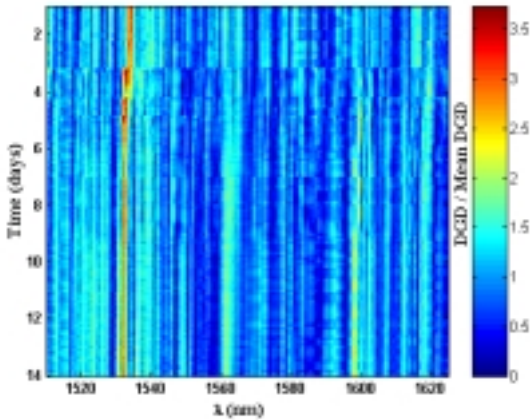
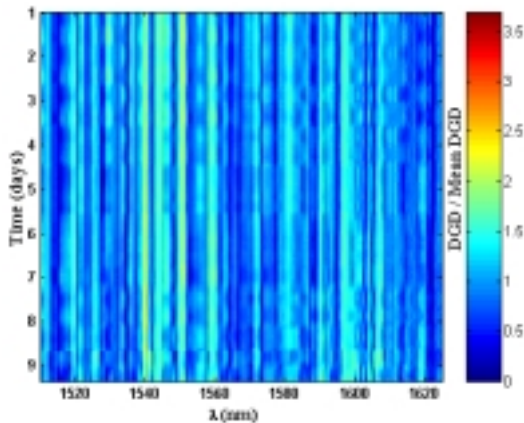


Figure 2. Measured, normalized DGD vs. wavelength and time for fiber span 2 (14 days of data).



(c)

Figure 3. Measured, normalized DGD vs. wavelength and time for fiber span 3 (9 days of data).

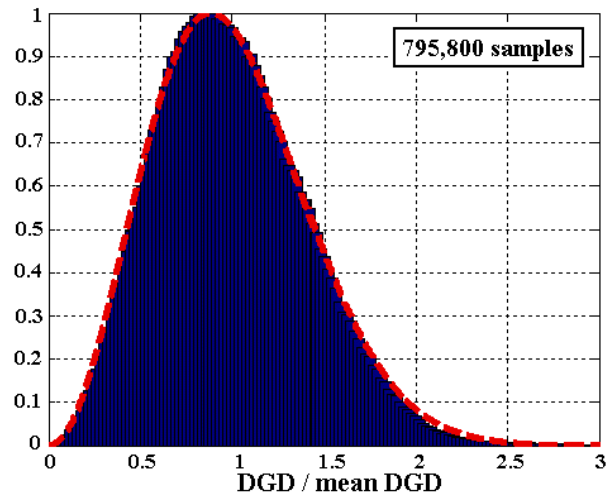


Figure 4. Histogram of measured, normalized DGD data on fiber span 1.

Similar histograms were obtained for the data on the other two fiber spans (plots not shown here) and they also showed good agreement with a Maxwellian distribution.

#### Mean DGD variation with time

To observe the time-dependent nature of DGD more closely, 1150 DGD measurements over all wavelengths were averaged together to obtain frequency-averaged DGD data, denoted as  $\langle \text{DGD} \rangle_\lambda$  normalized by the overall mean DGD (averaged over both time and frequency), denoted as  $\langle \langle \text{DGD} \rangle_\lambda \rangle_t$ . Since temperature is a known driver in changing DGD changes, hourly air temperature data for the region were collected as well. The variation of frequency-averaged DGD and temperature with time on the three fiber spans is shown in Figures 5, 6 and 7. From Figure 5 it can be observed that frequency-averaged DGD varies by only about  $\pm 10\%$  over 86 days of observations that included significant temperature swings. Since the entire length of the fiber is buried, the diurnal temperature variations do not represent the fiber temperature. Statistical analyses reveal no significant correlation between long-term temperature variations and the frequency-averaged mean DGD.

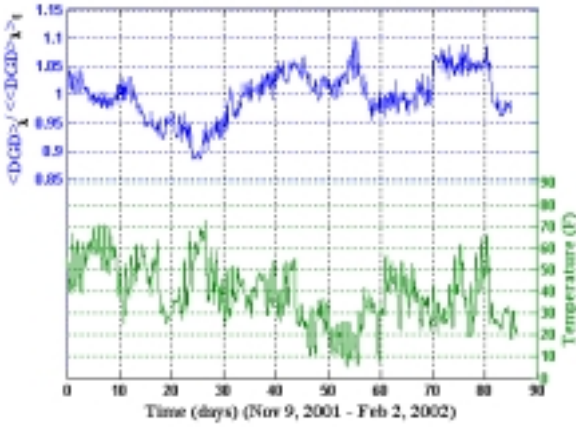


Figure 5. Frequency-averaged DGD and temperature vs. time for fiber span 1.

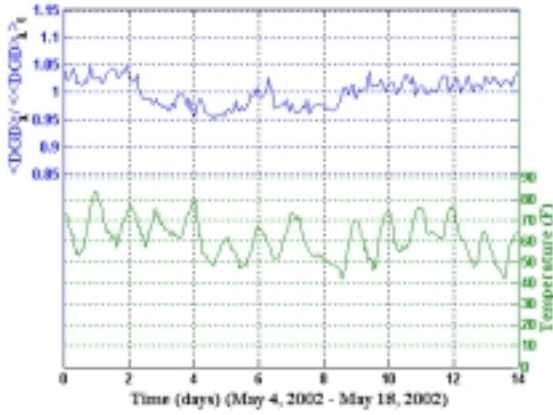


Figure 6. Frequency-averaged DGD and temperature vs. time for fiber span 2.

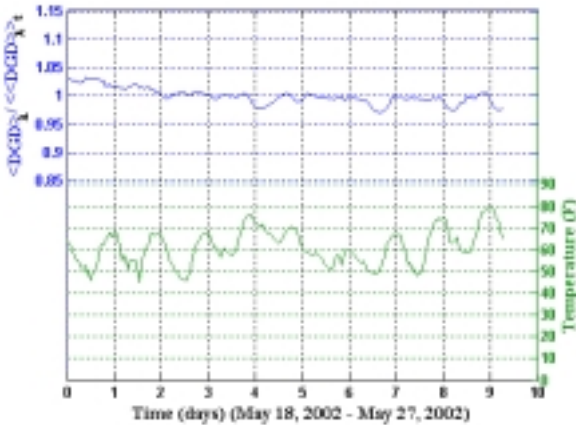


Figure 7. Frequency-averaged DGD and temperature vs. time for fiber span 3.

### System outage analysis

An outage event is one which exceeds the given threshold value of DGD,  $\Delta\tau_{th}$ . The outage probability  $P_{out}$ , expressed in minutes/year, can be calculated from

the Maxwellian probability distribution function (pdf),  $f_{\tau}(\cdot)$  as

$$P(\Delta\tau \geq \Delta\tau_{th}) = 1 - \int_0^{\Delta\tau_{th}} f_{\tau}(\Delta\tau) d\Delta\tau \quad (2)$$

and then multiplying the number of minutes in a year. As  $P_{out}$  is based on the Maxwellian pdf, it may be expressed as a function of one independent variable  $M = \Delta\tau_{th}/(\text{mean DGD})$  as  $P_{out}(M)$  and is clearly fiber independent and will be the same for all installations.

In cases where the probability of an outage is quite small,  $P_{out}$  represents the annualized outage probability based on long time records, however no insight is provided regarding the outage rates and their durations. Accurate estimation of the impact of PMD on network availability requires statistical analysis of the DGD variability. Caponi et al. [3] showed how the mean time between PMD-related outages could be estimated from the temporal characteristics of DGD variations and the Maxwellian probability density function. The mean outage rate,  $R_{out}$  (defined as the mean number of outage events per unit time with units of events/year), is found using [3]

$$R_{out} = \frac{1}{2} f_{\tau}(\text{threshold}) \int_{-\infty}^{\infty} f_{\tau}(\Delta\tau') |\Delta\tau'| d\Delta\tau' \quad (3)$$

where  $\Delta\tau'$  is the time derivative of the DGD, and  $f_{\tau}(\cdot)$  is the pdf of  $\Delta\tau'$ . Caponi et al. observed  $\Delta\tau$  and  $\Delta\tau'$  to be statistically independent and also found that  $R_{out}$  is cable and installation dependent.

Figure 8 shows the calculated outage probability,  $P_{out}$ , and the mean outage rate,  $R_{out}$ , for a given system threshold relative to the mean DGD on the three fiber spans.

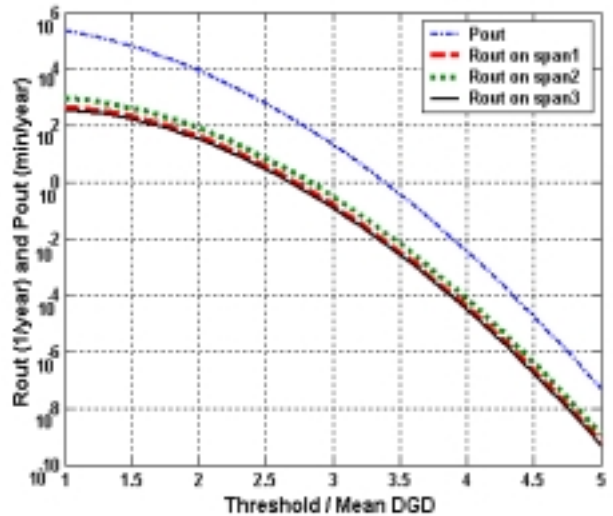


Figure 8. Calculated outage probability,  $P_{out}$ , and mean outage rate,  $R_{out}$ , versus Threshold / Mean DGD.

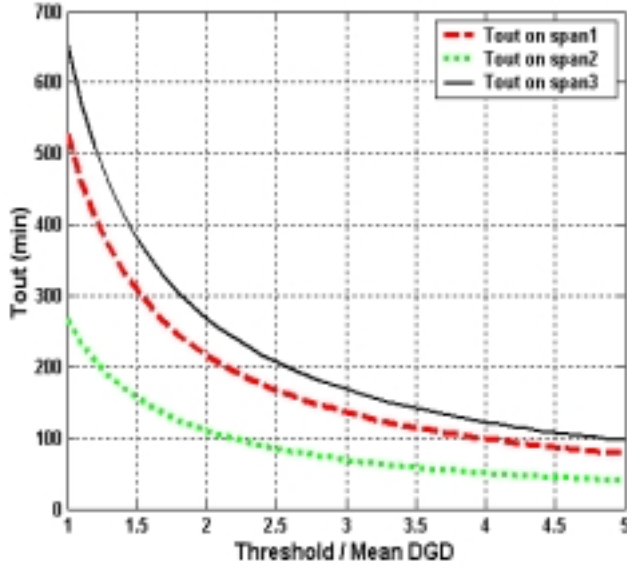


Figure 9. Calculated mean outage duration,  $T_{out}$ , as a function of Threshold/mean DGD.

Table 1. Predicted mean time between outages (MTBOs) and mean outage durations for different DGD tolerances

	$3*\langle DGD \rangle$	$3.7*\langle DGD \rangle$
Span 1		
MTBO	6.39 years	1648 years
Outage duration	136 min	108 min
Span 2		
MTBO	3.25 years	833 years
Outage duration	69 min	55 min
Span 3		
MTBO	7.91 years	2000 years
Outage duration	138 min	133 min

The mean duration of DGD-induced outages can be determined using statistical analysis as well. Caponi et al. [3] showed that the mean outage duration,  $T_{out}$ , is

$$T_{out} = P_{out} / R_{out} \quad (4)$$

which has units of minutes.

Figure 9 shows the calculated mean outage duration,  $T_{out}$ , as a function of system threshold relative to the mean DGD. Since  $T_{out}$  is found using  $R_{out}$ , which is cable and installation dependent,  $T_{out}$  will also be cable and installation dependent.

From the above analysis, we can estimate the mean outage time between outages (MTBOs) and mean outage durations for various DGD tolerances for these fiber spans. Table 1 lists these values for system thresholds of three and 3.7 times the mean DGD.

For comparison, Nagel et al. [4] predicted that for the 114-km buried link they studied, the DGD will exceed three times its mean value once every 3.5 years and estimated a mean outage duration of between 10 and 20

minutes for their link. From data measured on 37-km of buried cable, Caponi [3] predicted the DGD will exceed three times the mean DGD once every 2.5 years with a mean outage duration of 56 minutes.

### Conclusions

We have measured DGD data on three different 95-km fibers within a slotted-core, direct buried, standard single-mode fiber-optic. From these measurements we observed that DGD varies slowly over time but rapidly over wavelength or frequency. Episodes of higher-than-average DGD were observed and seen to be spectrally localized and of limited duration.

To investigate the role of changing temperature on mean DGD variations, frequency-averaged DGD data were compared to temperature histories. The frequency-averaged DGD varied by only about  $\pm 10\%$  over 86 days of observations that included significant temperature swings.

From this data predictions were made regarding the probability, and frequency of outage occurrence. While the statistics of Maxwellian processes adequately describe the annualized outage probability, further analysis of the DGD data revealed the mean time between outages and mean outage durations. For outages characterized by high DGD episodes (DGD more than three times the mean DGD), we found that the mean outage rates and durations for these three fibers to be similar. Our findings agree with reports by others that DGD excursions of three or more times the mean DGD are infrequent and relatively short lived. This finding is significant for network operators who must assess the impact of PMD on network reliability.

### Acknowledgment

This work was funded by Sprint Corporations Company, L. P. A special tribute is paid to Francis Yarkosky, for his leadership and support.

### References

- [1] Karlsson, M. and J. Brentel, "Autocorrelation function of the polarization-mode dispersion vector," *Optics Letters*, 24(14), pp. 939-941, 1999.
- [2] Karlsson, M., J. Brentel, and P. A. Andrekson, "Long-term measurement of PMD and polarization drift in installed fibers," *Journal of Lightwave Technology*, 18(7), pp. 941-951, 2000.
- [3] Caponi, R., B. Ripsati, A. Rossaro, and M. Schiano, "WDM design issues with highly correlated PMD spectra of buried optical fibers," *Proc. OFC 2002*, Anaheim, CA, Th15, pp. 453-455, 2002.
- [4] Nagel, J. A., M. W. Chbat, L. D. Garrett, J. P. Soigné, N. A. Weaver, B. M. Desthieux, H. Bülow, A. R. McCormick, and R. M. Derosier, "Long-term PMD mitigation at 10 Gb/s and time dynamics over high-PMD installed fiber," *Proc. ECOC 2000*, Munich, Germany Vol. II(4.2.1), pp. 31-32, 2000.